NPS-OC-94-009

NAVAL POSTGRADUATE SCHOOL
Monterey, California

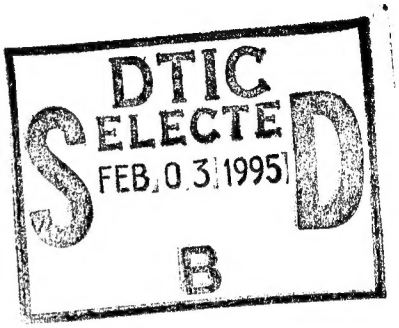

THESIS

MODELING STUDIES OF
THE LEEUWIN CURRENT OFF WESTERN
AND SOUTHERN AUSTRALIA

by

Christopher L. Butler

December, 1994

Thesis Advisor: Mary L. Batteen

Prepared for:
National Science Foundation
4201 Wilson Boulevard
Arlington, VA 22230

NAVAL POSTGRADUATE SCHOOL
Monterey, CA 93943

Rear Admiral Thomas A. Mercer
Superintendent

This thesis was prepared in conjunction with research sponsored in part by the National Science Foundation, 4201 Wilson Boulevard, Arlington, VA 22230.

Released by:

P.J. MARTO, Dean of Research

DISCLAIMER NOTICE

THIS DOCUMENT IS BEST QUALITY AVAILABLE. THE COPY FURNISHED TO DTIC CONTAINED A SIGNIFICANT NUMBER OF COLOR PAGES WHICH DO NOT REPRODUCE LEGIBLY ON BLACK AND WHITE MICROFICHE.

REPORT DOCUMENTATION PAGE

Form Approved OMB No. 0704-0188

1. AGENCY USE ONLY *(Leave blank)*	2. REPORT DATE December 1994	3. REPORT TYPE AND DATES COVERED Master's Thesis

4. TITLE AND SUBTITLE MODELING STUDIES OF THE LEEUWIN CURRENT OFF WESTERN AND SOUTHERN AUSTRALIA (U)

5. FUNDING NUMBERS

6. AUTHOR(S) Butler Christopher L. in conjunction with Mary Batteen

7. PERFORMING ORGANIZATION NAME(S) AND ADDRESS(ES)
Naval Postgraduate School
Monterey CA 93943-5000

8. PERFORMING ORGANIZATION REPORT NUMBER
NPS-OC-94-009

9. SPONSORING/MONITORING AGENCY NAME(S) AND ADDRESS(ES)
National Science Foundation
4201 Wilson Boulevard
Arlington, VA 22230

10. SPONSORING/MONITORING AGENCY REPORT NUMBER

11. SUPPLEMENTARY NOTES The views expressed in this thesis are those of the author and do not reflect the official policy or position of the Department of Defense or the U.S. Government.

12a. DISTRIBUTION/AVAILABILITY STATEMENT
Approved for public release; distribution is unlimited.

12b. DISTRIBUTION CODE

13. ABSTRACT *(maximum 200 words)*

A high-resolution, multi-level, primitive equation ocean model is used to examine the response of an eastern boundary oceanic regime to thermal and wind forcing. The focus of this study is the anomalous Leeuwin Current System off Western and Southern Australia.

Three types of experiments are conducted. The first type forces the model from rest with the Indian Ocean climatological temperature gradient as an initial condition only, while the second type repeats the first experiment with the added contribution of the North West Shelf water temperature profile. The role of irregular coastline geometry on the generation of currents and eddies is also examined by comparing these cases with and without an irregular (realistic) coastline. The third type, with an irregular coastline, forces the model from rest with constant thermal and wind forcing. A one-time application of the North West Shelf water is added during the model run.

In all experiments, surface currents, undercurrents, meanders, and eddies are generated. The results from experiments with an irregular, rather than an idealized coastline, show preferred eddy generation locations. The results from the third type of experiment, which has the most realistic features, agrees well with available observations off Western and Southern Australia. These results support the hypothesis that both thermal and wind forcing are important mechanisms for the generation of many of the observed features in the Leeuwin Current System.

14. SUBJECT TERMS Primitive equation model, Leeuwin Current System, currents, eddy generation, coastal oceanography, littoral oceanography.

15. NUMBER OF PAGES 158

16. PRICE CODE

17. SECURITY CLASSIFICATION OF REPORT	18. SECURITY CLASSIFICATION OF THIS PAGE	19. SECURITY CLASSIFICATION OF ABSTRACT	20. LIMITATION OF ABSTRACT
Unclassified	Unclassified	Unclassified	UL

NSN 7540-01-280-5500

Standard Form 298 (Rev. 2-89)
Prescribed by ANSI Std. 239-18

Approved for public release; distribution is unlimited.

MODELING STUDIES OF THE LEEUWIN CURRENT OFF WESTERN AND SOUTHERN AUSTRALIA

by

Christopher L. Butler
Lieutenant Commander, United States Navy
B.S., United States Naval Academy, 1983

Submitted in partial fulfillment
of the requirements for the degree of

MASTER OF SCIENCE IN
METEOROLOGY AND PHYSICAL OCEANOGRAPHY

from the

NAVAL POSTGRADUATE SCHOOL
December 1994

Author: Christopher L Butler
Christopher L. Butler

Approved by: Mary L. Batteen
Mary L. Batteen, Thesis Advisor

Curtis A. Collins, Second Reader

Robert H. Bourke
Robert H. Bourke, Chairman,
Department of Oceanography

ABSTRACT

A high-resolution, multi-level, primitive equation ocean model is used to examine the response of an eastern boundary oceanic regime to thermal and wind forcing. The focus of this study is the anomalous Leeuwin Current System off Western and Southern Australia.

Three types of experiments are conducted. The first type forces the model from rest with the Indian Ocean climatological temperature gradient as an initial condition only, while the second type repeats the first experiment with the added contribution of the North West Shelf water temperature profile. The role of irregular coastline geometry on the generation of currents and eddies is also examined by comparing these cases with and without an irregular (realistic) coastline. The third type, with an irregular coastline, forces the model from rest with constant thermal and wind forcing. A one-time application of the North West Shelf water is added during the model run.

In all experiments, surface currents, undercurrents, meanders, and eddies are generated. The results from experiments with an irregular, rather than an idealized coastline, show preferred eddy generation locations. The results from the third type of experiment, which has the most realistic features, agrees well with available observations off Western and Southern Australia. These results support the hypothesis that both thermal and wind forcing are important

mechanisms for the generation of many of the observed features in the Leeuwin Current System.

TABLE OF CONTENTS

ACKNOWLEDGEMENT

The author wants to thank Dr. Mary Batteen for her guidance and patience during the work in performing this investigation. A special thanks goes out to Dr. Curtis Collins for taking time to function as a second reader during a week of extensive oral surgery. Additional thanks to Mike Cook for his endless assistance with UNIX, FORTRAN, and MATLAB programming, and to Pete Braccio for his invaluable assistance with numerous model runs and visualization of the results. The author also wishes to thank Alan Pearce and Angela Way for their generous hospitality at the Commonwealth Scientific and Industrial Research Organisation's (CSIRO) Marine Laboratories, North Beach, Western Australia, where the author conducted preliminary research on the Leeuwin Current in the austral winter of 1994. Images used in the thesis were received by the Western Australian Satellite Technology and Applications Consortium (WASTAC), and processed by Angela Way (CSIRO, Division of Oceanography).

I. INTRODUCTION

Unlike other eastern boundary currents which flow equatorward in response to strong equatorial winds, the Leeuwin Current flows against the winds off Western Australia. The Leeuwin Current is a thermally driven, anomalous, Indian Ocean eastern boundary current which flows poleward along the Western Australian coast, down to Cape Leeuwin, and swings abruptly eastward extending as far east as the Great Australian Bight (e.g., Cresswell and Golding, 1980). This anomalous surface flow is credited with the appearance of tropical marine species off both the western and southwestern Australian coasts (Pearce and Griffiths, 1991). The current also can exhibit a strong seasonal variation which effects the flow into the Great Australian Bight, and the location of regional eddy pairs (Cresswell and Peterson, 1993). These characteristics of the Leeuwin Current provide a unique opportunity to examine the roles of wind and ocean thermal forcing on the generation and maintenance of an eastern boundary current and its associated eddies.

The Office of Naval Research has placed the study of eastern boundary currents (EBCs) and eddy generation mechanisms as an accelerated research initiative (Bayler and Batteen, 1991). By obtaining a better physical understanding of the roles of the forcing mechanisms and dominant instability mechanisms, oceanographers can provide a basis for predicting currents and eddies in EBC regions. This understanding can be expanded to provide accurate forecasts of fish migration for the fishing industry based on current strengths, local upwelling, or the presence of meanders and eddies. Knowledge of eddies, evolution and migration, and current variations can also provide an estimate of current impact on tactical sensor performance in the regions of EBCs.

This study examines the dynamics of the Leeuwin Current as it translates from north-south to west-east along the Australian coast. With the use of a model, the impact of climatological ocean thermal forcing and wind forcing and their effects on the instability mechanisms and current characteristics are explored. This study extends prior efforts which focused only on the Western Australian region by expanding the model domain eastward to include both the Western and Southern Australian coastal regions, and focusing on current dynamics and eddy generation in both regions.

The goal of this thesis is to carry out process-oriented modeling studies to examine and model the generation and stability of currents and eddies in the Leeuwin Current system in the region shown in Figure 1.1, with special concentration on the area around Cape Leeuwin and eastward to Esperance (entrance to the Great Australian Bight). This paper will focus on several elements. The first element is to determine current characteristics, such as the seasonal extent of the flow of the Leeuwin Current into the Great Australian Bight, and whether an undercurrent along Southern Australia exists similar to the undercurrent along Western Australia. The second element is to utilize energy analysis techniques to determine the dominant instability mechanisms for the eddies in the region. The last element will focus on the role of irregular coastline geometry in the generation of currents and eddies in the Leeuwin current as it translates from Western to Southern Australia. The additional contribution of the ocean thermal forcing from the North West Shelf (NWS) waters will also be addressed.

The organization of this paper is as follows: Chapter II presents a detailed descriptive and modeling background of the Leeuwin Current along with objectives of the study; Chapter III describes the numerical model, experimental design, analysis tools and techniques used; Chapter IV discusses model results and their significance; and Chapter V contains a

summary with conclusions and recommendations.

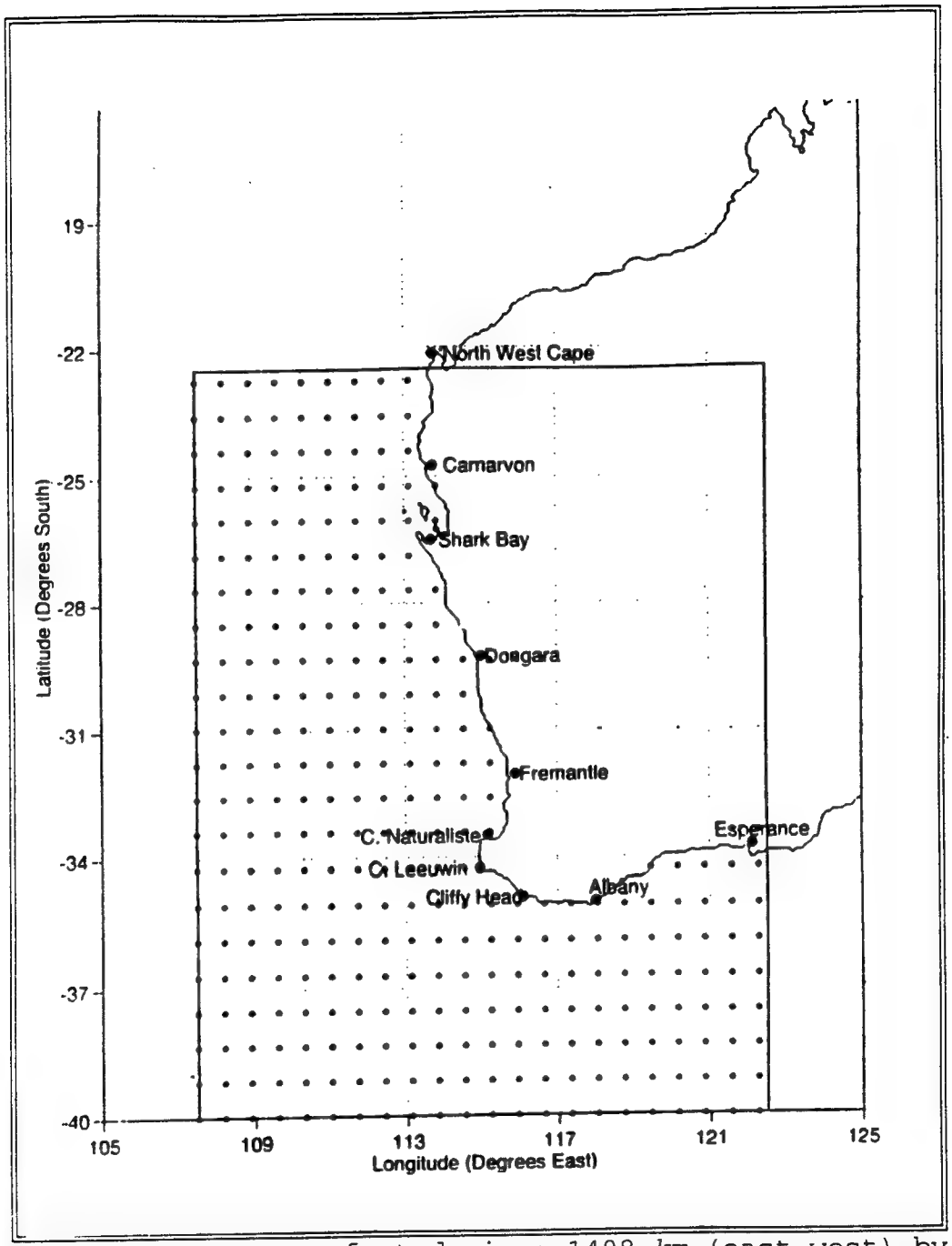

Figure 1.1: Area of study is a 1408 *km* (east-west) by 1792 *km* (north-south) box encompassing the west and south coast of Australia.

II. BACKGROUND

A. DESCRIPTION OF THE LEEUWIN CURRENT

The Leeuwin Current can be described as a body of warm low-salinity tropical water that forms a strong narrow current along the continental shelf edge, from about 22°S off the Western Australian coast, around Cape Leeuwin and into the Great Australian Bight (Cresswell and Golding, 1980). Satellite images (e.g., Figure 2.1) show a large wedge of warm water in the Northeast Indian Ocean being funneled into a narrow current near North West Cape, then moving south along the shelf and slope, until reaching Cape Leeuwin where it abruptly swings eastward and extends across the Great Australian Bight (e.g., Pearce and Cresswell, 1985). Both the satellite image and hydrographic data (not shown) show the Leeuwin Current undergoing a significant dynamical change as the flow approaches Cape Leeuwin. In particular, the warm water moves onto the shelf and the outer temperature front becomes stronger and more sharply defined. Maximum velocities at the southwest corner(~1.8 m/s) are found just beyond the shelf break (Griffiths and Pearce, 1985).

The Leeuwin Current is unlike any other EBC. The major subtropical EBCs such as the California, Canary, Peru, and Benguela currents are characterized by climatologically weak (<10 cm/s), broad (~1000 km wide) cold surface flow towards the equator in the direction of the prevailing winds, a poleward undercurrent, a shallow (<30 m depth) thermocline, and high biological production due to vast regional upwelling (Parrish et al., 1983). Observational studies along the coast of Western Australia have shown that the Leeuwin Current is characterized by a strong (>150 cm/s at times), narrow (<100 km wide), poleward surface current that flows opposite the prevailing wind direction (e.g., Cresswell and Golding, 1980; Godfrey et al., 1986), anomalous warm water at the surface, a deep (>50 m depth) thermocline (Thompson, 1984), and lower

biological production due to vast regions of downwelling (Batteen et al., 1992).

The Leeuwin Current appears to have its source in the Northeast Indian Ocean. The source is predominantly geostrophic inflow from the west (McCreary et al., 1986; Thompson, 1987). As a result of this strong inflow of subtropical water towards the coast, the Leeuwin Current intensifies poleward (Batteen et al., 1992).

Two major water masses occur for all or part of the year along the shelf region off Western Australia (see Figure 2.2): a warm (tropical) low salinity water mass from the North West Shelf (e.g., Weaver and Middleton, 1989) possibly having its origins in the Pacific Ocean (Godfrey and Ridgway, 1985), and a cooler (subtropical), higher saline water mass called the 'Western Australian Current' which is influenced by the presence of a large semi-permanent trough extending in a northeastward direction (Andrews, 1977).

The seas just south of Cape Leeuwin and eastward to the Great Australian Bight are influenced by several water types: 1) subtropical water from west of Western Australia carried in a branch of the Western Australian Current in summer (Andrews, 1977), 2) tropical water from north of Western Australia brought by the Leeuwin Current in autumn and winter (Rochford, 1969; Cresswell and Golding, 1980), 3) local Sub-Antarctic water characterized by its coldness and low salinity, and 4) a warm high salinity water mass located in the central and eastern Great Australian Bight most of the year (Rochford, 1986). Because of these various water masses along the southern coast of Australia, there is some evidence that the Leeuwin Current loses its identity within the Great Australian Bight by late winter by mixing with Bight waters (Pearce and Cresswell, 1985).

The generally accepted theory behind the origins of the Leeuwin Current is that it is generated by an established meridional pressure gradient resulting from the large amount

of heating in the equatorial region and excessive cooling near the poleward region. A net heat loss to the atmosphere occurs near the Western Australian coast poleward of 20°S. It extends down to a depth of 150 m and results in relatively low steric heights at the southern end of Western Australia (Tomczak and Godfrey, 1994). The meridional pressure gradient off Western Australia is comparable to the pressure gradient driving the strong western boundary currents in most of the other ocean basins (Figure 2.3). The resulting onshore geostrophic flow is strong enough to override the offshore Ekman flow (Tomczak and Godfrey, 1994). The resulting southward flow at the coast due to this strong meridional pressure gradient overwhelms the opposing equatorward wind stress (e.g., Batteen and Rutherford, 1990). The southward flow feeds the warm water polewards to maintain the surface heat loss. The process is self perpetuating, as southward flow is accompanied by surface cooling, and surface cooling produces southward flow (Tomczak and Godfrey, 1994).

The relative strength of the Leeuwin Current's pressure gradient forcing versus an opposing wind force, as shown in Figure 2.4, varies throughout the year as seasonal changes affect the Southern Hemisphere. The individual seasonal cycle of the pressure gradient/ thermal forcing mechanism reinforces seasonal trends of the wind forcing, creating a strong seasonal signal in the flow of the Leeuwin Current (Godfrey and Ridgway, 1985). The Leeuwin Current flows mainly but not exclusively in the austral autumn and austral winter (Church et al., 1989). The surface poleward current along the Western Australian coast is weakest and shallowest between November and January, followed by the period of strongest and deepest flow between March and May. During March through July the flow remains poleward but it is weaker, broader, and shallower and no longer confined to the upper slope (Smith et al., 1991). The warm water is generally seaward of the shelf break and in a band that is made very broad by seaward offshoots and

eddies. Cool water generally lies between the current and the coast (Griffiths and Pearce, 1985). Besides this anomalous poleward flow along the west coast, there is an equally significant anomalous equatorward undercurrent centered near 350 m depth that can attain speeds comparable to the surface flow, exceeding on the average 10 cm/s (Smith et al., 1991).

Near Cape Leeuwin, as shown in Figure 2.5, the Leeuwin Current moves from the shelf edge onto the shelf and slope region off Southern Australia (Griffiths and Pearce, 1985). The Leeuwin Current carries the warmest water mass of relatively low salinity principally along the shelf break as far east as 130°E. This water mass first enters the western end of the Bight region in May, disappears from the eastern end after July and from the western end by September (Rochford, 1986).

In the summer of 1986-1987, the Leeuwin Current carried subtropical water to the southern coast until March, when the current appeared to be arrested at about 34°S and an upwelling plume extended westward from the southern coast along the shelf and northward to Cape Naturaliste. In the one-month interval to April, the source of the current had switched from being subtropical to being tropical (Cresswell and Peterson, 1993). Anticyclonic and cyclonic eddies were found to exist along the Southern Australian Coast from offshoots of the Leeuwin Current (Legeckis and Cresswell, 1981). During the Franklin Cruise's (1987) crossing of the Leeuwin Current off Cliffy Head (coast of Southern Australia), a westward undercurrent of 0.2 m/s between 400 m and 700 m was discovered (Cresswell and Peterson, 1993), which may be comparable to the equatorward undercurrent along the western coast of Australia.

B. PREVIOUS MODELING STUDIES

Although these observations provide insight for the basic nature of the Leeuwin Current, modeling studies are also required to obtain a better understanding of the current

characteristics and dynamical forcing mechanisms around Cape Leeuwin and eastward to the Great Australian Bight. Recent modeling efforts have focused on process-oriented studies to better describe the contributing forcing mechanisms and their relative importance (Bayler and Batteen, 1991). Through the development of both linear and nonlinear analytical models, a better understanding of the characteristics and dynamics of the Leeuwin Current has been obtained.

1. Linear Models

McCreary et al. (1986) used linear models which produced currents, but failed to produce eddies. He concluded that the Leeuwin Current is significantly forced by a steady sea surface density field and seasonally varying wind stress. Additionally, he concluded that nonlinear remote forcing and other nonlinear enhancements could play a significant role in Leeuwin Current dynamics (McCreary et al., 1986). In their model, eddies were not produced presumably due to the lack of advection necessary for both barotropic (horizontal shear) instabilities and enhancement of the Leeuwin Current downstream (Weaver and Middleton, 1989; Batteen et al., 1992).

Thompson (1987) presented a linear analytical model which accounted for a significant portion of the observed phenomena. Thompson's theory provided a balance between the alongshore density gradient and the return flux in a frictional (i.e., Ekman) bottom layer over the shelf, producing a near bottom poleward alongshore current. This onshore flux created a cross-shelf pressure gradient to push the flux back out via the bottom Ekman layer, which in turn, created a poleward geostrophic current at the surface in addition to the equatorward flow generated by the bottom friction layer (Thompson, 1987). Thompson explained the flow into the wind, the equatorward undercurrent, and the existence of sharp fronts, but his linear model was confined to the shelf region and was well inshore of where eddies have been observed off

Western Australia (e.g., see Grunlingh, 1983).

The linear modeling studies of Weaver and Middleton (1989) concluded that a shelf is important to the Leeuwin Current dynamics. In the absence of vertical mixing, the presence of a sloping shelf is necessary for the existence of the trapped eastern boundary current. Without the sloping shelf, the current radiates offshore via baroclinic Rossby wave propagation (Weaver and Middleton, 1989) without producing eddies.

Weaver and Middleton (1990) also used a linear, steady-state, analytic model for the Leeuwin Current forced by a mean alongshore density gradient in the Indian Ocean and the seasonal winds. It was shown that during the season when the winds are strongest (September-February), the forcing due to the alongshore density gradient in the Indian Ocean off the coast of Western Australia is sufficient to overcome the opposing wind effect, with the net result that a strong southward flow exists near the shelf break in the top 200 m (Weaver and Middleton, 1990).

2. Nonlinear Models

Semtner and Chervin (1988) derived a nonlinear model to study global circulation. However, their global model had horizontal resolution too coarse (i.e., half a degree grid spacing) to adequately resolve the narrow Leeuwin Current and its associated eddy fields (Batteen et al., 1992).

Weaver and Middleton (1989) developed a nonlinear numerical model that allowed for the advection of temperature and salinity within a closed basin. An initial north-south density gradient based on annual mean data from Levitus (1982) and Rochford (1962,1969) was imposed in the top 500 m of the ocean domain. In the absence of external forcing, the ocean was allowed to geostrophically adjust over time. The model included a sloping shelf, vertical mixing and bottom friction, each of which has been shown capable of generating an

alongshore current independently (as shown in previous linear model studies). The North West Shelf waters were simulated as a "dam-breaking", and was initiated on the onset of the model run. The model ran for 80 days, produced a current but no eddies (probably due to the use of Laplacian rather than biharmonic lateral diffusion). The current was an initially strong eastern boundary current, which intensified and surged in velocity as a nonlinear feedback mechanism took effect (model day 55), then eventually dissipated through westward migration and friction, eliminating poleward surface flow. Weaver and Middleton (1989) noted that the presence of a strong offshore temperature gradient at the onset of the model run generated thermal winds that significantly enhanced the poleward flow via nonlinear feedback. They also ruled out the NWS waters as a primary driving mechanism for the Leeuwin Current and concluded that the NWS waters only provided a significant enhancement to the flow (Weaver and Middleton, 1990; Batteen and Bayler, 1991).

The nonlinear model studies of Batteen and Rutherford (1990) advanced the Leeuwin Current modeling efforts by simulating the generation of realistic mesoscale (eddy) features along the Western Australian coast, in addition to creating a poleward surface current and an equatorward undercurrent. For the current driven only by the Indian Ocean temperature gradient, barotropic instability developed as the dominant instability mechanism in the poleward end of the model domain. The addition of North West Shelf waters created a far more energetic and unstable current adding to the baroclinicity of the flow. The scales of their model-generated current and mesoscale features (missing from previous modeling studies) were comparable with available observations (Batteen and Rutherford, 1990). Batteen et al. (1992) added idealized wind forcing to the Western Australian model domain and concluded that wind forcing effects were only discernible at the equatorward end of their model domain.

Bayler and Batteen (1991) added continuous ocean thermal and wind forcing to the seasonal mean climatological data to generate the Leeuwin Current. The seasonal variation of the ocean thermal forcing provided little enhancement of the current structure, although the seasonal variation did enhance eddy generation during the period of strong thermal gradients. Wind forcing significantly inhibited the poleward coastal flow, but did not eliminate it. Seasonal wind forcing generated a strong seasonal signal in the poleward coastal flow, but never dominated over the pressure gradient forcing.

C. OBJECTIVES OF THE STUDY

The above paragraphs summarize the major modeling studies that have contributed to the understanding of the Leeuwin Current off the coast of Western Australia. A more thorough review of the theoretical models and relevant observations is given in Batteen and Rutherford (1990).

To date, no modeling studies have effectively simulated the Leeuwin Current dynamics and eddy formation mechanisms off the Southern Australian coast. Little is known about the circulation in or off the shelf east of Cape Leeuwin (Pearce and Cresswell, 1985).

Because previous studies have been limited to the western coast of Australia or along the coast to the shelf regions only (Batteen et al., 1992; Weaver and Middleton, 1990), the present modeling study will use a model domain which encompasses both the Western and Southern Australia regions to study the Leeuwin Current dynamics as the current abruptly shifts from poleward to eastward. A full primitive equation (PE) model will be used to carry out process-oriented studies to investigate the effects of wind and thermal forcing on the ocean circulation in the region around Cape Leeuwin and eastward to Esperance (entrance to the Great Australian Bight). To achieve this objective, the studies of Batteen et al. (1992) will be extended by examining the effects of forced

density forcing from the Levitus climatological Indian Ocean thermal structure, the influx of warm, low salinity water from the North West Shelf, and the climatological wind stress, to better describe the contributing forcing mechanisms and the relative importance in generating currents and eddies. The dynamical reasons for the generation and growth of eddies in the ocean circulation will also be investigated using the same energy techniques as Batteen et al. (1992). Finally, a comparison between model results and observational data will be made to access consistency of the model with characteristic features of the eastward flowing Leeuwin Current. The role of irregular coastline geometry on the generation of currents and eddies in the Leeuwin Current will also be explored by comparing cases ran with and without an irregular (realistic) coastline.

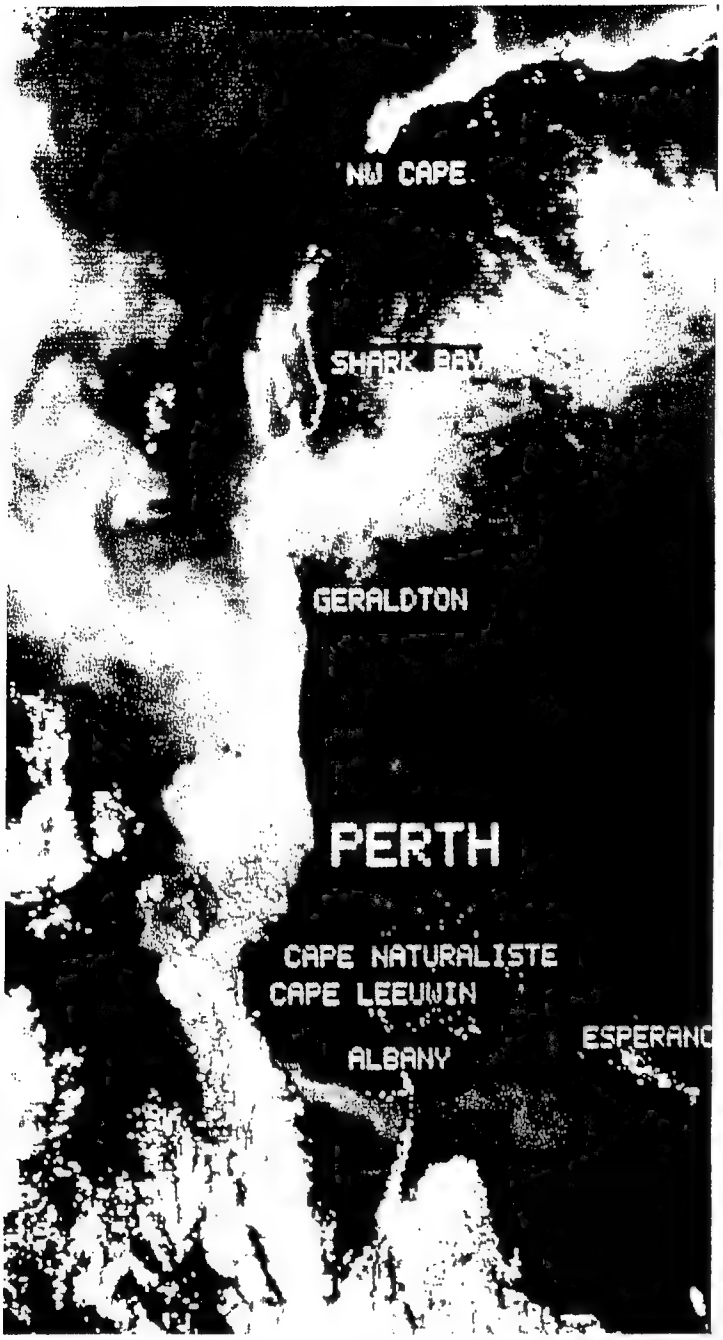

Figure 2.1: Surface temperature image from the NOAA7 satellite. Warmer water appears as red with the coolest water a dark blue. Note the strong southward jet of the Leeuwin Current (from Pearce and Cresswell, 1985)

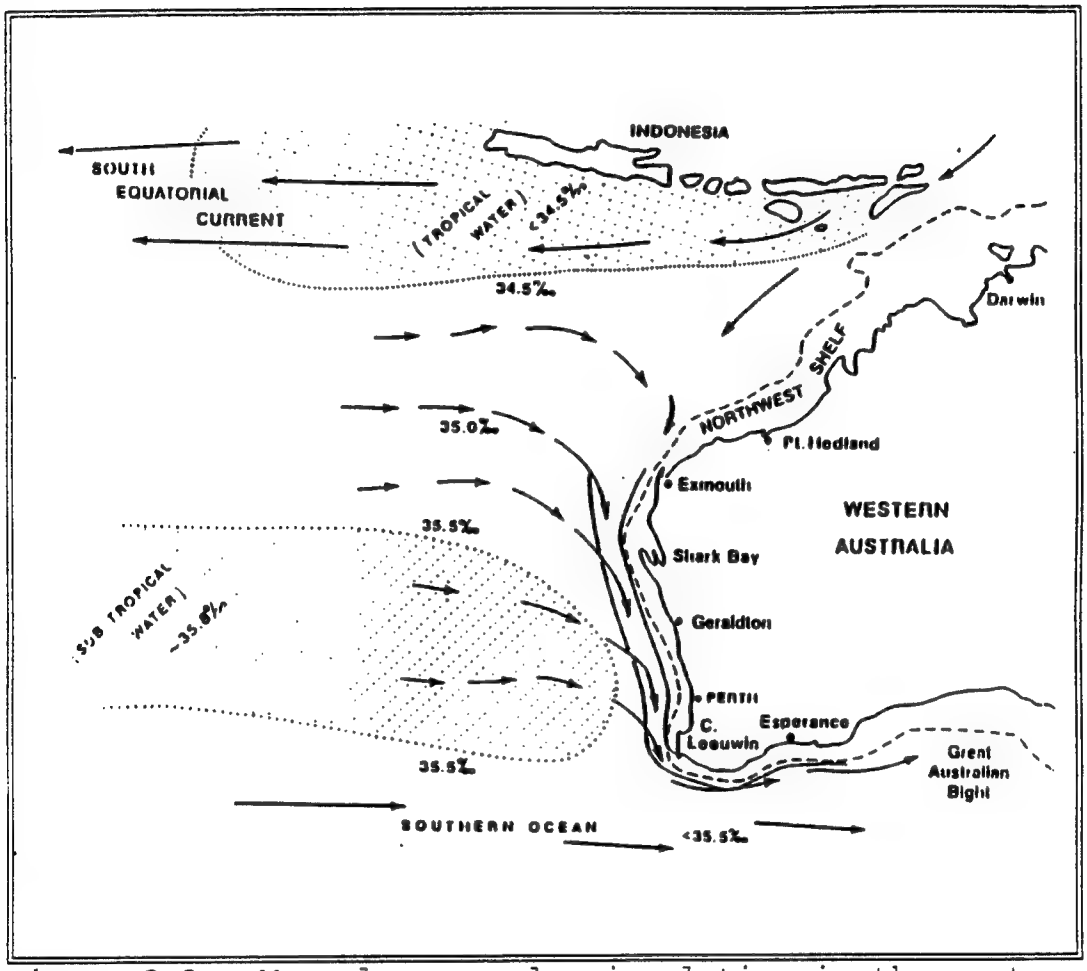

Figure 2.2: Mean large-scale circulation in the eastern Indian Ocean. The Leeuwin Current is the southward flow of warm low-salinity water down the Western Australian shelf break (from Pearce and Cresswell, 1985)

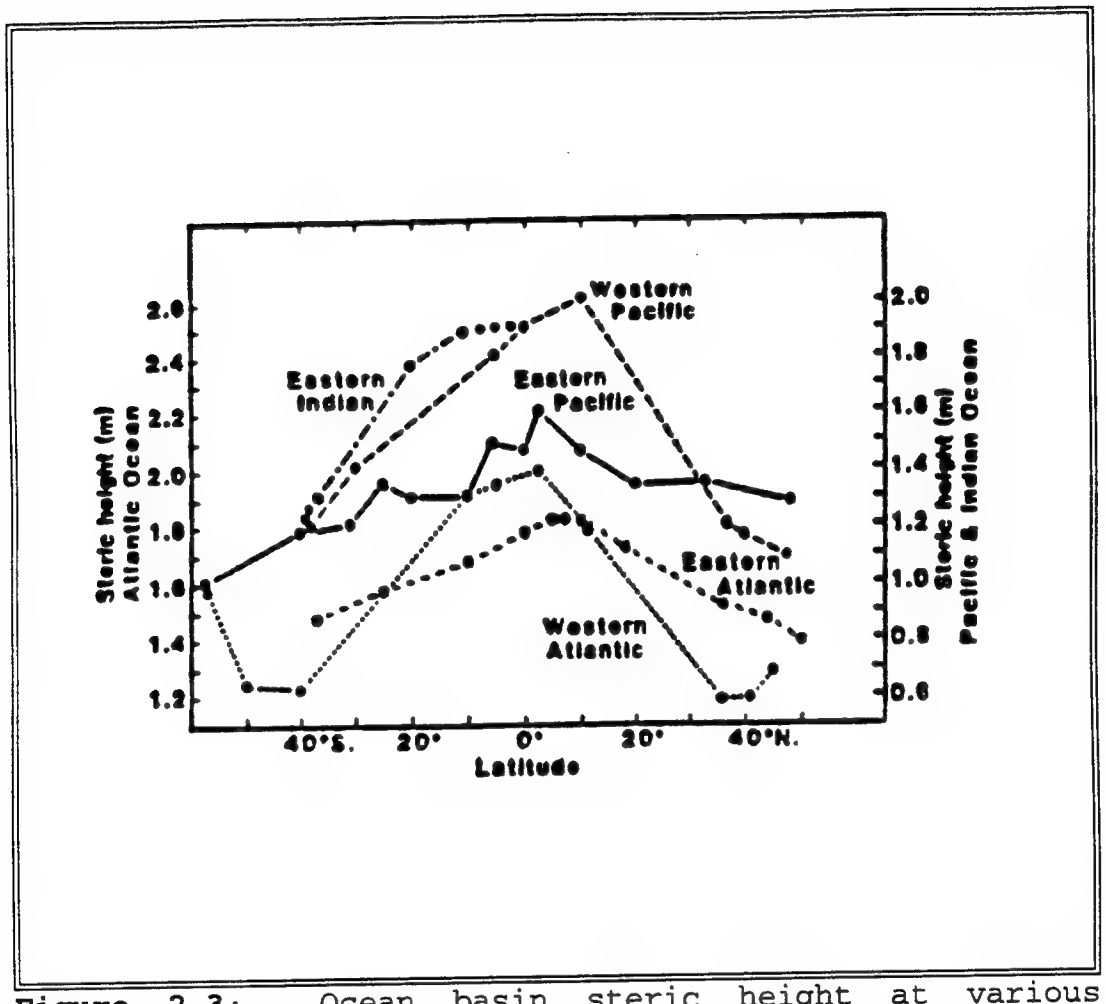

Figure 2.3: Ocean basin steric height at various latitudes reflecting sea surface slopes (from Godfrey and Ridgway 1985)

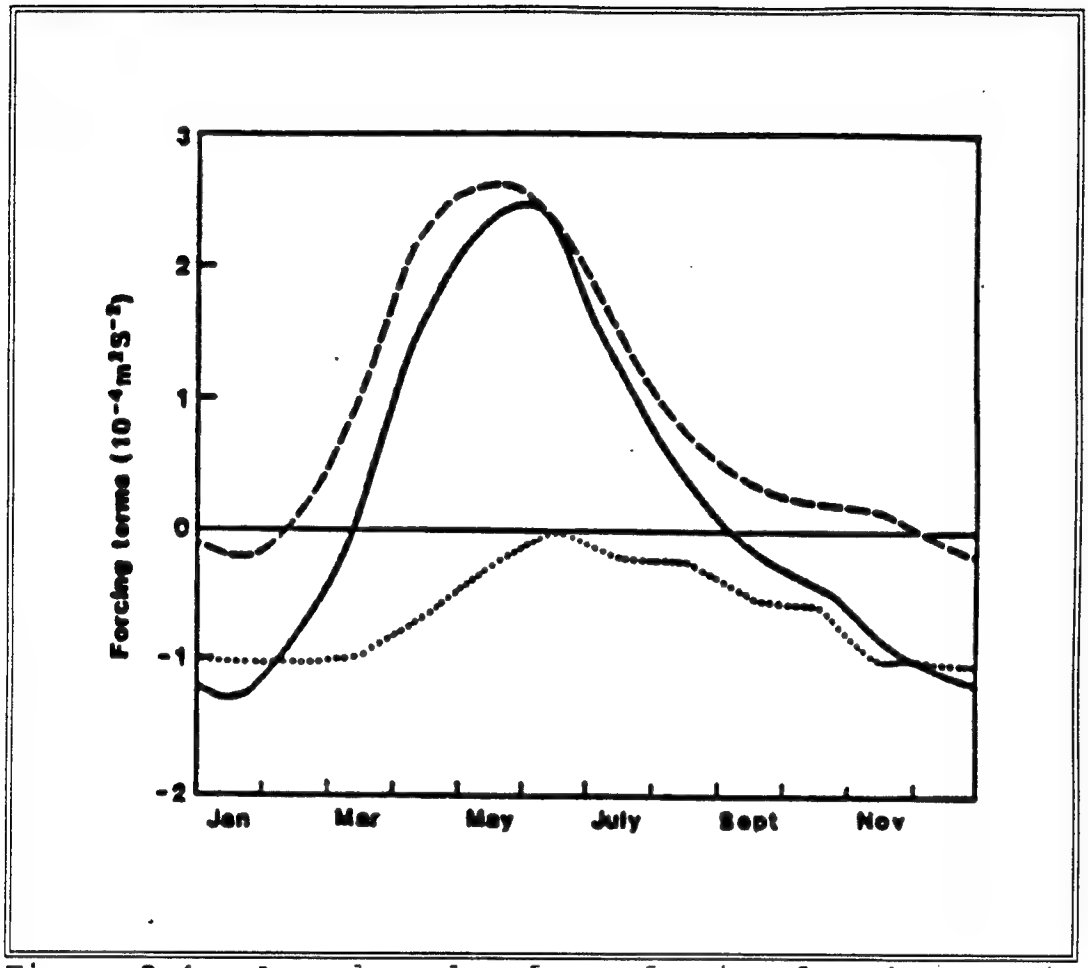

Figure 2.4: Annual cycle of net forcing for the Leeuwin Current: Dashed line, observed pressure gradient forcing; dotted line, alongshore wind stress (positive is southward); solid line, net forcing (from Godfrey and Ridgway 1985).

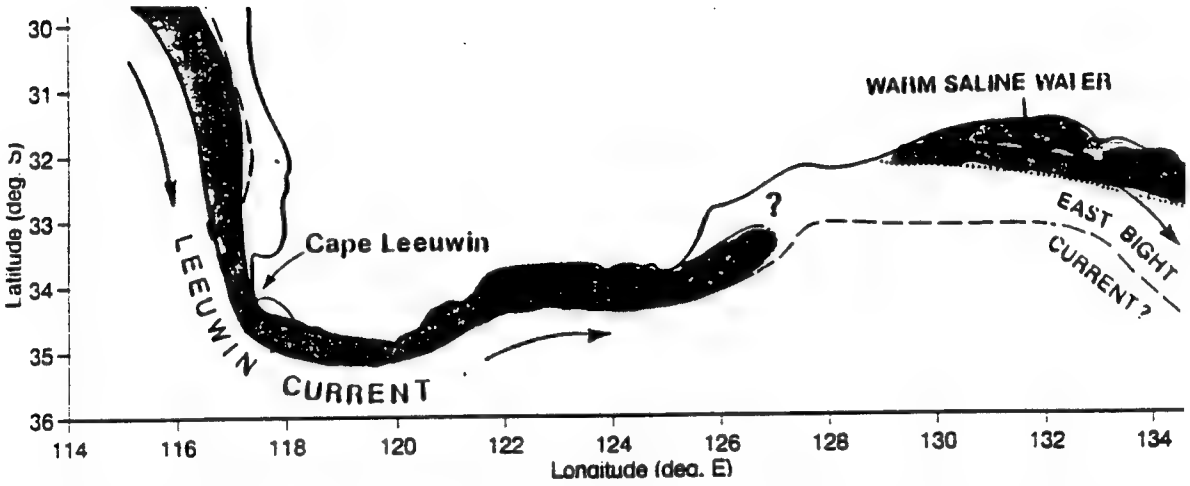

Figure 2.5: Behavior of the Leeuwin Current as it approaches and rounds Cape Leeuwin and flows towards the Great Australian Bight. The long dash line represents the continental shelf (from Pearce and Cresswell, 1985)

III. MODEL DESCRIPTION AND EXPERIMENTAL DESIGN

A. MODEL DESCRIPTION

1. Basic Model

The model used in this research is a slightly modified version of that used by Batteen et al. (1989, 1992) which was adapted from Haney's (1974, 1985) closed basin model. This limited area EBC model is multi-level, uses non-adiabatic primitive equations on a β plane, and has both barotropic and baroclinic components. The following approximations are made: hydrostatic, Boussinesq, and rigid lid. (For a more detailed summary of the model and the governing equations, refer to Batteen et al., 1989).

2. Friction

The type of diffusion used can be important for the generation of mesoscale eddies. Biharmonic rather than Laplacian lateral heat and momentum diffusion is used in this study. The use of biharmonic lateral diffusion allows mesoscale eddy generation via barotropic (horizontal-shear) or baroclinic (vertical-shear) instability mechanisms, or both, as Holland (1978) and Holland and Batteen (1986) have shown. The biharmonic coefficients are the same (i.e., 2.0×10^{17} cm^4s^{-1}) as used in Batteen et al. (1989). Weak (0.5 cm^2s^{-1}) vertical eddy viscosities and conductivity are used. A simplified quadratic drag law is used to parameterize bottom stress (Weatherly, 1972).

3. Boundary Conditions

The domain of the model along the coastal boundaries uses a closed boundary condition. A no-slip condition on the alongshore velocity is used. The kinematic boundary condition of no flow through the coastal boundary is imposed on the cross-shore velocity component. A modified version of the radiation boundary conditions of Camerlengo and O'Brien (1980) is used for the open ocean domain boundaries to the north,

south, east, and west. Some spatial smoothing is applied in the vicinity of the open boundaries.

At the surface, the rigid lid approximation filters out external gravity waves and allows a longer time step. On the ocean bottom, no vertical heat flux or vertical velocity is allowed.

4. Domain and Resolution

The domain of the model is a corner shaped region encompassing the west and south coast of Australia from 22.5°S to 40°S, 107.5°E to 122.5°E as shown in Figure 1.1. This covers an area of 1408 km in the cross-shore (east-west) and 1792 km in the alongshore (north-south) directions. The horizontal resolution is 11 km in the cross-shore direction and 14 km in the alongshore direction. Mesoscale features within the Leeuwin Current system should be resolvable with this resolution because typical eddy wavelengths are around 150 km (Batteen et al., 1992). Bottom topography has been omitted to focus on the roles played by thermal and wind forcing, as well as the effects of an ideal versus an irregular coastline (see Figures 3.1 and 3.2).

5. Finite Difference Scheme

A staggered grid model, using the Arakawa and Lamb (1977) B-scheme is used in the horizontal. Variables are defined as follows: u, v, and w are velocity components eastward, northward and vertical, respectively, t denotes time, T is temperature, ρ is density, p is pressure, and ψ is the streamfunction. The center of each grid point defines u and v while T, ρ, ψ, w, and p are defined at the corners. The B-scheme is used because it gives a superior representation of the geostrophic adjustment process (Batteen and Han, 1981).

The model uses ten layers in the vertical, with constant z-levels, at depths of 13, 46, 98, 182, 316, 529, 870, 1416, 2283, and 3656 m. This spacing scheme concentrates more layers above the thermocline in the dynamically active portion

of the ocean, consistent with Haney (1974). Variables are staggered in the vertical with u, v, ρ, and T defined at each level, while w and p are defined between the levels which lie between the ocean surface (w=0) and at the bottom (z=-H, where H is the depth). A Matsuno time step followed by ten leapfrog time steps is used and continuously repeated during the model run.

6. Method of Solution

The method of solution is straightforward with the rigid lid and flat bottom assumptions because the vertically integrated horizontal velocity is subsequently non-divergent. The vertical mean flow can be described by a streamfunction ψ which can be predicted from the vorticity equation, while the vertical shear currents can be predicted after the vertical mean flow is subtracted from the original equations. The other variables T, ρ, w, and p can be explicitly obtained from the thermodynamic energy equation, equation of state, continuity equation, and hydrostatic relation, respectively.

7. Initial Conditions

The initial temperature profile was derived from Levitus (1982) climatological data. Levitus provided quarterly temperature climatological data to describe the upper 250 m of the model ocean, and annual average temperature for filling the model levels below this depth. This data was linearly interpolated in time to provide daily temperature values. The daily temperature values for the north and south grid boundaries were linearly interpolated vertically to model level values from the data levels. To fill the interior grid values, the north-south thermal gradient was approximated with a meridional linear interpolation for each model level. The resulting thermal gradient closely approximates the general eastern Indian Ocean environment (Bayler and Batteen, 1991). Figure 3.3 shows the approximated temperature profile, which is used as an initial condition in the model simulations.

The above initial condition should allow the model to evolve the eastern boundary thermal characteristics. Note that data immediately adjacent to the coast is not incorporated into the initialization, because these values reflect advection by the Leeuwin Current and they distort the representation of open ocean geostrophic inflow forcing. In addition, starting the model near the beginning of the year (within days 1-73) when the Leeuwin Current is the weakest is done to minimize the influence of the Leeuwin Current on the initial temperature profile, as well as to allow the model to geostrophically adjust prior to the austral summer transition to austral autumn when the Leeuwin Current begins its primary surge (Church et al., 1989; Weaver and Middleton, 1989).

8. Wind Forcing

The winds used to force the model are from the European Centre for Medium-Range Weather Forecasts (ECMWF) (Trenberth et al., 1990) and have been provided by the National Center for Atmospheric Research. Winds were extracted from world wide mean monthly wind velocities that were provided at 2.5 degree spacing for the years 1980 to 1989 along with 120 month climatology for the area of study. This data was linearly interpolated in space and then in time to provide daily forcing at the desired grid points.

The wind forcing used in the model shows significant meridional and zonal variability in the wind stress, especially in the vicinity of Cape Leeuwin. Figure 3.4 shows a characteristic profile for the area of study.

9. Ocean Thermal Forcing

These studies focus on the existing thermohaline structure of the eastern Indian Ocean and its ability to create a Leeuwin Current type of flow. The oceanic thermal forcing used in this model study is similar to that used by Bayler and Batteen (1991), but differs by the location of the applied thermal forcing and the extent of smoothing into the

unforced segment. Also techniques which incorporate thermal forcing once a day (when the wind forcing mechanism is deactivated), as well as a continuous forcing effort which uses the daily averaged temperature gradient at every time step (when the wind forcing mechanism is activated), are used.

The thermal forcing is applied by daily specifying the north and south grid point temperature values along the western boundary, and the associated thermal gradient. These values are derived from Levitus (1982) by linearly interpolating in time from one season to the next, with the seasonal magnitude achieved at the midpoint of each season. The boundary forcing values for the upper four model layers increment each model day while the lower six layers are held constant (since only annual data is available from Levitus, 1982 for these layers). Daily varying only the upper four model layers (fourth layer being at 182 m) is consistent with the shallow character of the Leeuwin Current which is strongest at the surface, and near-zero at ~ 150 m depth (Bayler and Batteen 1991; Thompson 1987). This thermal forcing technique simulates the persistent equator-to-pole thermal gradient found in the open eastern Indian Ocean. The use of daily forcing allows for geostrophic adjustment prior to the next forcing increment. Figure 3.5a-b shows the characteristic daily forcing for model level 1 (13 m) and level 4 (182 m).

The North West Shelf (NWS) waters provide a significant influx of warm low salinity tropical water to the Leeuwin Current and is used as an additional thermal forcing source. The climatology of Levitus (1982) provides a representative temperature profile for the NWS waters. This study employs the same choice as Batteen and Rutherford (1990) for the NWS temperature profile (Table 3.1), which incorporates an equivalent temperature to compensate for variations in density due to significant NWS deviations from a mean salinity of 35.6 psu (see Bayler and Batteen, 1991 for more information). The

NWS water is modeled as a horizontal homogeneous raft of warm water simulating a "dam breaking" applied to the model domain (at the north eastern ocean boundary) only once during a model year. This model approach is consistent with the hypothesis of flow reversals as a function of monsoonal winds isolating water on the NWS, which subsequently flow poleward (Gentilli, 1972).

The specific timing of the dam break was inferred from observations of Cresswell and Peterson (1993). They observed a drastic decrease of salinity in the Leeuwin Current (measured near Rottnest Island) between the March and April time frame and have indicated this as the onset of the NWS waters influence on the Leeuwin Current. This is also consistent with available satellite observations (see Cresswell and Peterson, 1993) which show the onset of the Leeuwin Current surge in the austral autumn to occur in the Mid-March time frame. Based on the above reports, the chosen day for the simulated dam break of NWS waters into the model ocean domain is 15 March (model day 74).

After applying the NWS water dam break, the model is allowed to evolve through geostrophic adjustment. All adjustments to the existing velocity fields are made by the model in response to the inserted thermal forcing (Bayler and Batteen, 1991).

B. SPECIFIC EXPERIMENTAL DESIGN

Table 3.2 provides a summary of the experiment runs. Experiments 1 and 2 study the model response to an initialized climatological thermal forcing using an annual mean temperature gradient for the Indian Ocean. The ocean is then allowed to adjust in the absence of external forcing. Experiment 1 uses the ideal coastline (Figure 3.1), while Experiment 2 uses the irregular coastline (Figure 3.2). Experiments 3 and 4 study the additional impact of the NWS waters on the Leeuwin Current System using the Indian Ocean

climatological mean temperature for mid-March to initialize the model. The ocean is then allowed to adjust in the absence of external forcing. Experiment 3 uses the ideal coastline, while Experiment 4 uses the irregular coastline. Experiments 1-4 examine the model results for the first 150 model days to concentrate on the initial current characteristics and eddy formation mechanisms. Experiment 5 uses an irregular coastline along with continuous thermal and wind forcing to examine the effects of daily climatological thermal and wind forcing on the Leeuwin Current System. In experiment 5, model day 1 corresponds to the first day of the calendar year. The NWS waters are introduced into the model as a "dam break" at model day 74 (corresponding to the mid-March time frame). Figure 3.6 provides classification and definition of mesoscale features used to describe the model current characteristics in Chapter IV.

C. ENERGY ANALYSIS TECHNIQUES

The energy technique used is the same as that used and described in Batteen et al. (1992), and is based on that of Han (1975) and Semtner and Mintz (1977). This is done to gain a better understanding of the flow within the Leeuwin Current system and of the types of energy transfer during unstable flow. A brief summary of the method follows.

Kinetic energy is calculated for the horizontal components. After quasi-steady state is reached where the total kinetic energy is nearly constant, mean and eddy kinetic energies are calculated using the averaged sum of squared mean and eddy horizontal fields, respectively. Next, the available potential energy is calculated and used to determine when a quasi-steady state is reached and when statistics should be collected. Then, both mean and eddy available potential energy are computed. The energy transfers follow that of Semtner and Mintz (1977), and are used to argue for the type of instability mechanism (e.g., barotropic, baroclinic, or

mixed) which leads to the initial eddy generation in each experiment.

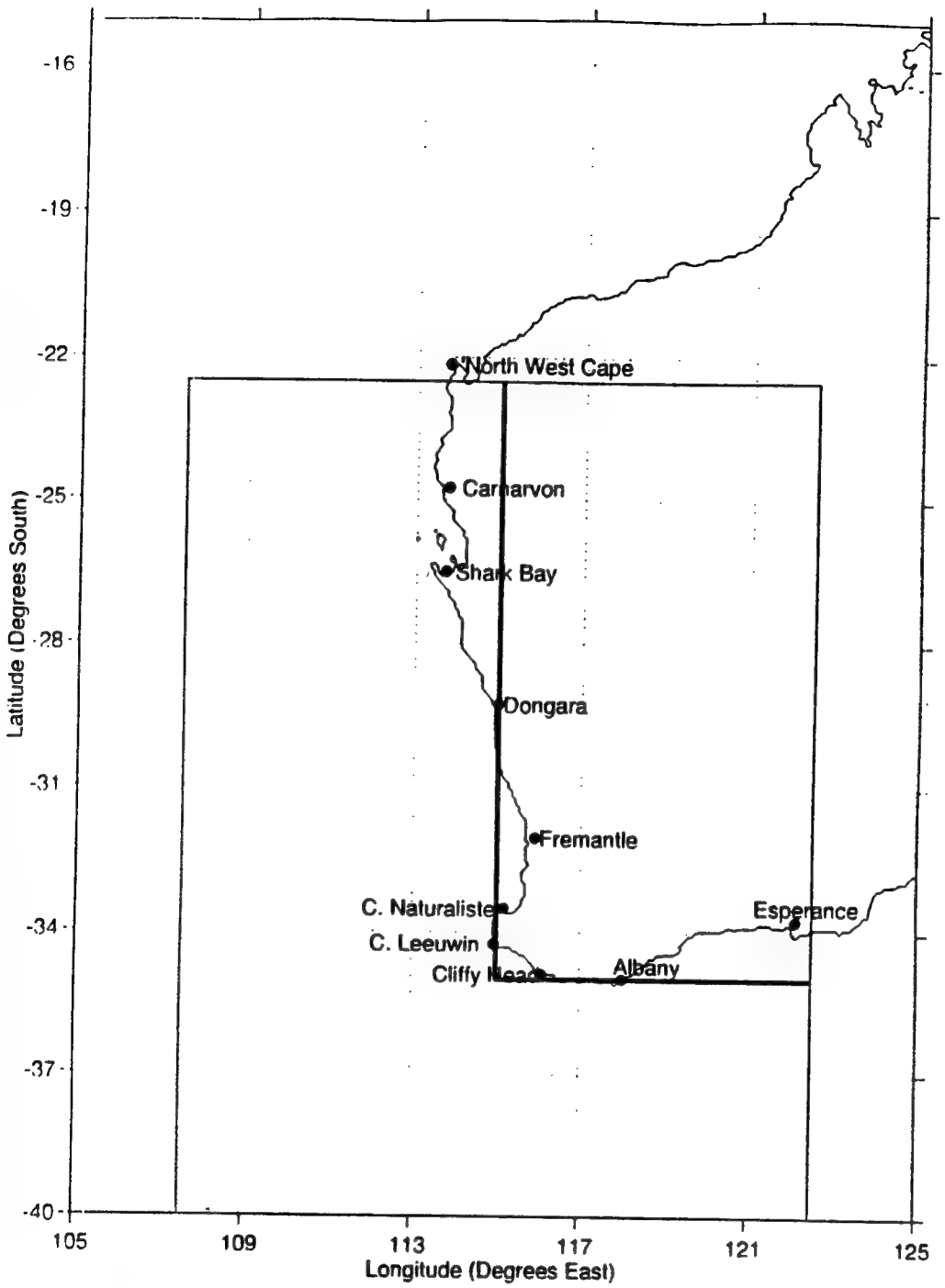

Figure 3.1: The "ideal coastline" (a first order model simulation) uses a straight coast depiction of Western and Southern Australia. The 90° corner is the model representation of Cape Leeuwin.

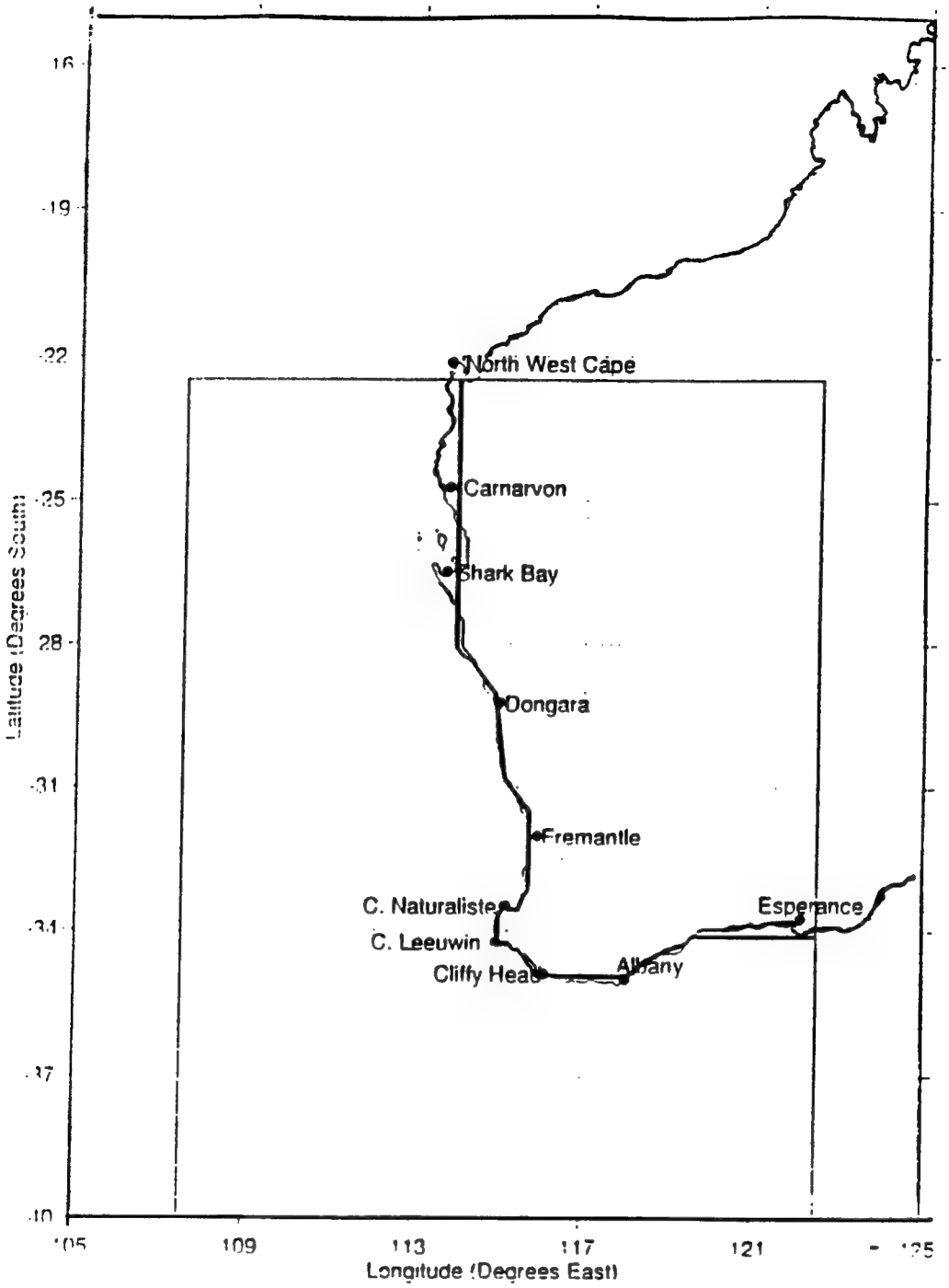

Figure 3.2: The "irregular coastline" (a second order model simulation) features the general characteristics and irregularities (e.g., coastal indentation south of Shark Bay, Dongara, Fremantle, Cliffy Head, and Albany) along the western and southern coast of Australia (including a realistic representation of Cape Leeuwin).

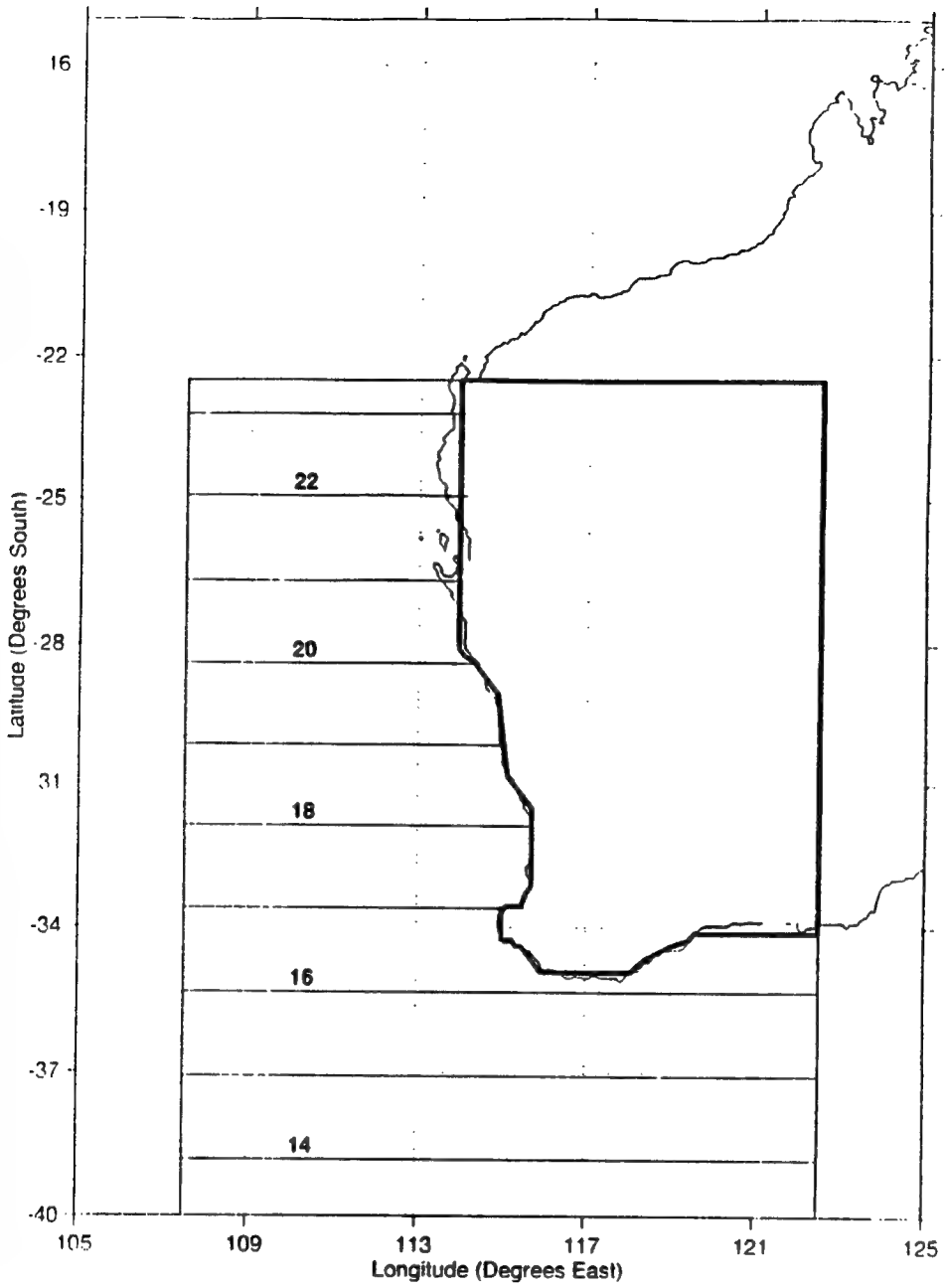

Figure 3.3a: The Indian Ocean climatological temperature gradient profile used to initialize the interior ocean of the model domain. The above temperature profile is for model level 1 (13 m). It is representative of the temperature profile used as an initial condition in Experiments 1, 2 and 5.

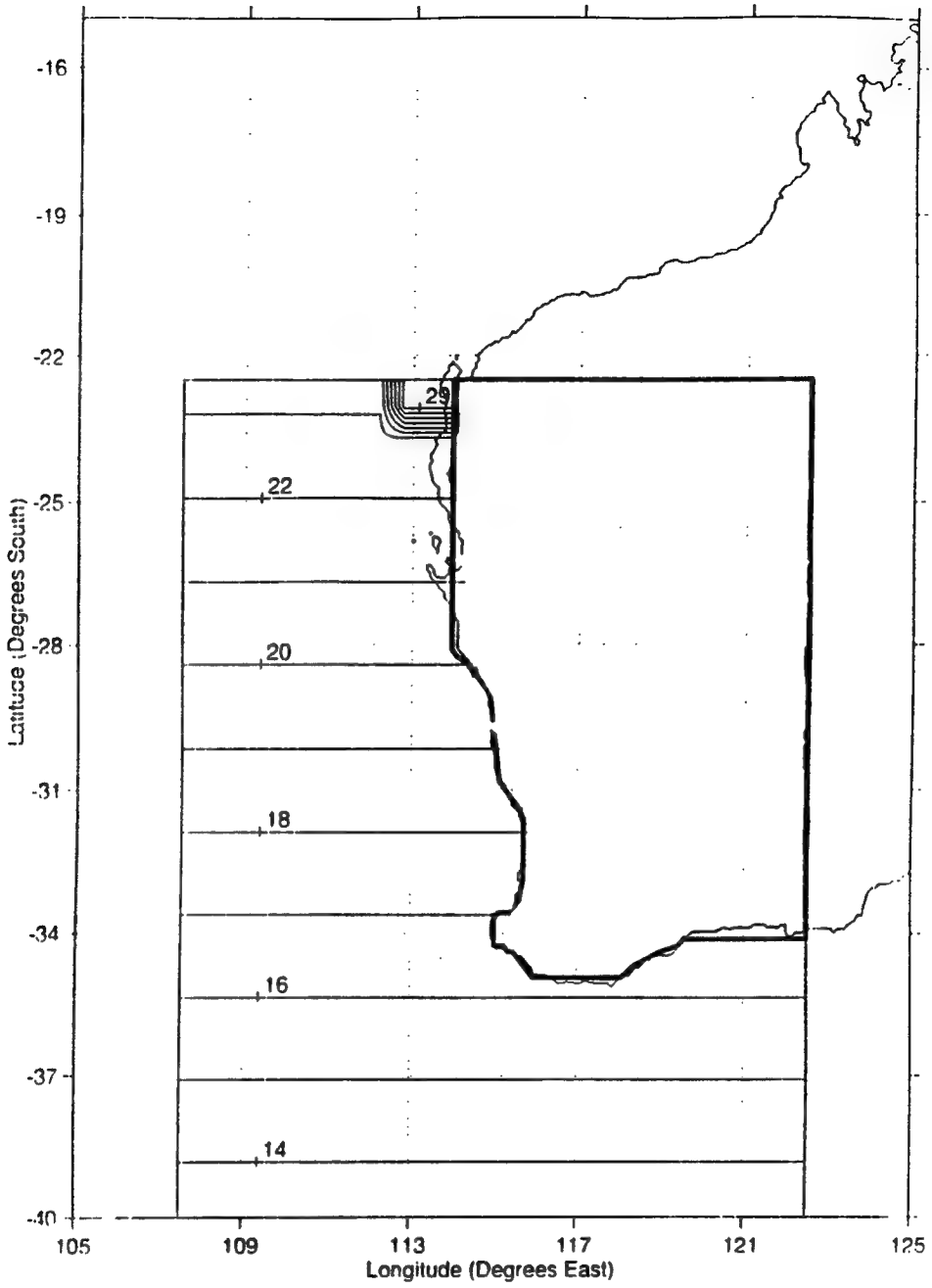

Figure 3.3b: The Indian Ocean climatological temperature gradient profile along with the North West Shelf water temperature profile used to initialize the interior ocean of the model domain for Experiments 3 and 4. The above temperature profile is for model level 1 (13 m).

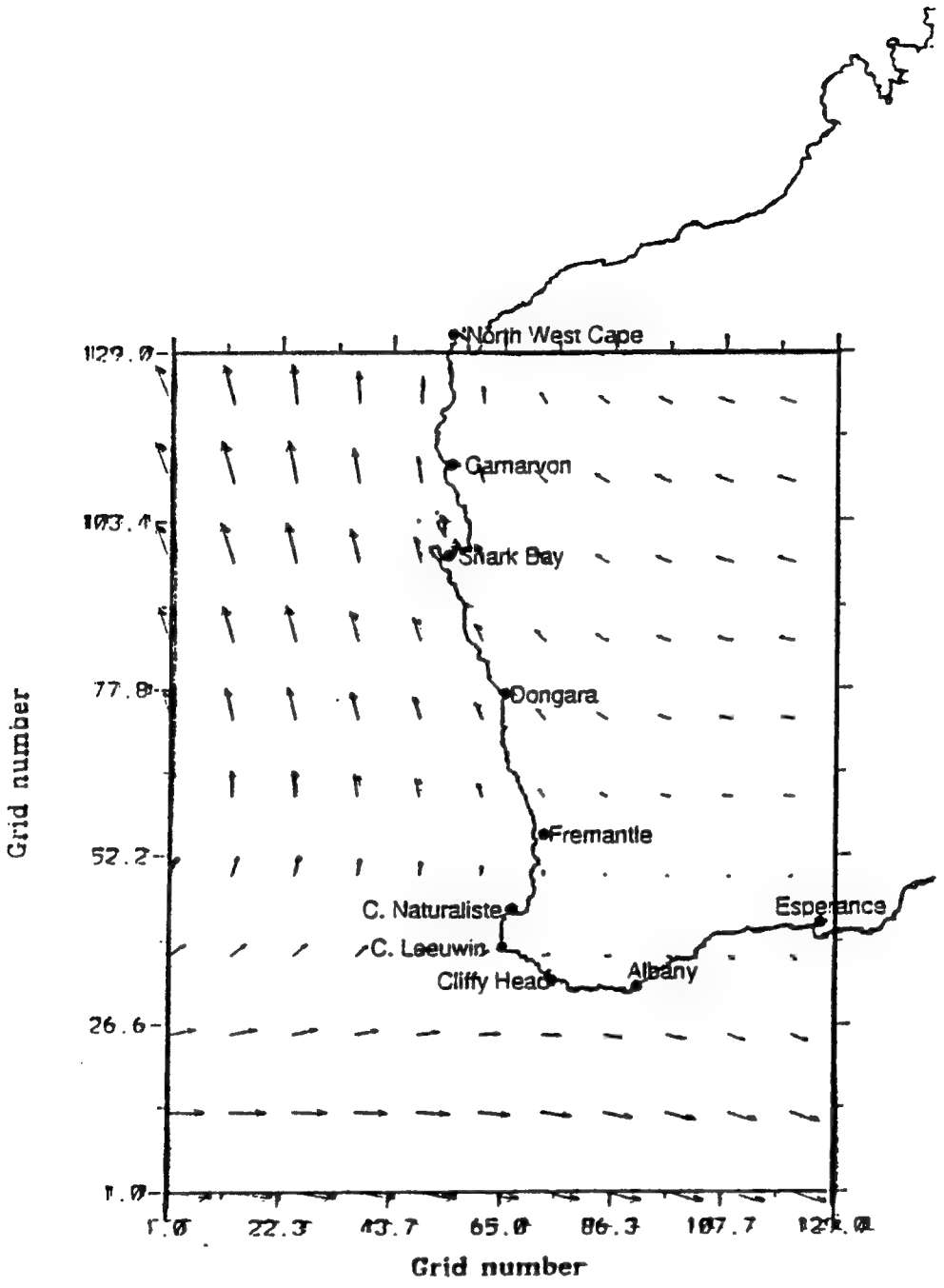

Figure 3.4 Characteristic wind profile for Western and Southern Australia obtained from the climatological (1980 - 1989) ECMWF winds in m s^{-1}: the profile displayed is an annual average for the ten year time period. The latitudinal grid point 1 (129) corresponds to 40° S (22.5° S); so that the latitudinal grid point of 78 corresponds to 29° S. Maximum wind vector is 20 m s^{-1}.

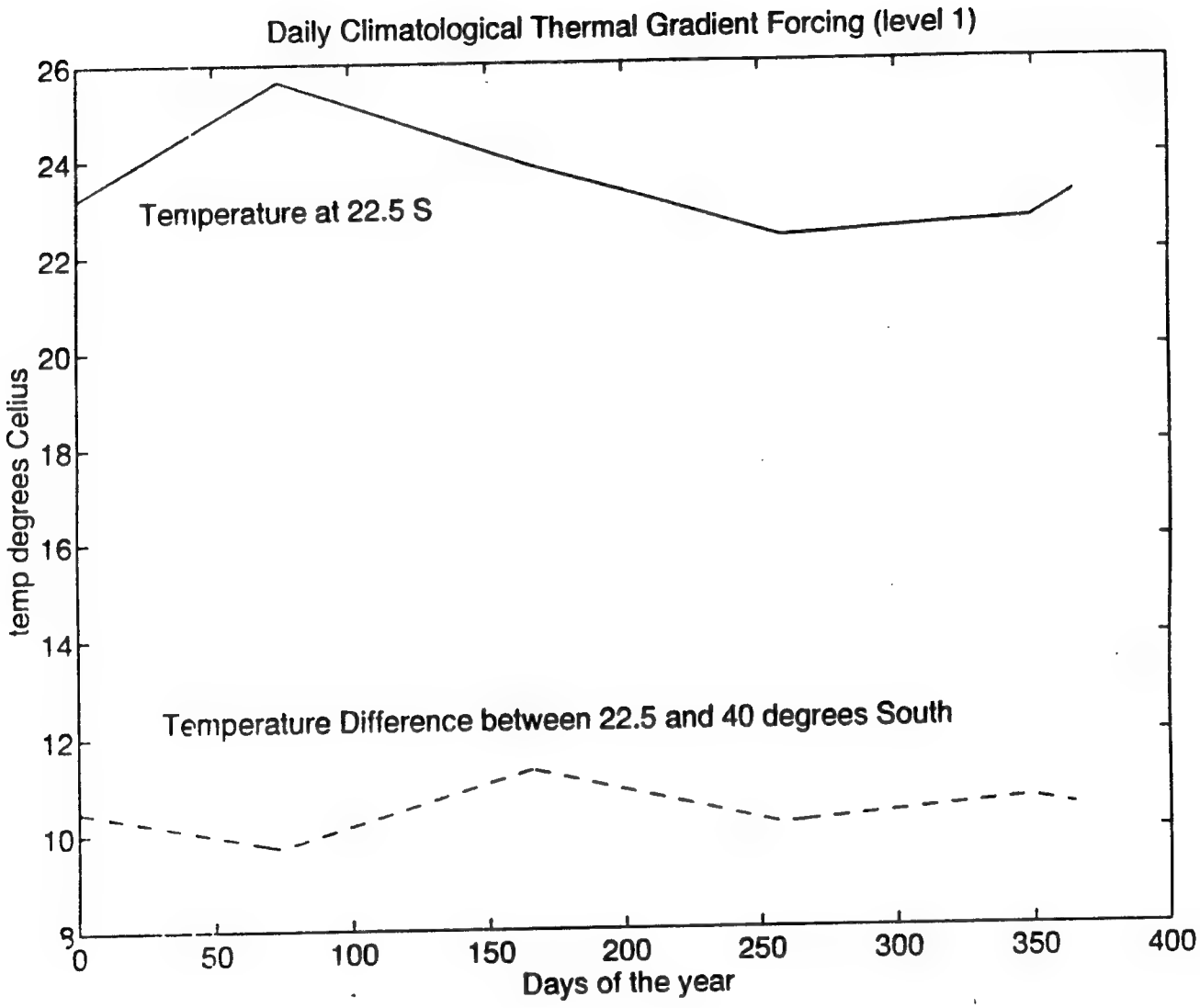

Figure 3.5a: The characteristic daily climatological thermal gradient forcing used in Experiment 5. The above temperature profile is for model level 1 (13 m). The solid line is the temperature at 22.5°S, 107.5°E. The dashed line is the temperature difference between 22.5°S and 40°S at longitude 107.5 E.

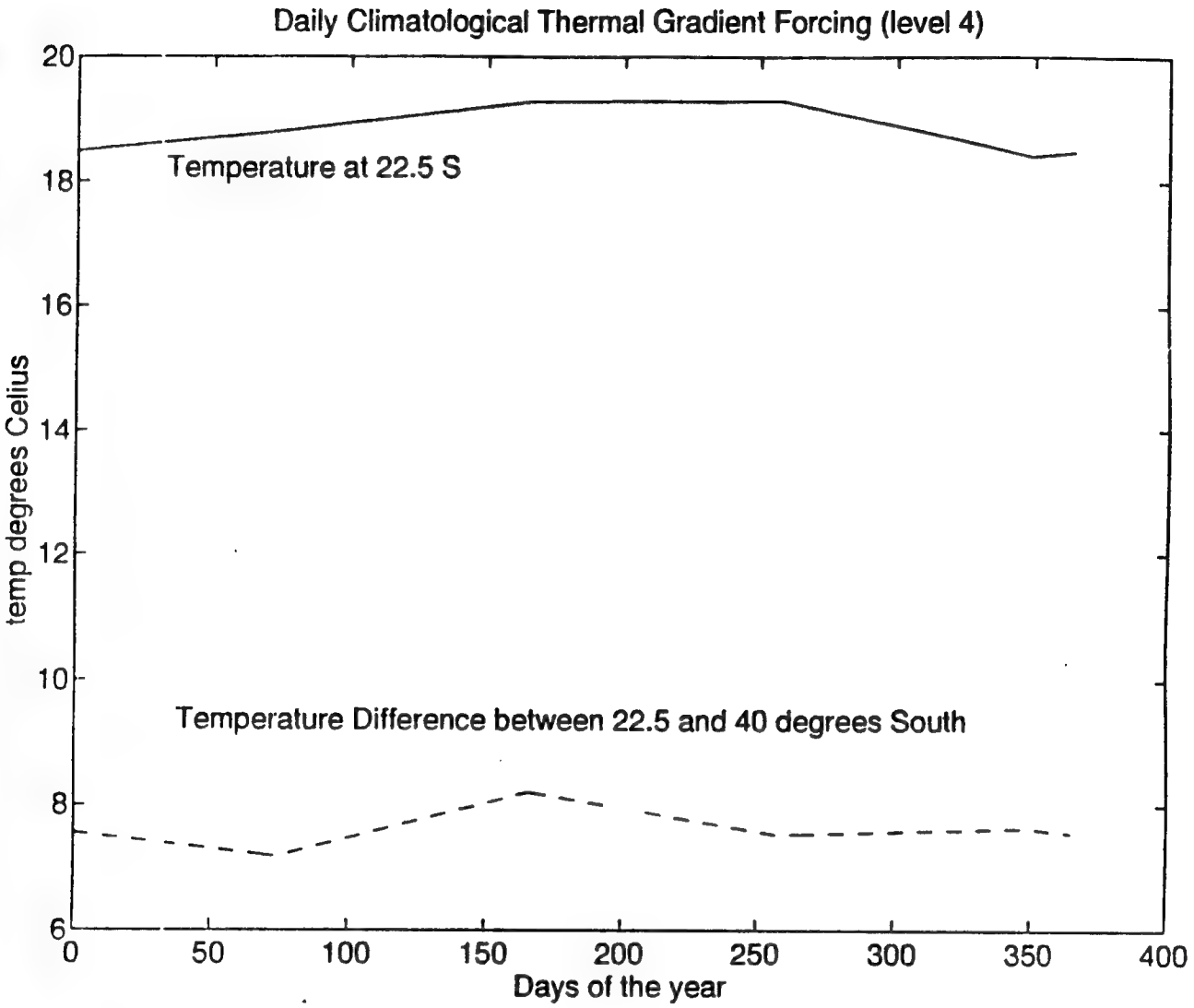

Figure 3.5b: The characteristic daily climatological thermal gradient forcing used in Experiment 5. The above temperature profile is for model level 4 (182 m). The solid line is the temperature at 22.5°S, 107.5°E. The dashed line is the temperature difference between 22.5°S and 40°S at longitude 107.5 E.

Layer	Temperature (°C)
1	29.5
2	28.5
3	26.0
4	20.5
5	15.7

Table 3.1 TEMPERATURE PROFILE: NORTH WEST SHELF WATERS

CASES	Thermal forcing (Initial Condition (IC) only or Forced Every Time Step ?)	North West Shelf waters added into model?	Ideal coastline utilized?	Irregular coastline utilized?	Winds Forced over Entire Domain Every Time Step ?
1	IC only	no	yes	no	no
2	IC only	no	no	yes	no
3	IC only	yes	yes	no	no
4	IC only	yes	no	yes	no
5	Forced Every Time Step	yes (day 74)	no	yes	yes

Table 3.2 SUMMARY OF SPECIFIC EXPERIMENTAL DESIGN

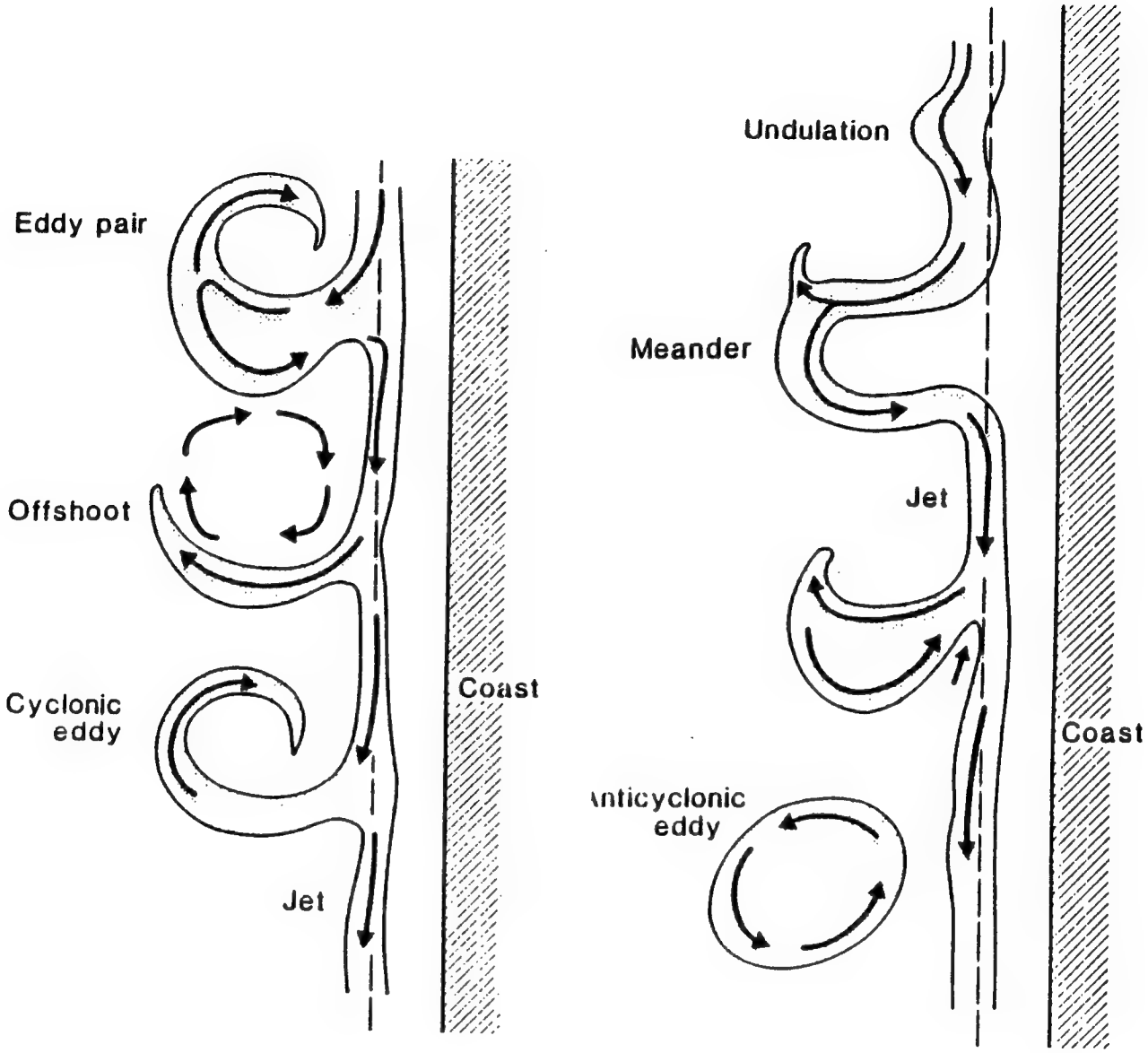

Figure 3.6 Postulated classification and definition of observed mesoscale features: Current characteristics on the right suggest the evolution from a jet flow along the shelf break through a fully developed meander to a free anticyclonic eddy; the left represents an eddy pair, an offshoot, and a cyclonic eddy. In each case, the coast is shaded and the shelf break is indicated by the dashed line (from Pearce and Griffiths, 1991).

IV. RESULTS OF EXPERIMENTS

A. EXPERIMENTS INITIALIZED WITH THERMAL GRADIENT ONLY

1. Experiment 1 - Ideal Coastline

a. Generation of Currents and Eddies

(1) Pre-eddy period (days 0-36). The current produced by the model is consistent with existing theory on the Leeuwin Current System. Due to the initial alongshore temperature field, the resulting pressure gradient establishes an onshore geostrophic inflow from the interior of the ocean. The onshore flow varies between 2 and 10 cm/s. As the flow approaches the eastern boundary, it turns and forms a narrow poleward boundary current with velocities as high as 55 cm/s at y ~850 km, off Fremantle (Figure 4.1a). By model day 6 (not shown), the current has entered the Great Australian Bight (with eastward velocities of ~20 cm/s and accelerating). Additional onshore flow augments the coastal current causing the magnitude of the current to increase in both the poleward and eastward directions. The poleward current increases in magnitude such that by day 36 (Figure 4.1b), maximum velocities of the order of 1 m/s are observed near Cape Leeuwin. The eastward current continues to accelerate from 20 cm/s on day 3 (Figure 4.1a) to 1.28 m/s at day 36 (Figure 4.1b) due to nonlinear feedback from instabilities, i.e., strong thermal fronts caused by initial poleward advection generate thermal winds that feed back to enhance the poleward and eastward surface flow (Batteen and Rutherford, 1990). Additionally, by day 36, the onshore geostropic flow has slightly weakened and is maintained at 2 cm/s near-shore and 6 cm/s in the interior ocean. Likewise, with the slowing down of the geostrophic adjustment process with time, the model Leeuwin Current significantly broadens due to westward Rossby wave propagation.

The pressure gradient in the Indian Ocean due to the thermal profile is sufficient to establish an equatorward flowing undercurrent along Western Australia, and a westward flowing undercurrent along Southern Australia. The strongest equatorward flow is north of Cape Leeuwin (24 cm/s) (Figure 4.2a) and is maintained throughout. Along Southern Australia the westward undercurrent between Albany and Esperance ranges between 17-23 cm/s throughout the pre-eddy period. The westward undercurrent near Cliffy Head ranges between 47-53 cm/s (see Figure 4.2b, for example). The variations in the westward undercurrent velocity are primarily due to increasing instabilities within the Leeuwin Current along Southern Australia. The average core depth of the undercurrent is between 200-350 m depth.

The initial temperature field changes dramatically as the Leeuwin Current System develops. Warm water is rapidly advected poleward and eastward throughout the domain, but subsequently decreases with time. By model day 36 (Figure 4.3), 19°C water has been advected poleward and around Cape Leeuwin and has reached the Great Australian Bight. Additionally by model day 36, 20.5°C water only extends as far as off the coast of Albany, 22°C water is held abate off the coast of Fremantle, and 23.5°C water extends no further than Dongara.

(2) Eddy generation period (days 36-135). The Indian Ocean climatological thermal gradient is sufficient to establish an unstable flow in the Leeuwin Current System. With the addition of Southern Australia to the model domain, large current offshoots are evident as early as model day 6 (not shown), as the current shifts from poleward around Cape Leeuwin to eastward towards the Great Australian Bight. These offshoots are likely due to the Coriolis force acting on the flow of the current around the landmass, which would introduce anticyclonic vorticity into the region. An anticyclonic

meander in the vicinity of Cape Leeuwin and Albany is established and intensifies with time. Along the south coast of Australia, the current "jets" around the Cape Leeuwin meander and continues to accelerate advecting anticyclonic vorticity downstream and intensifying undulations and offshoots at Esperance (entrance to the Great Australian Bight). The eastward current magnitude is greater towards the coast and decreases offshore. Near-shore the current velocity varies as nonlinear feedback causes surges from 1.28 m/s at day 36 (Figure 4.1b) to 1.0 m/s by day 63 (Figure 4.1c).

The mesoscale features in the current intensify and grow, such that by day 63 (Figure 4.1c), the Cape Leeuwin meander develops into an anticyclonic eddy. Undulations in the poleward current intensify as far up the coast as Dongara. Offshoots and meanders encompass the entire coast of Southern Australia well into the Great Australian Bight. By day 90 (4.1d), an anticyclonic eddy forms in the vicinity of Fremantle. Meanders near Esperance simultaneously intensify. By day 135 (Figure 4.1e), the Fremantle anticyclonic eddy begins a westward propagation. The poleward Leeuwin Current intensifies as nonlinear effects result in a "jet" between the eddy and the coast. These effects translate downstream to augment the eastward current's instability as nonlinear effects cause current surges to peak velocities of 2.1-2.3 m/s. The continuation of the geostropic inflow at Cape Leeuwin deforms the round anticyclonic Cape Leeuwin eddy and southern meanders, impeding eddy growth as well as causing the eddy to propagate westward at a slower rate than the eddies along Western Australia. An eddy pair is clearly visible near Cape Leeuwin as it is formed from offshoots from the anticyclonic limb of the Cape Leeuwin eddy and becomes fully developed into two counter-rotating cells which extend eastward pass Albany.

The formation of eddies contributes to a significant amount of advection of warm water offshore by the anticyclonic eddies (Figure 4.3b). The warm core eddy in the vicinity of Fremantle propagates westward and brings 22°C water into the interior ocean. The Cape Leeuwin warm core eddy embodies 20.5°C water which spans the offshore waters of the cape, while the cold core eddy embodies 16°C water and establishes a sharp temperature front in the peripheral of the eddy pair as the meander continues to intensify. The current is augmented by offshoots of warmer water previously held abate by upstream eddy development. These offshoots act to enhance mesoscale development, as pools of warm water entrain into the core of downstream meanders and eddies

b. Analysis of Eddy Generation Mechanisms

The dynamical reasons for the generation and stability of eddies in the Leeuwin Current System are examined using the energy techniques described in Chapter III. From the energy transfer analysis the location and magnitude of baroclinic and barotropic transfers can be found and examined to argue for the type of instability mechanism (e,g,. barotropic, baroclinic, or mixed) which leads to the initial eddy generation. Those waves which are unstable and in particular the fastest growing waves, can be determined from the internal Rossby radii.

Plots of the total kinetic energy over the entire domain and for all layers were plotted in a time series (Figure 4.4). As the model adjusts geostropically to the forcing, a quasi-steady state is reached between days 36 to 63. This corresponds to the period of eddy generation, since the velocity plots show the formation of the Cape Leeuwin eddy by day 63 (Figure 4.1c).

Analysis of horizontal plots of the energy transfer can be used to find the location and magnitude of barotropic and baroclinic transfers. Figure 4.5 shows horizontal plots

for (a) the transfer between mean and eddy kinetic energy (barotropic mechanism), and (b) the transfer between eddy potential and eddy kinetic energy (baroclinic mechanism) for the time period 36-63. The transfer plots emphasizes the dynamic nature of the Leeuwin Current as the current abruptly shifts from poleward to eastward, and clearly show the strongest energy transfers occurring in the regions of eddy development. A comparison of Figures 4.5a with 4.5b, which have the same contour intervals, shows that mixed instability (i.e., both baroclinic and barotropic) mechanisms are providing eddy kinetic energy, with barotropic instability dominant over baroclinic instability for this time period. Mixed instability transfers (not shown) are also responsible for the eddy development that occurred by day 90 off of Fremantle, and for the Southern Australia eddy pair which developed by day 135 between Cape Leeuwin and Albany.

2. Experiment 2 - Irregular Coastline

a. Generation of Currents and Eddies

(1) Pre-eddy period (days 0-36). In Experiment 2, the initial current characteristics are similar to the initial characteristics of Experiment 1. The onshore velocities of the geostropic flow varies between 2 and 10 cm/s as in Experiment 1. The poleward velocities at the irregular coastline are slightly higher at 68 cm/s (off the coast of Dongara) and located further to the north than Experiment 1 (55 cm/s off the coast of Fremantle). By model day 6 (not shown), the current has entered the Great Australian Bight (eastward current magnitude is 20 cm/s and accelerating). Augmentation from additional geostrophic flow increases the magnitude of the poleward current such that by model day 9 (not shown), a maximum current velocity of 1.1 m/s is observed near Cape Leeuwin. By day 36 (Figure 4.6a), the onshore geostropic flow has slightly weakened (to ~2 cm/s near-shore

and ~6 cm/s in the interior ocean), and the poleward current has broadened (due to Rossby wave propagation) and decelerated to 82 cm/s near Fremantle (due to increased nonlinear feedback occurring in the current downstream). The eastward current continues to accelerate from 20 cm/s at day 3 to 1.58 m/s on day 36 as nonlinear feedback occurs in the current.

The pressure gradient in the Indian Ocean establishes an equatorward undercurrent along Western Australia, and a westward undercurrent along Southern Australia. The strongest equatorward flow (17.5 cm/s) is north of Cape Leeuwin and is maintained between 10.5-17.5 cm/s throughout the pre-eddy period. Along Southern Australia the westward undercurrent ranges from 10-22.5 cm/s, between Albany and Esperance, and from 19.5-28.5 cm/s near Cliffy Head. The variations in the westward undercurrent velocity are primarily due to increased instabilities within the Leeuwin Current along Southern Australia.

The initial temperature field changes less dramatically than in Experiment 1, as the Leeuwin Current System develops along the irregular coastline. Warm water is advected poleward and eastward throughout the domain, but subsequently decreases with time. By day 36 (Figure 4.7), 17.5°C water has been advected poleward and around Cape Leeuwin and has reached the Great Australian Bight. Additionally, 19°C water only extends as far as off the coast of Albany; 20.5°C water is held abate off the coast of Fremantle (with the exception that an offshoot of 20.5°C does form a warm pool offshore of Cliffy Head); 22°C water extends to Dongara; an offshoot of 22°C water forms a small pocket at Fremantle; and 23.5°C water extends no further than just south of Shark Bay.

(2) Eddy generation period (days 36-150). The addition of a irregular coastline results in significant

instability from the onset of the model run. Large current offshoots are evident as early as model day 3 (not shown). These offshoots occur at preferred locations, specifically along the west coast irregular coastline, and around Cape Leeuwin where the current changes direction. This is likely due to the Coriolis force acting on the flow of the current around the landmass, which introduces anticyclonic vorticity into the region. Anticyclonic meanders (one just south of Shark Bay, one between Dongara and Fremantle and one in the vicinity of Cape Leeuwin and Cliffy Head) are established and instabilities subsequently intensify. The growth of these meanders effects the current characteristics both upstream and downstream. By day 36 (Figure 4.6a) the current along the west coast of Australia has large undulations near the Shark Bay and Fremantle meanders. The current continues to decelerate from 82 cm/s to 77 cm/s until day 42 (Figure 4.6b), after which this same velocity is maintained.

Along the south coast of Australia, the current "jets" around the Cape Leeuwin meander and continues to accelerate advecting anticyclonic vorticity downstream and intensifying undulations and offshoots at Esperance (entrance to the Great Australian Bight). Near-shore the current velocity varies (due to nonlinear feedback causing surges) from 1.58 m/s at day 36 (Figure 4.6a) to 1.4 m/s by day 42 (Figure 4.6b). The eastward current magnitude is greater towards the coast and decreases offshore.

The mesoscale features in the current intensify and grow. By day 45 (Figure 4.6c), the Shark Bay, Fremantle, and Cape Leeuwin meanders develop into anticyclonic eddies. The poleward current "jets" around these meanders. Offshoots and meanders encompass the entire coast of Southern Australia well into the Great Australian Bight. By day 72 (Figure 4.6d), an anticyclonic eddy forms in the Leeuwin Current System Southern Australian branch between Albany and

Esperance. Additionally, within this time frame a cyclonic meander southwest of Esperance intensifies. The Fremantle eddy begins its westward propagation. By day 144, the Shark Bay, Fremantle and Cape Leeuwin anticyclonic eddies have propagated westward well into the interior ocean. The southern coast eddies also propagate westward. The westward propagation speeds are ~10 km/day, consistent with Rossby wave propagation speed. Eddy pairs are clearly visible throughout the coastal region. These pairs form from the anticyclonic limb of the established warm core eddies and then develop into two counter-rotating cells. The poleward Leeuwin Current intensifies as nonlinear effects result in a "jet" between the eddy and the coast. A new Shark Bay anticyclonic eddy has formed as instabilities along the coast continue. These effects translate downstream to the eastward current's instability as nonlinear effects cause current surges with velocities between 1.4-1.86 m/s. By day 144 (Figure 4.6e) along the Southern Australian coast, the Leeuwin Current is no longer distinctly defined; instead eddies and meanders saturate the coastal region.

The formation of eddies contributes to a significant amount of advection of warm water offshore by the anticyclonic eddies. The warm core eddy in the vicinity of Shark Bay propagates westward and brings 23.5°C water into the interior ocean. The warm core eddy in the vicinity of Fremantle propagates westward and brings 22°C water into the interior ocean. The Cape Leeuwin warm core eddy embodies 20.5°C water which spans the offshore waters of the cape, while the cold core eddy embodies 16°C water and establishes a sharp temperature front in the peripheral of the eddy pair as the meander continues to intensify. The current is augmented by upstream offshoots of warmer water previously held abate by eddy development. These offshoots act to

enhance mesoscale development, as pools of warm water entrain into the core of downstream meanders and eddies.

b. Analysis of Eddy Generation Mechanisms

The total kinetic energy over the entire domain and for all layers were plotted in a time series (Figure 4.8). As the model adjusts geostropically to the forcing, a quasi-steady state is reached between days 39 to 57, corresponding to the period of eddy generation for the Shark Bay, Fremantle, and Cape Leeuwin eddies.

Analysis of horizontal plots of the energy transfer are used to find the location and magnitude of both barotropic and baroclinic transfers. Figure 4.9a-b shows horizontal plots for (a) the transfer between mean and eddy kinetic energy (barotropic mechanism), and (b) the transfer between eddy potential and eddy kinetic energy (baroclinic mechanism) for the 39-57 day period. As expected, the strongest energy transfers occur in the regions of eddy development. A comparison of Figure 4.9a with Figure 4.9b, which have the same contour interval, shows that mixed (i.e., both baroclinic and barotropic) instability mechanisms are present. Further examination of the magnitudes of both instability mechanisms show that barotropic instability dominates over baroclinic instability. This is also the case for eddy development at days 72 (not shown) and 144 (not shown).

3. Summary of Experiments Initialized with Thermal Gradient Only

Initialization using the climatological mean temperature for the Indian Ocean, and allowing the ocean to geostrophically adjust in the absence of external forcing produces a model Leeuwin Current (and associated undercurrent) that is unstable and generates mesoscale eddies. The surface current is augmented by onshore geostrophic inflow and accelerates downstream. With the addition of the Southern

Australian coast to the model domain, a significant amount of horizontal and vertical shear is added to the region.

The results of Experiment 1 (ideal coastline) reveal how the current dynamics around Cape Leeuwin increase instability by inducing anticyclonic vorticity into the system. This anticyclonic vorticity is likely a result of the current shifting from poleward to eastward via the Coriolis and geostrophic forces acting on the current, as well as regional horizontal and vertical shear forces. Mesoscale features result in nonlinear feedback mechanisms which cause surges in the current velocity. The poleward current is observed to peak at Cape Leeuwin at 1.0 m/s by day 36, and to decrease to 60 cm/s by day 63. Off Southern Australia current surges causes peak velocities of 2.1-2.3 m/s.

Both equatorward and westward undercurrents with maximum velocities near Cape Leeuwin were observed. The magnitude of the undercurrents decrease both equatorward and eastward. Eddy generation occurs on the offshore side of the core of the current. The initial eddy develops at Cape Leeuwin by day 63, with subsequent eddies upstream (off of Fremantle by day 90) and downstream (Cape Leeuwin, Albany eddy pair by day 135). The primarily anticyclonic eddies form in horizontal and vertical shear zones. In these regions instabilities are mixed with barotropic instability dominant.

The results of Experiment 2 reveal the significance of adding a realistic coastline. The irregular coastline establishes a more energetic and dynamic current, but effectively decreased the magnitude of the undercurrents. The poleward current velocities are generally higher than those for the ideal coastline, and occur at an earlier time period (i.e., 1.1 m/s velocities at day 9, which subsequently decrease and surge to 70-76 cm/s by day 39). Off the southern coast of Australia, current velocities with current surges of ~1.4-1.86 m/s, are slightly lower than those for the ideal

magnitudes of the undercurrents both equatorward and westward, also decreased. Initial eddy development occurs much earlier (i.e., by day 45), and develops in the vicinity of coastal indentations along Western Australia and near Cape Leeuwin. Subsequent eddies also develop earlier (i.e., by day 72) and are further spread throughout the region of Southern Australia to the point that the southern branch of the Leeuwin Current System is no longer distinctly defined by day 144. The formation of all the eddies result from mixed instabilities, with barotropic instability dominant.

In both experiments the eddies have time scales of months. The wavelengths for the west coast eddies are larger (~150 km) than those off the southern coast of Australia (which have wavelengths ~112 km). This is likely due to ongoing geostropic inflow which acts to deform the eddy shape (subsequently inhibiting the growth rate of eddies) and to impede the westward Rossby propagation of eddies. These length scales are consistent with the Rossby radius of deformation of ~30 km, and with the results of Batteen and Rutherford (1990).

B. EXPERIMENTS INITIALIZED WITH THERMAL GRADIENT AND THE NORTH WEST SHELF (NWS) WATERS

1. Experiment 3 - Ideal Coastline

a. Generation of Currents and Eddies

(1) Pre-eddy period (days 0-27). With the addition of the NWS waters to the climatological thermal gradient of the Indian Ocean, a more energetic and dynamic current than that in Experiment 1 is established. From the onset of the model run, the NWS waters add strong horizontal shear to the coastal equatorial region of the domain, and vertical shear to the inshore current. Away from the source region, the influence of the NWS waters diminishes poleward, but is still strong enough to augment the onshore geostrophic

inflow with the result that a stronger current is established throughout the coastal regions of Australia. The initial onshore geostrophic inflow from the interior of the ocean is of the same magnitude (i.e.,~2-10 cm/s) as in Experiment 1; however the narrow poleward flowing boundary current has magnitudes on the order of 1.5 m/s off Shark Bay, and 1.1 m/s just south of Dongara. The current entering the Great Australian Bight is larger than that of Experiment 1 with a magnitude of 40 cm/s and accelerating, as shown in Figure 4.10a. Continual onshore geostrophic inflow and nonlinear feedback mechanisms augment the poleward and eastward current. By day 18 (not shown), the poleward current has reached a maximum of 2.2 m/s, at Cape Leeuwin. By day 27 (Figure 4.10b), the geostrophic inflow has weakened and the current has broadened due to Rossby wave propagation. The poleward current velocity has decreased to 94 cm/s at Shark Bay and to 1.6 m/s at Cape Leeuwin. The eastward current continues to accelerate from 40 cm/s at day 6 to 2.2 m/s at day 27.

The addition of the NWS water also results in the establishment of a stronger undercurrent than in Experiment 1. The strongest equatorward flow (45 cm/s) is north of Cape Leeuwin at day 12 (not shown). It subsequently decreases to 36-38 cm/s and maintains this speed throughout the pre-eddy period. Along Southern Australia the westward undercurrent ranges from 25-36 cm/s between Albany and Esperance throughout the pre-eddy period, while the westward undercurrent ranges from 69-74 cm/s near Cliffy Head. These undercurrent velocities, like the surface current velocities, are significantly higher than in Experiment 1.

The initial temperature field changes dramatically due to the addition of the NWS water. The advection of the NWS water results in a narrow core of warmer water along the entire coastal boundary. By day 27 (Figure 4.11a), 20.5°C water has been advected poleward and around Cape Leeuwin and

has reached the Great Australian Bight; 22°C water extends between Albany and Esperance; and 23.5°C water extends around Cape Leeuwin to just west of Albany. A strong temperature front is also established along the Southern Australian coast.

(2) Eddy generation period (days 27-129). The addition of the NWS water adds significant instability to the source region and throughout the coast region of Australia. As a result of this more vigorous and unstable current, an earlier eddy generation period than in Experiment 1 is observed. The stronger surface current, along with the NWS water temperature gradient produces a large horizontal shear zone in the coastal equatorial region. Coupled with a stronger undercurrent, greater baroclinic instability contributes to a larger vertical shear zone throughout the entire coastal region. As early as day 6 (Figure 4.10a), an anticyclonic eddy is formed near the source region, and large offshoots are observed at Cape Leeuwin. Instabilities intensify such that by day 27 (Figure 4.10b), a large undulation occurs in the current along both the western and southern coastal branches resulting in anticyclonic meanders, one just south of Shark Bay, and one at Cape Leeuwin. Current offshoots occur in the vicinity of Fremantle and east of Albany. Nonlinear feedback continues to increase the current surges along the west coast of Australia from 0.94-1.6 m/s by day 27 (Figure 4.10b) to 0.61-1.3 m/s by day 42 (Figure 4.10c). Along the southern coast the current continues to accelerate to 2.5 m/s by day 42 (Figure 4.10c).

The mesoscale features rapidly form eddies. The current characteristics at day 45 (Figure 4.10d) show anticyclonic eddies near the NWS water source region, Shark Bay, Fremantle and Cape Leeuwin. Offshoots and meanders encompass the entire coast of Australia. By day 66 (not shown), the NWS, Shark Bay, and Fremantle eddies have propagated westward. By day 87 (Figure 4.10e), an

anticyclonic eddy has formed between Albany and Esperance. By day 129 (Figure 4.10f), the above eddies have propagated westward. Also, eddy pairs are visible throughout the coastal region. By this time, the Leeuwin current has been forced off the coastal boundary into the interior ocean due to westward eddy propagation and to coastline meanders.

Since the NWS water addition advects warmer water throughout the entire Australian coast, it also results in the advection of warmer waters offshore by the anticyclonic eddies. Overall, the eddies developed in Experiment 3 are 1.5-3°C warmer (Figure 4.11b) than the initial eddies formed in Experiment 1.

b. Analysis of Eddy Generation Mechanisms

With the NWS water acting in conjunction with the Indian Ocean thermal gradient, a quasi-steady state is reached between days 42 to 63 (Figure 4.12). This corresponds to the same eddy generation period as in Experiment 1. The energy transfers for this time period (Figure 4.13a-b) show mixed instabilities present with the barotropic instability mechanism dominant. This is also the case for eddy development at day 87 (not shown); however, analysis of the energy transfers for the eddies formed by day 129 (Figures 4.14a-b) reveal that baroclinic instabilities dominates over barotropic instability in the NWS water's source region. This could possibly be caused by the interaction of northern eddy pairs propagating westward with the onshore geostropic eastward flow with the result that transitory vertical shear regions are generated.

2. Experiment 4 - Irregular Coastline

a. Generation of Currents and Eddies

(1) Pre-eddy period (days 0-24). As expected, in Experiment 4 the addition of the realistic irregular coastline introduces even greater instabilities into the model Leeuwin

Current System than in previous experiments. Current velocities of the poleward boundary current are generally higher than those established in Experiment 3. A new regional maximum of 2.06 m/s is observed off of Shark Bay by day 9 (Figure 4.15a). Also by day 9, the current velocity at Dongara is 1.2 m/s, 1.35 m/s at Cape Leeuwin and the eastward current is 1.19 m/s and accelerating. By day 12 (not shown), the Cape Leeuwin poleward velocity peaks at 1.69 m/s and the eastward current peaks at 1.58 m/s. By day 24 (Figure 4.15b), the current velocities have decreased, and a range from 1.0-1.4 m/s along the western coast, and 1.0-1.16 m/s along the southern coast is maintained throughout the pre-eddy period.

The irregular coastline reduces the overall magnitude of the undercurrent compared to previous experiments. The equatorward undercurrent maintains a range of 22-26 cm/s north of Cape Leeuwin. Along Southern Australia the westward undercurrent ranges from 17.9-23.3 cm/s between Albany and Esperance, and from 20-42 cm/s near Cliffy Head.

The irregular coastline limits the extent of the advection of the NWS warmer waters along the Australian coast. By day 24 (Figure 4.16), only 17.5°C water has been advected into the Great Australian Bight; the 19°C water extends between the coast of Albany and Esperance; the 20.5°C water extends around Cape Leeuwin to just west of Albany; and the 22°C and 23.5°C waters are held abate at Fremantle. The temperature front along the southern coast of Australia is much more relaxed compared to the front established by Experiment 3.

(2) Eddy generation period (days 24-135). As in Experiment 3, as early as day 6 (not shown), an eddy pair is observed near the coast of the NWS water source region. Current shifts along the irregular coastline produce undulations and large offshoots. By day 9 (Figure 4.15a), large offshoots are observed near Shark Bay, Fremantle, around

Cape Leeuwin, and as far east as Albany. By day 24 (Figure 4.15b), these offshoots intensify to form anticyclonic meanders. By day 27 (Figure 4.15c), anticyclonic eddies have formed at Shark Bay and Fremantle. Instabilities increase downstream such that by day 42 (Figure 4.15d), anticyclonic eddies form in the vicinity of Cape Leeuwin and Cliffy Head, and off the coast of Albany. Also by day 42, the Fremantle eddy has begun its westward propagation. By day 60 (Figure 4.15e), a second eddy has formed in the NWS water source region (near North West Cape), and eddy pairs are visible along the entire southern coast of Australia. Regional instabilities continue to intensify such that by day 135 (Figure 4.15f), a new anticyclonic eddy has formed off the coast of Dongara, and eddy pairs are established throughout the entire coast of Australia. By this time Rossby wave propagation, eddies and meanders have forced the model Leeuwin Current System far offshore away from the coastal regions.

Since the irregular coastline effectively limits the advection of the warmer NWS waters along the Australian coastline, the eddies propagate offshore with cooler waters than in Experiment 3. The warm core eddy in the vicinity of Shark Bay propagates westward and brings 23.5°C water into the interior ocean. The warm core eddy in the vicinity of Fremantle propagates westward and brings 22°C water into the interior ocean. The Cape Leeuwin warm core eddy embodies 20.5°C water which spans the offshore waters of the cape. By day 135 a sharp temperature front has been established off the coast of Southern Australia as cooler 14.5°C water is entrained into the region.

b. Analysis of Eddy Generation Mechanisms

A plot of the total kinetic energy over the entire domain (Figure 4.17) shows that a quasi-steady state period is reached between days 24 to 45, covering the time period for

the formation of the Shark Bay, Fremantle, Cape Leeuwin and Albany eddies.

Analysis of horizontal plots of the energy transfer for this time period (Figure 4.18a-b) shows that mixed instabilities are present, with barotropic instability mechanisms dominant. This is also the case for eddy development at days 60 (not shown) and 135 (Figure 4.19a-b). The result for the latter period is different than the baroclinic instability domination displayed in Experiment 3, which was observed by day 144 in the interior ocean. This may be a function of lower undercurrent velocities contributing less to vertical shears zones established in the latter days of the model run.

3. Summary of Experiments Initialized with Thermal Gradient and the North West Shelf Waters

In both experiments 3 and 4, initialization using climatological mean temperatures for the Indian Ocean and the NWS waters, followed by the geostrophic adjustment of the ocean in the absence of external forcing, produces a model Leeuwin Current (and associated undercurrent) that is more vigorous and unstable than that of previous experiments with the result that mesoscale eddies are generated at an earlier time period. The NWS waters augment the onshore geostrophic inflow to produce a stronger current and undercurrent throughout the entire domain, adding to the baroclinicity of the current through vertical shear forces. The NWS waters also add a significant amount of horizontal shear near the equatorial source region. The influence of the NWS waters diminish away from the source region but contribute significantly to downstream current characteristics. Greater current velocities are observed throughout the entire coastal regions of Australia. The observed undercurrents are significantly higher than in previous experiments. Also the

warmer NWS waters are advected further south which results in warmer waters in the Great Australian Bight region. This leads to the establishment of strong temperature fronts along Southern Australia as cooler Sub-Antarctic Water is entrained into the southern branch of the current system.

Eddies form along the equatorial region at the onset of the experiment rather than later, with subsequent eddies developing along the western coast of Australia, as far north as Shark Bay, and as far south as Cape Leeuwin. Along the southern coast of Australia eddies and eddy pairs also form earlier than in previous experiments.

The NWS waters increase the barotropic instability near the source region. As in Experiments 1 and 2, initial eddies form as warm core, anticyclonic eddies. Eddy formation occurs through mixed instabilities with barotropic instabilities dominant for the first two major formation periods of Experiments 3; however, during the latter period of eddy development (day 129) in Experiment 3, baroclinic instability mechanisms become dominant as the offshore propagating eddy pairs interact with the onshore geostropic flow. In Experiment 4, however, mixed instabilities are present; however barotropic instabilities dominate throughout the entire model run.

The addition of the irregular coastline (Experiment 4) further increases the observed velocities of the surface boundary current, but lower the undercurrent velocities observed north of Cape Leeuwin and Cliffy Head. This effectively reduces the regional vertical shear throughout the model domain. The irregular coastline limits the extent of the poleward advection of the warmer NWS water. Initial eddy formation occurs much earlier off Western Australia, Cape Leeuwin and off the coast of Albany, than in Experiment 3. This is also the case for the appearance of eddy pairs throughout the entire domain.

In both experiments 3 and 4, the eddies have time scales on the order of months. The NWS waters increased the scale at which the dominant eddy growth occurred by modifying the thermal structure in the inshore region. The dominant scale of eddy generation for the west coast eddies in the current is 180 km. As in experiments 1 and 2, eddies off the south coast are generally smaller (~140 km) than eddies off Western Australia. This scale is consistent with the Rossby radius of deformation of ~30 km in this strongly baroclinic flow, and is also consistent with the results of Batteen and Rutherford (1990).

C. EXPERIMENT 5: CLIMATOLOGICAL THERMAL AND WIND FORCING

As Table 3.2 shows, Experiment 5 uses two opposing forces (i.e., wind and thermal) applied every time step over the irregular coastal model domain. The NWS water "dam-breaking" is introduced into the model at day 74. The model response should produce a more complex flow regime than that observed in previous experiments: the equatorward wind forcing directly opposes the poleward thermal forcing along Western Australia but acts to augment the eastward thermal forcing along the coast of Southern Australia (since the wind forcing is also eastward in that region). As a result, along Western Australia the wind forcing should establish local upwelling coastal regions due to the Ekman force, while in the interior ocean, the wind forcing should create significant shear zones (especially in the equatorial region where the wind forcing has strong equatorial and offshore components). Along Southern Australia, the wind forcing, which has a strong eastward component (and onshore near Cape Leeuwin) should augment the eastward Leeuwin Current flow, and should enhance regional dynamics as the current shifts poleward around Cape Leeuwin and then eastward. It should also promote a stronger temperature gradient along the southern coast than in previous experiments.

1. Generation of Currents and Eddies

a. Pre-Eddy Period (Days 0-30)

As in previous experiments, the pressure gradient establishes a predominantly onshore geostropic flow in the interior ocean. The wind forcing acts to establish an offshore flow in the northwest equatorial region of the model domain, and acts to decrease the magnitude of the onshore geostrophic flow. As a result, the onshore flow varies between 2-6 cm/s along Western Australia, but increases to 8 cm/s near Cape Leeuwin. As the flow approaches the eastern boundary, it turns and forms a narrow poleward boundary current with velocities as high as 55 cm/s near Dongara (Figure 4.20a). By model day 6 (not shown), the current has entered the Great Australian Bight with eastward velocities of ~60 cm/s and accelerating. With the additional onshore flow augmenting the coastal current, the poleward current increases in magnitude to a maximum velocity by day 9 (not shown) of ~96 cm/s near Cape Leeuwin. By day 30 (Figure 4.20b), the geostrophic inflow has weakened (~2-4 cm/s along Western Australia), and the current has broadened due to wind effects creating shear forces, coupled with westward Rossby wave propagation. The poleward current velocity has decreased to 40 cm/s at Dongara and to ~69 cm/s at Cape Leeuwin. The eastward current continues to accelerate from ~60 cm/s at day 6 to ~1 m/s by day 30.

The established undercurrent (like the surface current) is weaker than in previous experiments. North of Cape Leeuwin, the equatorward flow ranges from ~11-14 cm/s. Along Southern Australia the westward undercurrent ranges from 14-19 cm/s between Albany and Esperance, and between 16-21 cm/s near Cliffy Head. These undercurrent magnitudes are maintained throughout the pre-eddy period. The core of the undercurrents is at ~200-325 m depth.

Due to the addition of wind forcing, the initial temperature fields changed less dramatically than in previous experiments. The wind acts to limit the southern advection of warmer equatorial waters. By day 30 (Figure 4.21a), 23°C water is held abate off of Carnarvon; 22°C water extends to Shark Bay (with offshoots down to Dongara); 20°C water is held abate just north of Cape Leeuwin; 19°C water extends to Albany; and only 16°C water extends into the Great Australian Bight. Additionally, the offshore and equatorward components of the wind force establish regions of local upwelling evident offshore of Carnarvon, Shark Bay, and along the coast between Dongara and Fremantle. A moderate temperature front exists along the southern Australian coast. It is weaker than in previous experiments due to warmer waters held abate upstream along the western coast.

b. Eddy Generation Period (Days 30-150)

The opposing wind and thermal forcing establish an unstable complex flow regime that results in the development of eddies. Offshoots appear at Carnarvon, Dongara, and Cape Leeuwin by day 6 (not shown), and intensify to form large anticyclonic meanders by day 30 (Figure 4.20b). By day 36 (Figure 4.20c) anticyclonic eddies form near Shark Bay, and north of Fremantle, resulting in current surges between 57-66 cm/s in the vicinity of Cape Leeuwin. These eddies subsequently propagate westward (see Figure 4.20d) at a rate of ~12 km/day causing a current "jet" along the coast. The westward Rossby wave propagation of these eddies (along with increased horizontal shear forces from the offshore climatological winds) subsequently splits the onshore geostrophic inflow. The split geostropic inflow establishes an offshore poleward current in the interior ocean in addition to an inshore coastal poleward current. These two poleward currents reunite at Cape Leeuwin and proceed eastward into the Great Australian Bight. During this time period, wind effects

along Southern Australia also intensify the current shift around Cape Leeuwin such that the south coast meanders develop into anticyclonic eddies south of Cape Leeuwin, and near Albany.

The eddies continue to develop and grow, with the west coast eddies larger (wavelength ~300 km) than the south coast eddies (~120 km). This is possibly due to the different climatological winds, coupled with the variation in intensity of the geostrophic inflow in the west and south coast regions. By day 72 (Figure 4.20e), eddy pairs encompass the coast of Australia as far north as Dongara, and as far east as Esperance. The offshore poleward current velocity is ~20 cm/s. The inshore poleward current increases to ~1 m/s at Cape Leeuwin (due to coastal current "jets" and nonlinear feedback mechanisms). The eastward current consequently increases to ~1.4 m/s near Albany.

The NWS water "dam-break" at model day 74 results in a warm water poleward "jet" along the irregular coastline. The inshore poleward current increases from ~22 cm/s near Shark Bay, and 1 m/s near Cape Leeuwin at day 72 (Figure 4.20e), to ~1 m/s and ~1.2 m/s respectively, by day 93 (not shown). This accelerated current regenerates instabilities along the west coast. New meanders intensify near Shark Bay, Dongara, and Fremantle. The growth of these meanders deform pre-existing eddy pairs due to the increased horizontal shear. This increased regional shear accelerates the westward propagation of the eddy pairs to ~15 km/day, which in turn acts to further split the onshore geostrophic inflow. The offshore poleward current intensifies to ~40 cm/s. The intensification of the poleward currents creates a strong current surge along Southern Australia, accelerating the eastward current to ~1.68 m/s by day 93 (not shown). This eastward surge forces the Cape Leeuwin and Albany eddy pairs further downstream (towards the Great Australian Bight).

By day 105 (Figure 4.20f), the west coast meanders, formed by the addition of the NWS water, develop into new anticyclonic eddies. These eddies intensify the regional shear forces acting on the offshore poleward current. This shear force drives the offshore current further into the interior ocean. Offshore poleward velocities increase to ~50 cm/s. The inshore coastal current velocities are maintained at ~60 cm/s at Shark Bay, ~1.5 m/s at Cape Leeuwin, and ~1.9 m/s east of Esperance. The offshore and inshore poleward current also acts to restrict the growth of eddies in the interior ocean in addition to decreasing the westward propagation speed to ~10 km/s by day 150 (Figure 4.20g). The eddy pair just north of Fremantle and the eddy pair south of Cape Leeuwin appear to be semi-permanent due to the reunion of the offshore and inshore poleward currents at Cape Leeuwin, and strong regional onshore climatological winds. The Albany and Esperance eddy pairs also propagate slower than the west coast eddies (> 5 km/day). Additionally, throughout this period, the wind forcing acts to refine the inshore poleward current to a narrow current "jet" along the coast. The poleward current velocity decreases near Carnarvon to ~20 cm/s, yet maintains a velocity of ~1.8 m/s at Cape Leeuwin. The eastward current velocity remains ~1.4 m/s near Albany.

Since the wind forcing effectively limits the advection of the warmer waters along the Australian irregular coastline, the eddies formed by day 57 (Figure 4.21b) propagate offshore with cooler waters than in previous experiments. The warm core eddy in the vicinity of Shark Bay propagates westward and brings 22°C water into the interior ocean. The warm core eddy in the vicinity of Fremantle propagates westward and brings 20.5°C water into the interior ocean. The Cape Leeuwin and Albany warm core eddies embody 18°C water. During this time period, the wind forcing has intensified the temperature front along the south coast by

entraining cold Sub-Antarctic Water into the eastward current. The NWS water "dam-break" at day 74 (not shown) advects warmer waters along the entire coast. By day 105 (Figure 4.21c), new eddies formed in the above mentioned regions are generally 2°C warmer. A stronger temperature front is established off the coast of Southern Australia as warmer water is advected into the Great Australian Bight. By day 150 (Figure 4.21d), the wind forcing acts to recede the bulk of the warmer NWS water back up the irregular coastline to just north of Carnarvon, and establishes a strong temperature front along the west coast of Australia. These effects significantly add to the baroclinicity of the current, and to the vertical shear of the interior ocean.

2. Analysis of Eddy Generation Mechanisms

A plot of the total kinetic energy over the entire domain (Figure 4.22) shows that a quasi-steady state period is reached between days 36 to 57, consistent with the formation of the Shark Bay and Fremantle eddies which form by day 36, and with the formation of the Cape Leeuwin and Albany eddies which form by day 57.

Analysis of horizontal plots of the energy transfer for this time period (Figures 4.23a-b) shows that mixed instabilities are present, with barotropic instability dominant along the Southern Australian coast, and baroclinic instability dominant along the Western Australian coast. This is also the case for eddy development at days 105 (not shown) and 150 (Figure 4.24a-b). The baroclinic instability domination along the west coast region of the model domain is different from the results of all previous experiments except Experiment 3. This may be a function of the larger vertical shear zones established along the irregular coastline and in the interior ocean, due to the added wind forcing and opposing thermal forcing invoked every time step throughout the model run.

3. Comparison With Observations

The model results from Experiment 5 will be used for comparison with available field observations because the results have the most realistic features of the Leeuwin Current System. General features of the Leeuwin Current are apparent from satellite images as well as measured current data. The discussion in the ensuing paragraphs detail the general features, and then discuss the specific magnitudes and characteristics along the Western and Southern Australian coast. Overall, the results of Experiment 5's complex flow regime highlights the major characteristics of the Leeuwin Current with vividly impressive similarities to field observations.

a. Comparison of Ocean Currents

In Experiment 5 the numerical model, through the use of climatological data, developed an ocean current that contained many features observed in the Leeuwin Current System. The existence of an onshore geostropic flow which turns south at the coastal boundary and forms a narrow poleward current advecting warm tropical waters southward to Cape Leeuwin then eastward into the Great Australian Bight has been observed in numerous satellite images. These images reveal a system of meanders, eddies, along-shelf jets, on a range of length scales (e.g., Legeckis and Cresswell, 1981; Griffiths and Pearce, 1985a,b; Prata and Wells, 1990; Prata et al., 1986; Cresswell and Peterson, 1993). The observation that the Leeuwin Current is not a steady flow has been made by Legeckis and Cresswell (1981), and by Pearce and Griffiths (1990). They both observed current surges, "jets", and large spatial variations due to intensification of instabilities and nonlinear feedback mechanisms. The experiment results document several current surges due to nonlinear feedback mechanisms, as well as large spatial variations in the current

from Rossby wave propagation. The "Western Australian Current" (an offshore poleward current) and the inshore Leeuwin Current uniting at Cape Leeuwin has been described by Andrews (1977), and is consistent with the split geostropic flow documented in the above results. Andrews (1977) also described the dynamical nature of the current shift around Cape Leeuwin. The model established equatorward and westward undercurrent had a core at ~200-325 m depth, and magnitudes consistent with observations from current measurements noted by Cresswell and Peterson (1993) and from LUCIE data noted by Boland et al. (1988).

(1) The Current Off of Western Australia. The major characteristics of the modeled Leeuwin Current off Western Australia is consistent with field observations. The sustained magnitudes of the model poleward (5-69 cm/s) and equatorward (5-14 cm/s) current prior to the "dam-breaking" of the NWS waters compare favorably with LUCIE data measured during the austral winter. For example, off of Dongara by day 30 (Figure 4.20b) the model poleward current measures ~40 cm/s, and undercurrent ~5 cm/s (not shown), while LUCIE current meter data at Dongara (83 m) measures 38.5 cm/s for the poleward current, and 5.9 m/s for the undercurrent (Boland et al., 1988).

With the inclusion of the NWS waters, the simulated poleward velocity increased to ~1.5 m/s at Cape Leeuwin by model day 105 (Figure 4.20f), which is consistent with surface current measurements greater than 1 m/s measured by the RV Franklin at Cape Leeuwin (Cresswell and Peterson, 1993). From the CDT measurements of Cresswell and Peterson (1993) it is observed that the NWS water increases coastline temperatures ~2°C by advecting warmer "tropical" waters previously held abate by the wind. This observation is consistent with the simulated temperature field shown in Figure 4.21. Model day 150 revealed how the winds receded the

bulk of the NWS waters to north of Carnarvon, which resulted in a narrow poleward current with a strong temperature front. Figure 2.1 (NOAA7 satellite image) shows that the bulk of NWS water arrested north of Dongara. Additionally, Weaver and Middleton (1989) deduced a strong temperature front ~3°C along Western Australia from the advection of warm NWS waters. These observations support the model results for current characteristics off of Western Australia.

(2) The Current Off of Southern Australia. Griffiths and Pearce (1985) used high resolution infra-red images from NOAA7 to reveal that the poleward flow off the west coast of Australia moves against the coastline as it approaches Cape Leeuwin and continues to hug the coast as it flows eastward. They also observed that the largest current velocities (~1.8 m/s) along the southern coast of Australia occurs near Cape Leeuwin where the dynamics is influenced by the 90° corner. Godfrey and Vaudrey (1986) noted the strongly nonlinear dynamics in the neighborhood of Cape Leeuwin. Experiment 5 showed this dynamic shift, along with maximum currents and undercurrent that occurred in the vicinity of Cape Leeuwin. The magnitude of the model eastward surface current was ~0.9-1.4 m/s while that of the westward undercurrent was ~16-21 cm/s, which agrees favorably with current measurement from Cresswell and Peterson (1993), which showed eastward surface velocities of 1-1.6 m/s, and westward undercurrent velocities of ~20 cm/s at Cliffy Head.

The inclusion of the NWS waters in the model act to drive warmer waters into the Great Australian Bight and to intensify the current velocity and temperature fronts. This is consistent with observations. Rochford (1986) observed that by May the Leeuwin Current had carried the warmest water mass of relatively low salinity into the Great Australia Bight as far as 130°E. Pearce and Cresswell (1985) observed that in the austral winter a surface temperature gradient up to 5°C

may be encountered in the Leeuwin-to-Esperance region. Cresswell and Peterson (1993) also observed a Leeuwin Current recession from southern Australia by 6 March 1987. Rochford (1986) noted that the warmest water mass carried by the Leeuwin Current disappears from Southern Australia by September-October. This is consistent with the model's wind forcing effect that causes the bulk of NWS water to recede to north of Carnarvon by model day 150.

b. Comparison of Eddies

Consistent with the buoy observations of Cresswell and Golding (1979, 1980), and satellite observations of Griffiths and Pearce (1985), eddy generation occurs on the offshore side of the core of the Leeuwin Current. In Experiment 5 (and in previous experiments with an irregular coastline), the onset of instabilities occurs at preferred locations. These locations were where the coastline significantly changed, i.e., near Shark Bay, between Dongara and Fremantle, Cape Leeuwin and off the coast of Albany (see Figure 4.25 and 4.26a). Figure 4.26b shows a satellite image that agrees with the west coast preferred locations for the formation of meanders and eddy positions, while Figure 4.26c shows the south coast meanders and eddies. The eddies have time scales of months, can be anticyclonic or cyclonic, and can exist in pairs or as a separate entity, (Hamon 1965,1972; Condie and Lvey, 1988; Pearce and Griffiths, 1991). Through satellite images, semi-permanent eddies have been observed in the vicinity of Cape Leeuwin (e.g., Cresswell and Golding 1979; Godfrey et al., 1979), and there have been observations that eddies along the south coast propagate westward at a relatively slower rate (~2-5 km/day) (Cresswell and Peterson, 1993). This is consistent with the semi-permanent nature of the simulated eddies in the vicinity of Cape Leeuwin where the two poleward currents merge, the geostropic inflow is greatest, and climatological winds shift to predominantly

eastward. The two dominant eddy wavelengths of the west coast eddies of ~150 and 300 km are consistent with length scales proposed by Andrews (1983) and observed by Hamon and Cresswell (1972) and Golding and Symonds (1978) (Batteen et al., 1992). The smaller eddies of the south coast are consistent with the small eddy pairs observed by Griffiths and Pearce (1985). Griffiths and Pearce also attributed baroclinic instability as the major cause of large disturbance. They concluded based on the dimensions, separation distance, growth rates and life times of the waves and eddies, that these structures were the results of baroclinic instability. However, Experiment 5 results indicate barotropic rather than baroclinic instability as the dominant instability mechanisms. The smaller size and growth rate of eddies is thought to be a function of the increased horizontal shear force from winds and geostropic inflow.

The variety of length scales, life time scales, in conjunction with the differences in field observations themselves, emphasize the complex flow region of the Leeuwin Current System. Except for the disagreement with Griffiths and Pearce (1991) about the dominant instability mechanism for eddy development, overall, the numerical model of results of Experiment 5 have striking similarities to the field observations.

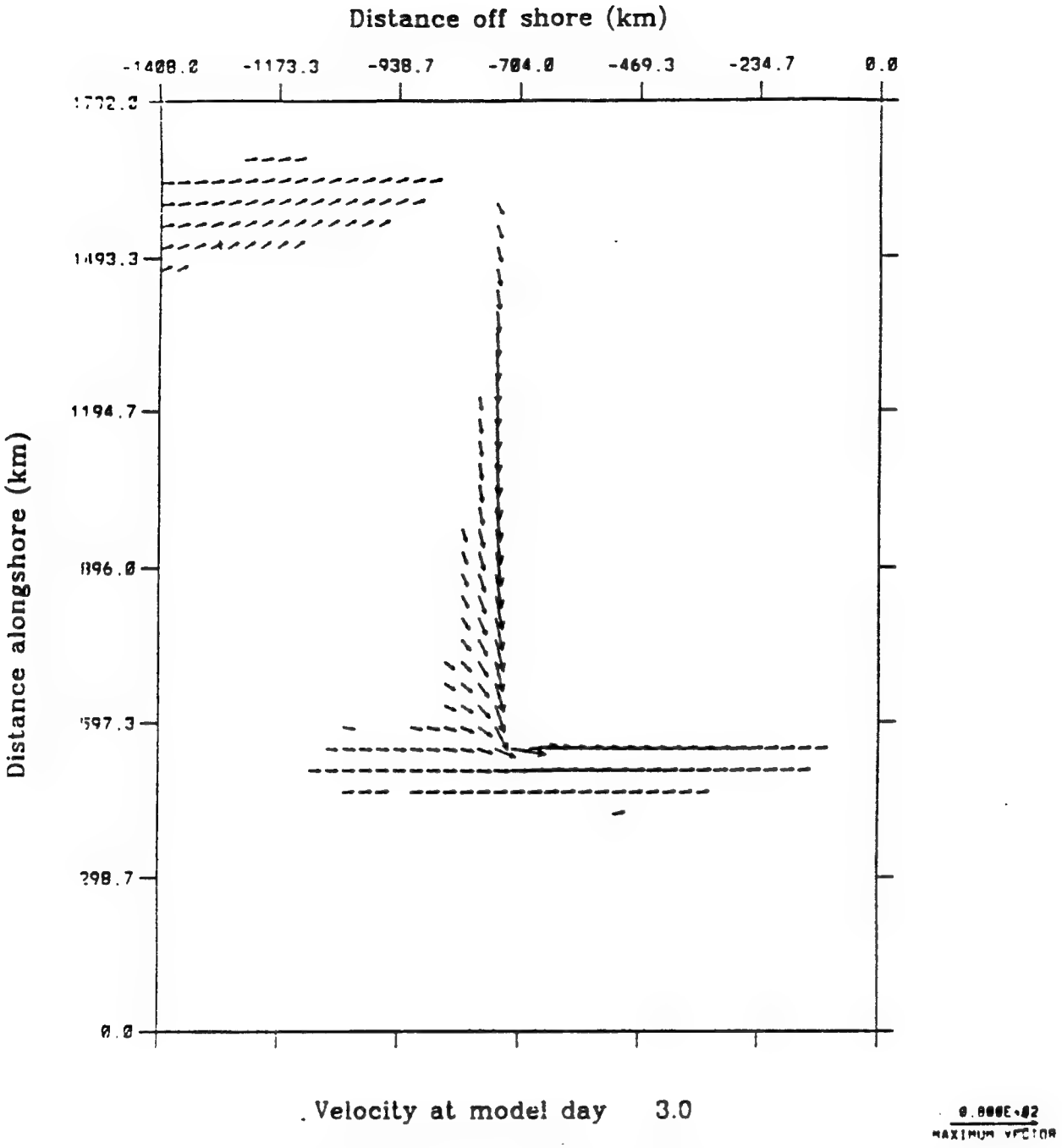

Figure 4.1a Experiment 1: Surface velocity vectors at day 3. To avoid clutter, velocity vectors are plotted at every third grid point in both the cross-shore and alongshore direction, and velocities less than 5 cm s^{-1} are not plotted.

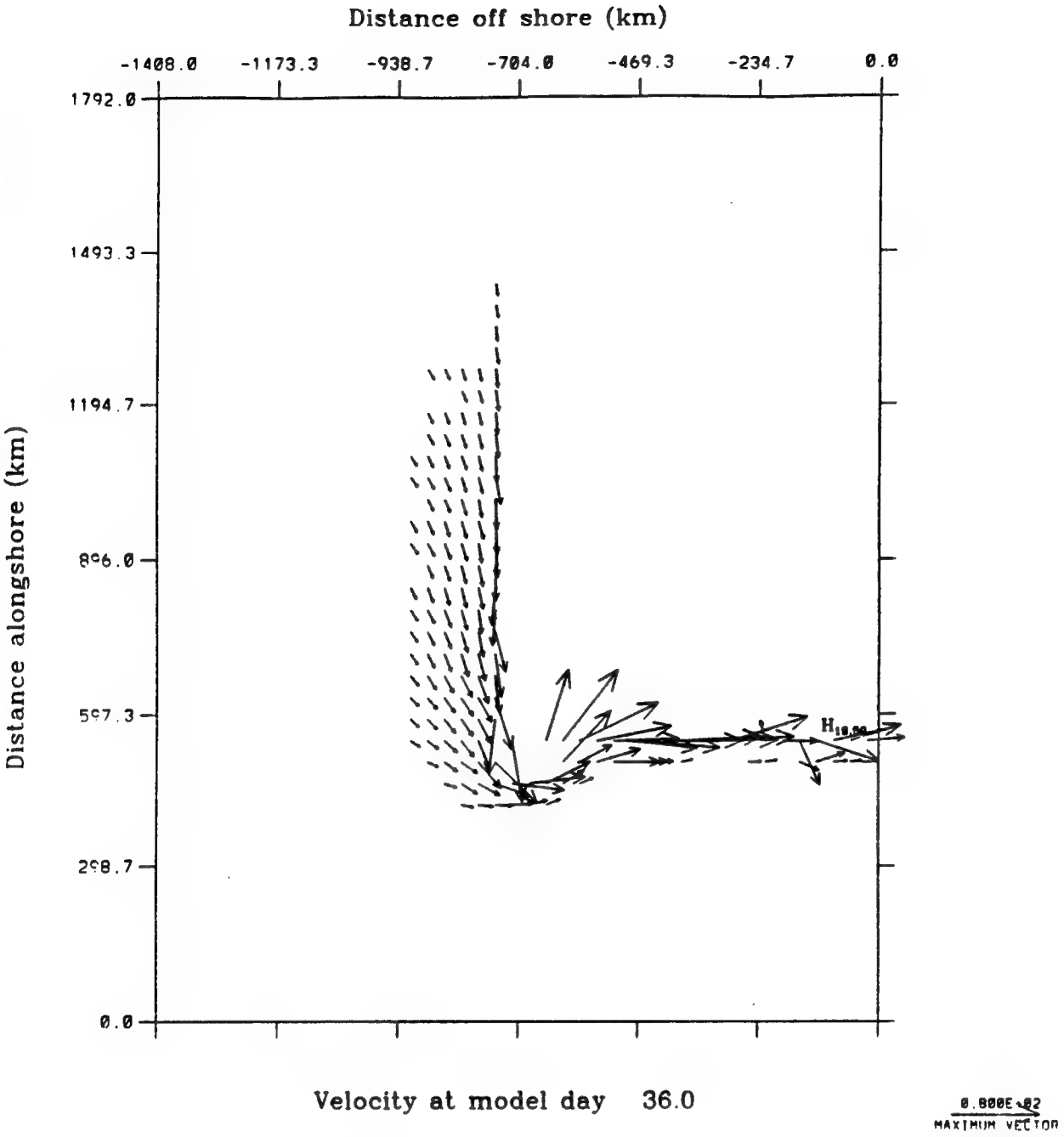

Figure 4.1b Experiment 1: Surface velocity vectors at day 36. To avoid clutter, velocity vectors are plotted at every third grid point in both the cross-shore and alongshore direction, and velocities less than 5 cm s^{-1} are not plotted. In this and the following figures, the numbers associated with the highs (H) and lows (L) correspond to temperature, not velocity. Note start of a meander at Cape Leeuwin (y~500 km).

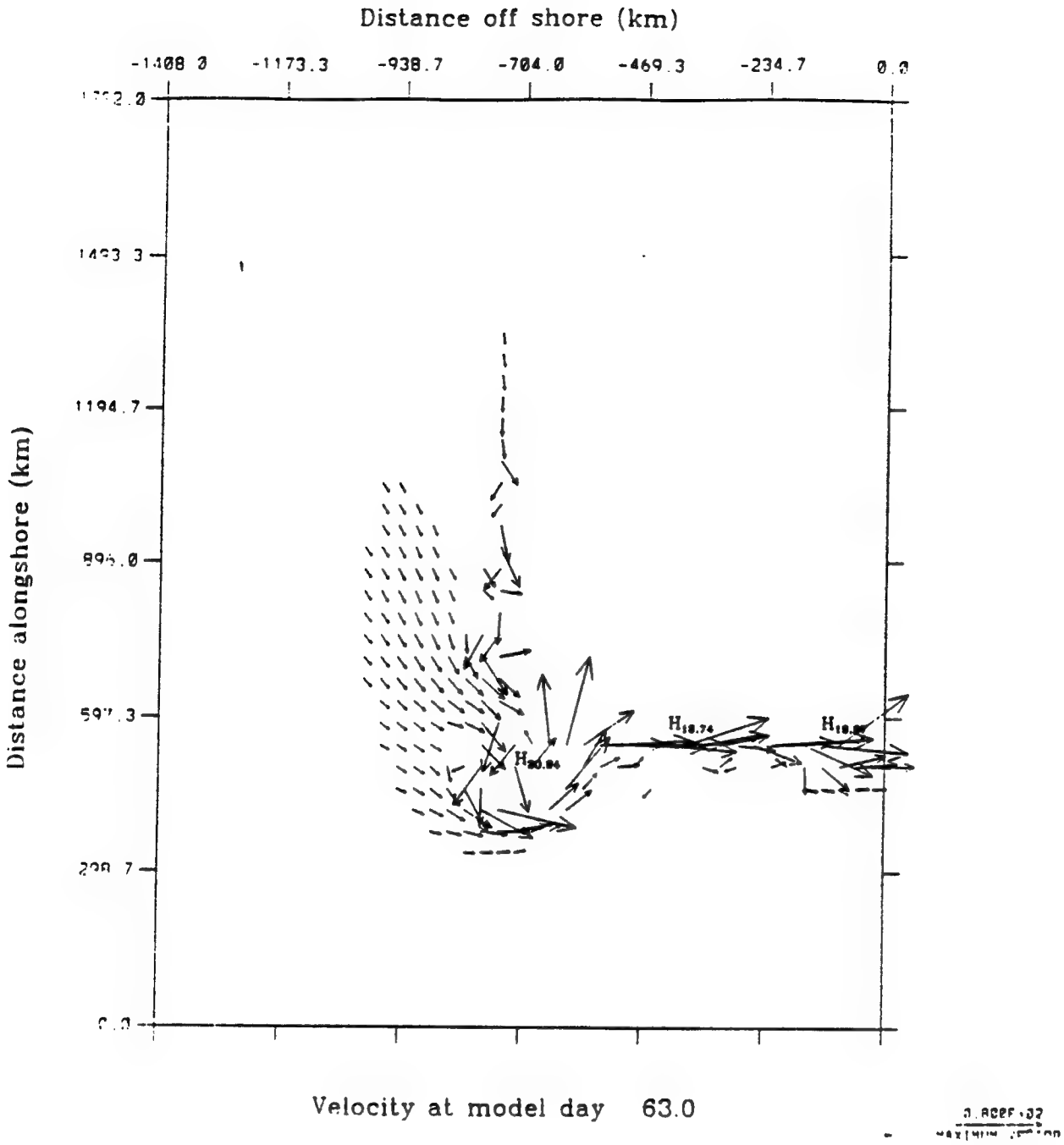

Figure 4.1c Experiment 1: Surface velocity vectors at day 63. To avoid clutter, velocity vectors are plotted at every third grid point in both the cross-shore and alongshore direction, and velocities less than 5 cm s^{-1} are not plotted. Note the formation of an anticyclonic eddy at Cape Leeuwin (y~500 km).

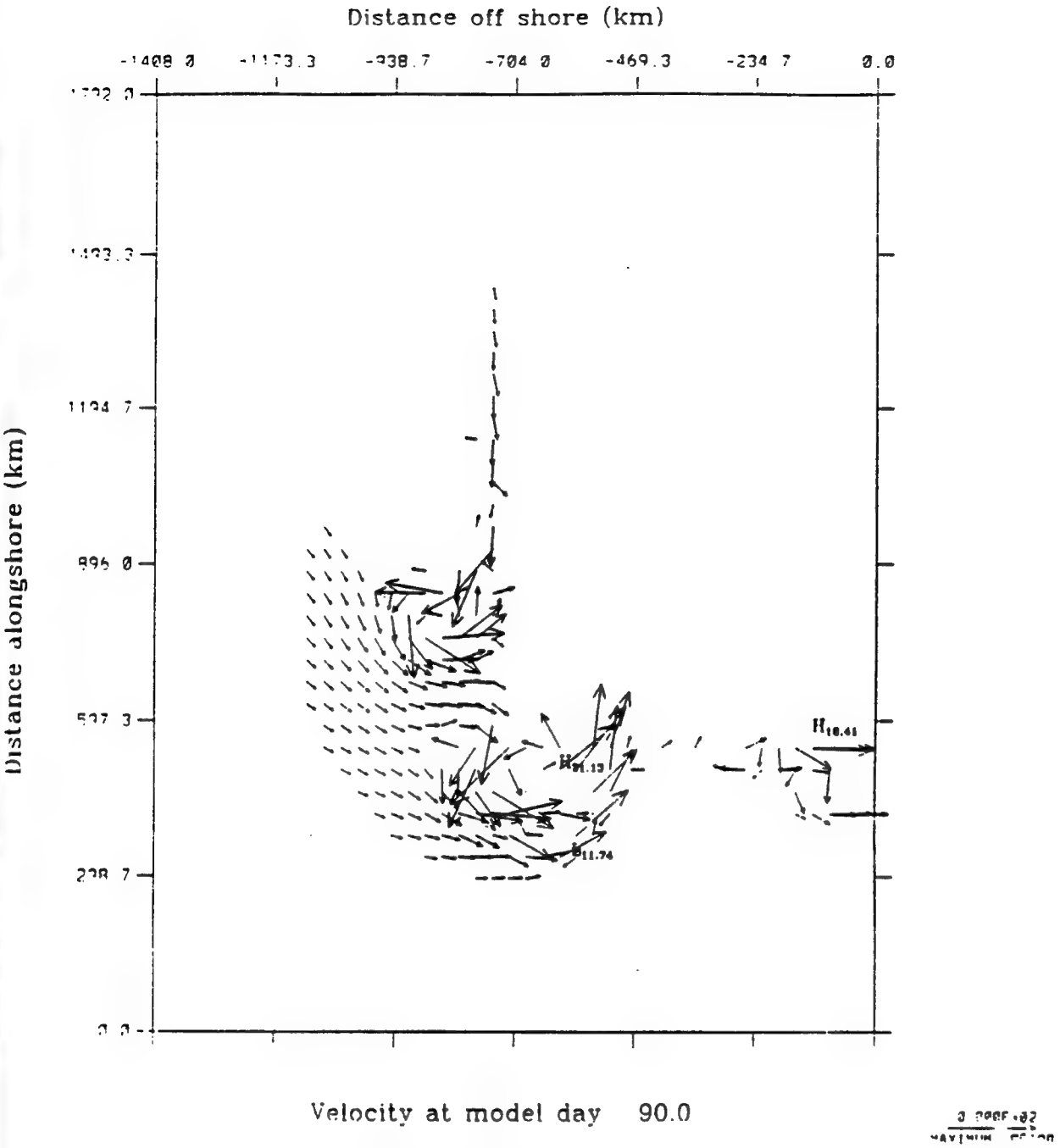

Figure 4.1d Experiment 1: Surface velocity vectors at day 90. To avoid clutter, velocity vectors are plotted at every third grid point in both the cross-shore and alongshore direction, and velocities less than 5 cm s^{-1} are not plotted. Note the formation of an anticyclonic eddy at Fremantle (y~850 km).

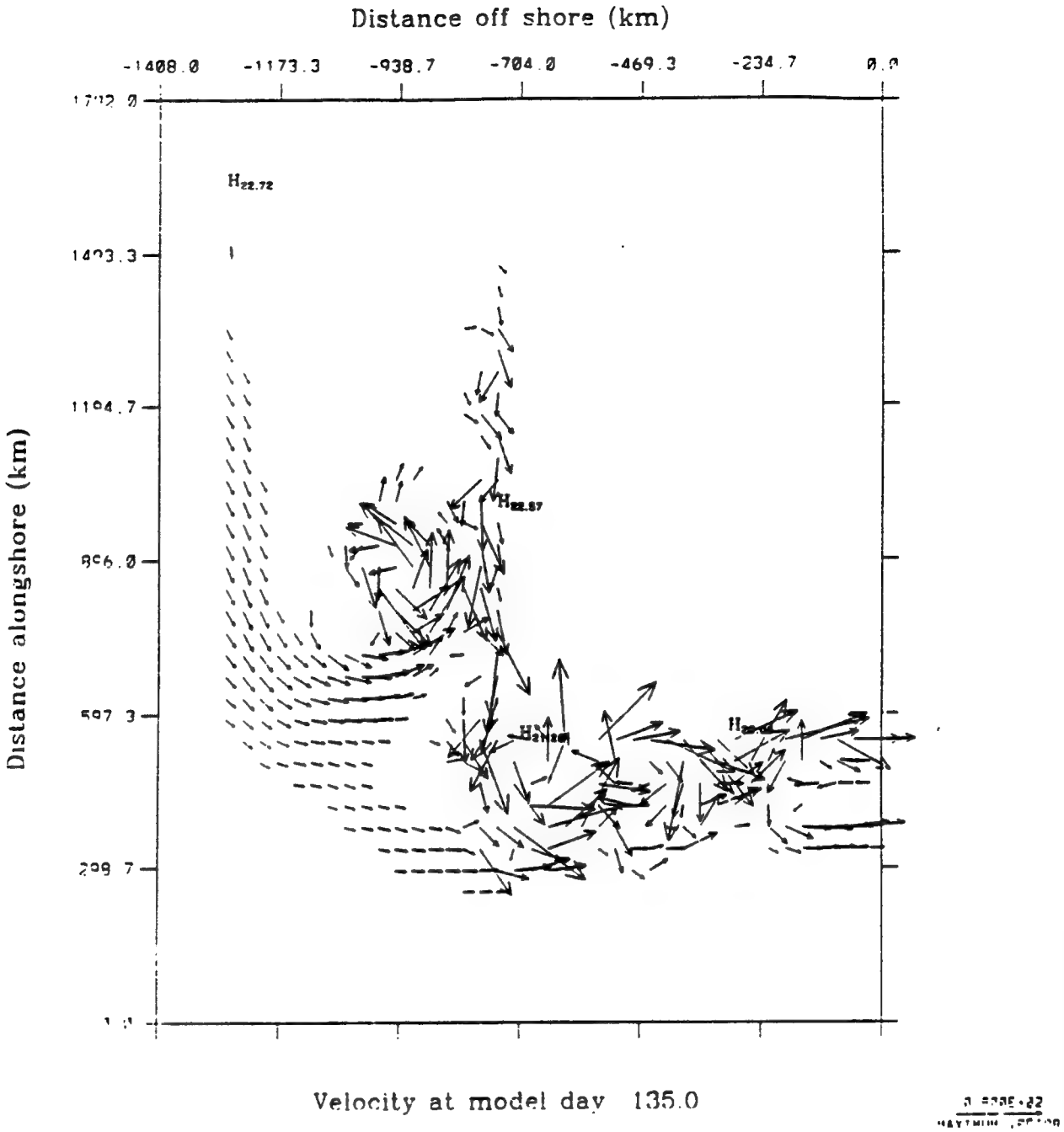

Figure 4.1e Experiment 1: Surface velocity vectors at day 135. To avoid clutter, velocity vectors are plotted at every third grid point in both the cross-shore and alongshore direction, and velocities less than 5 cm s^{-1} are not plotted. Note the formation of an anticyclonic eddy pairs along the south coast at y~500 km, x~500 km.

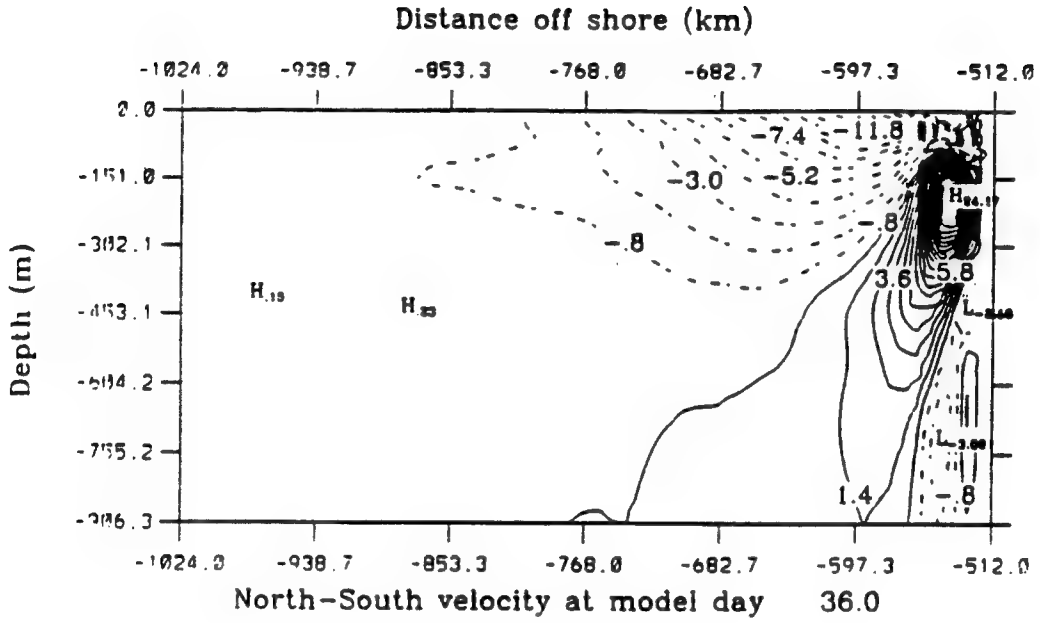

Figure 4.2a Experiment 1: Cross-section north of Cape Leeuwin (y~715 km) (32.5° S) of the north-south component of velocity at day 36. Solid lines indicate equatorward flow, while dashed lines indicate poleward flow.

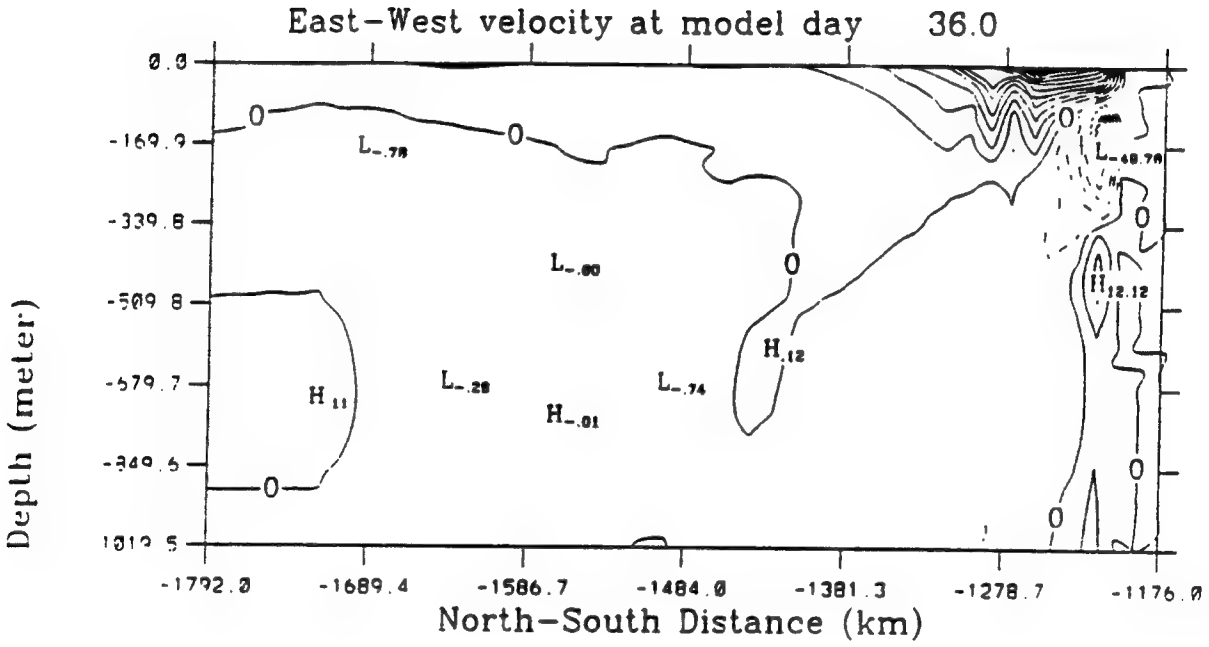

Figure 4.2b Experiment 1: Cross-section at Cliffy Head (x~770 km) (116° S) of the east-west component of velocity at day 36. Solid lines indicate eastward flow, while dashed lines indicate westward flow.

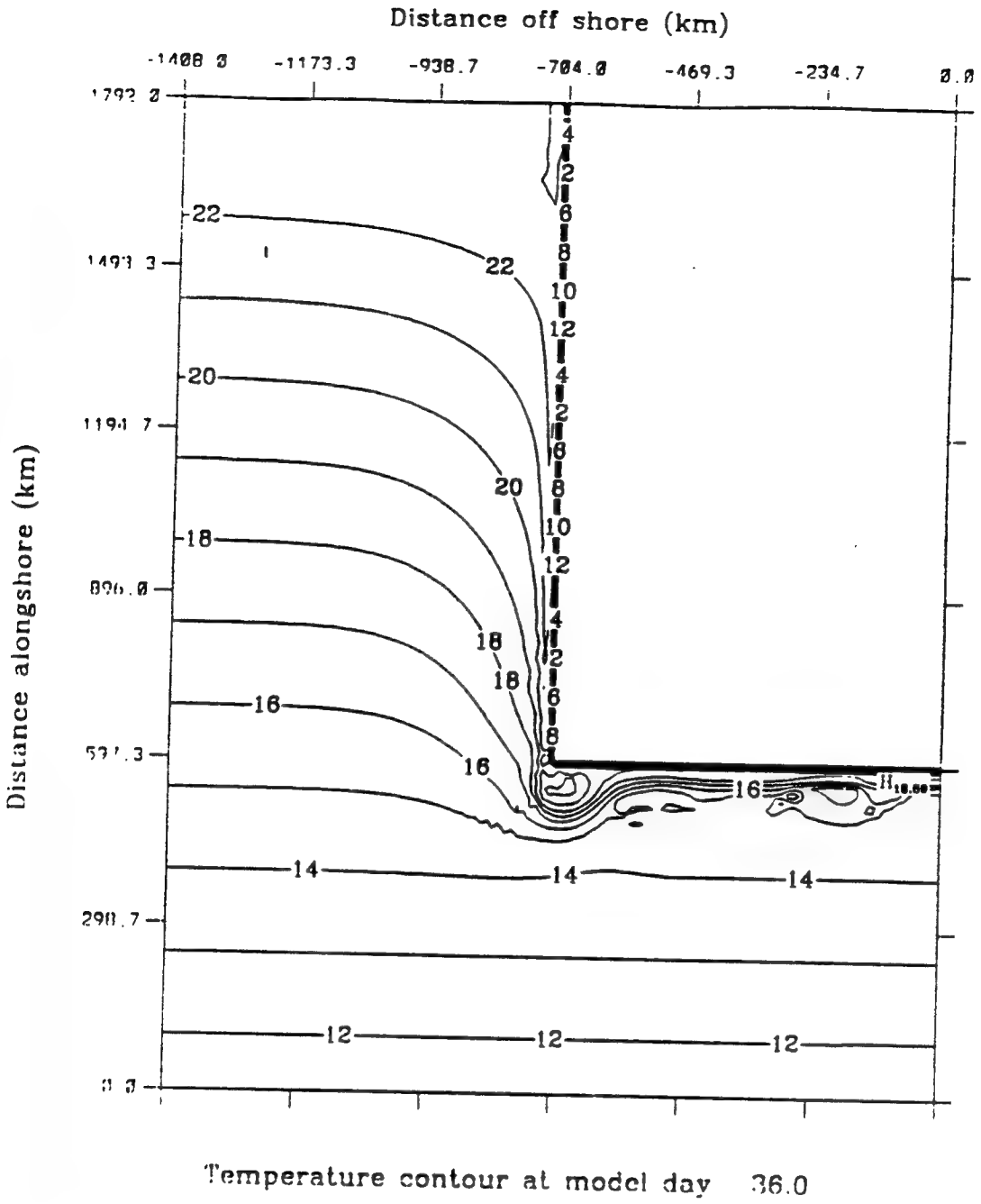

Figure 4.3a Experiment 1: Surface temperature at day 36. The contour interval is 1° C. The temperature increases towards the west coast.

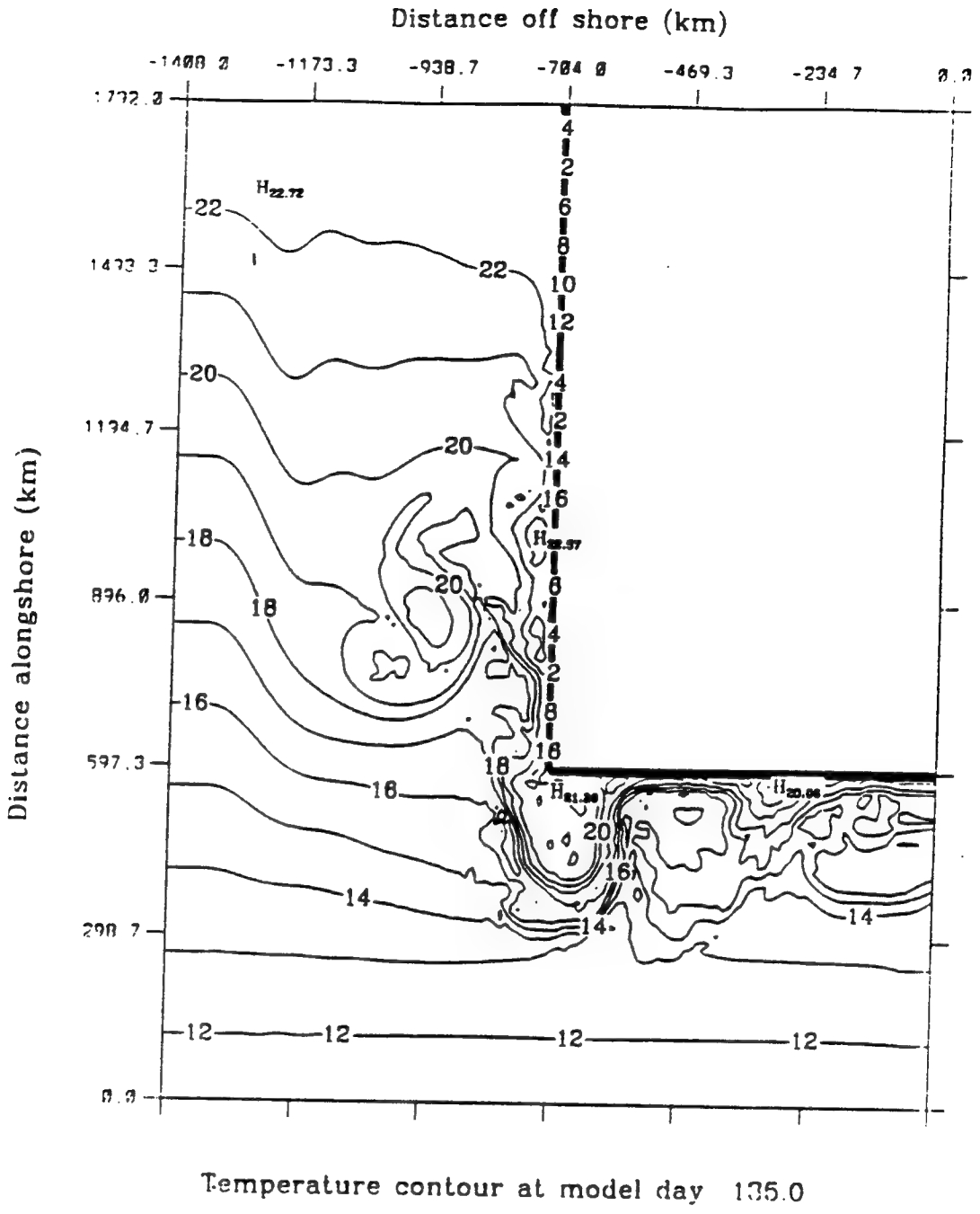

Figure 4.3b Experiment 1: Surface temperature at day 135. The contour interval is 1° C. The temperature increases towards the west coast.

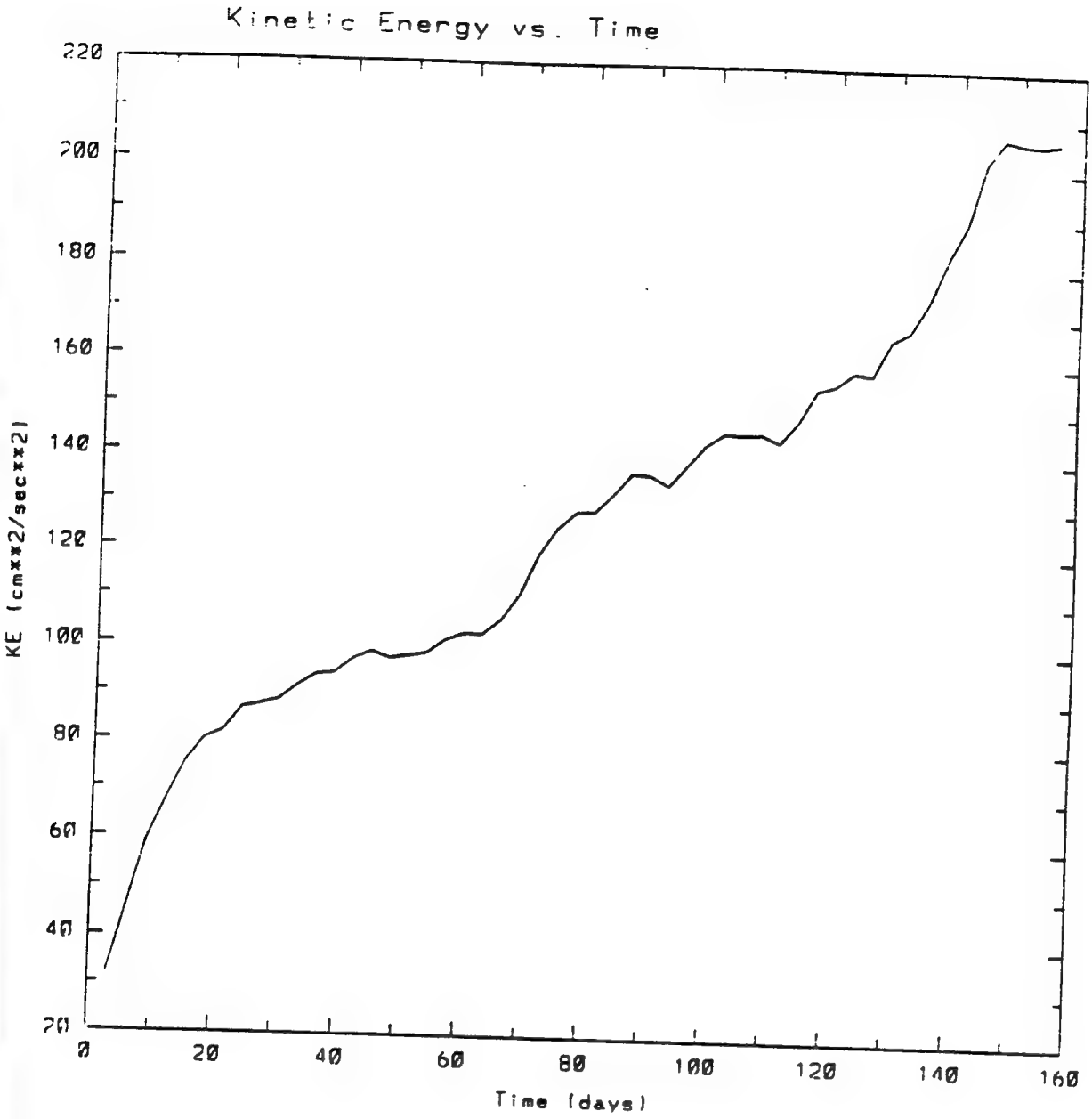

Figure 4.4 Experiment 1: Total kinetic energy per unit mass time series for the first 150 model days averaged over the entire domain (Units of the kinetic energy are cm^2s^{-2}).

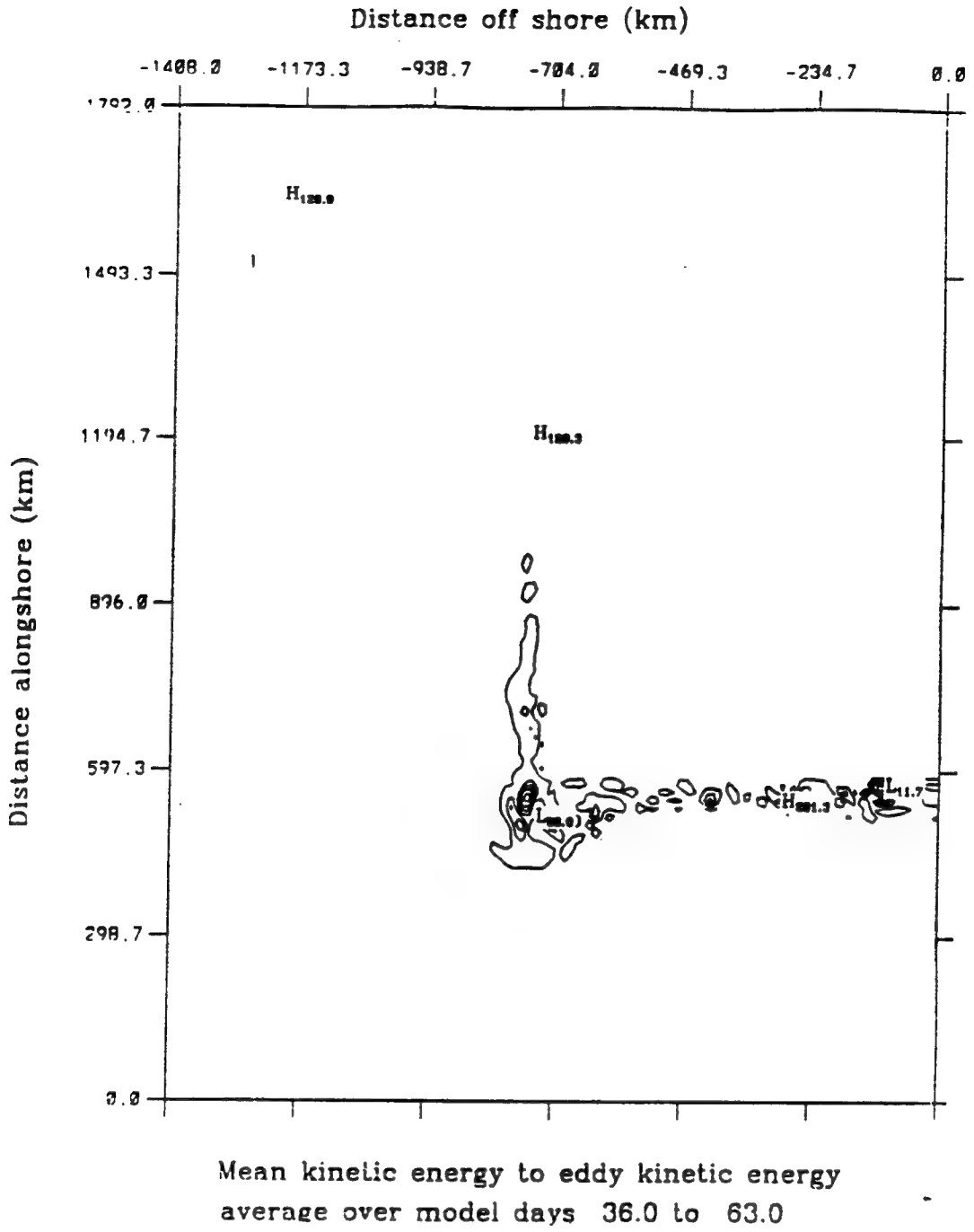

Figure 4.5a Experiment 1: Energy transfers of mean to eddy kinetic energy (i.e., barotropic energy transfer) for model days 36 to 63. The contour interval is 1 ergs cm^{-3} s^{-1}.

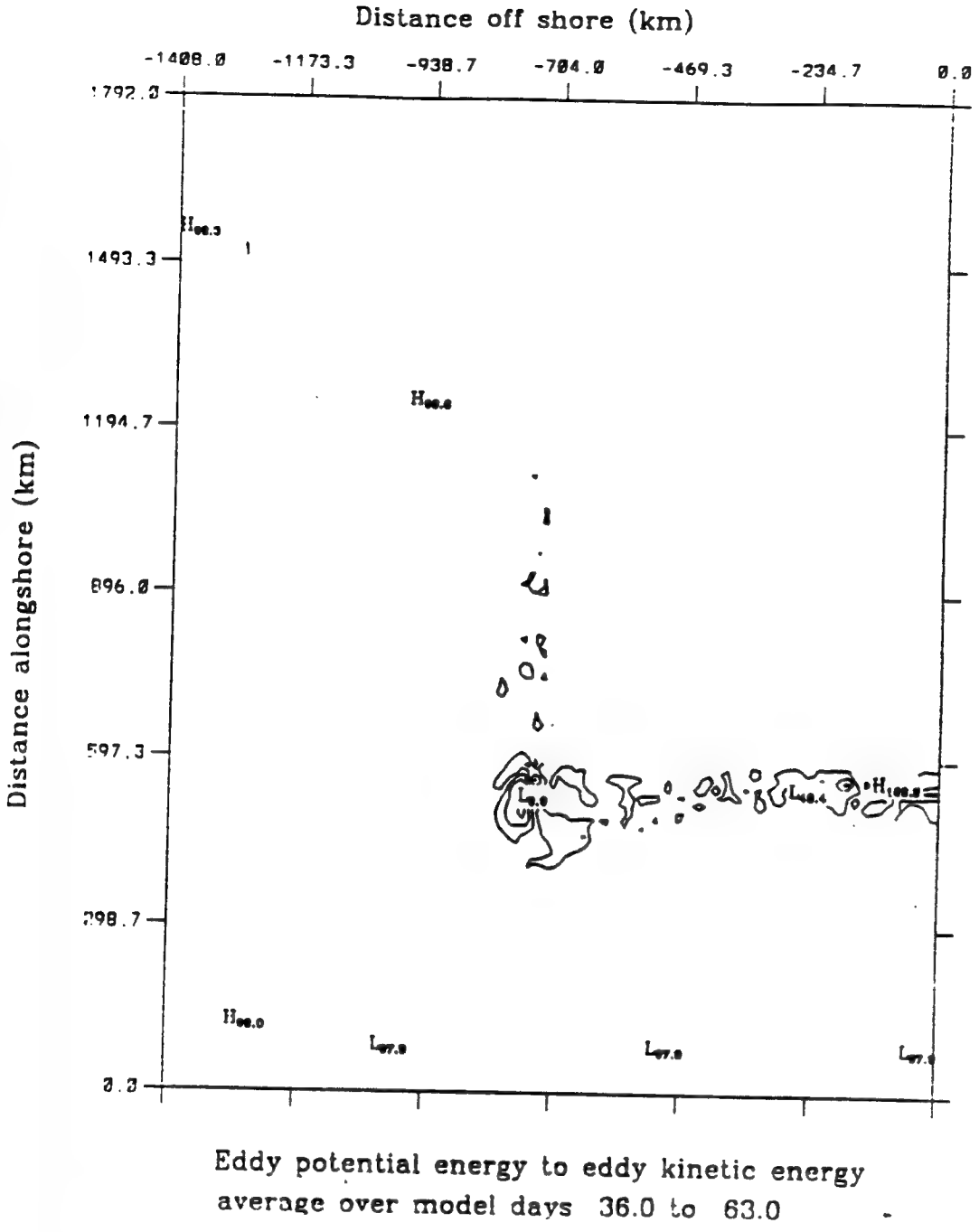

Figure 4.5b Experiment 1: Energy transfers of eddy potential to eddy kinetic energy (i.e., baroclinic energy transfer) for model days 36 to 63. The contour interval is 1 ergs cm^{-3} s^{-1}.

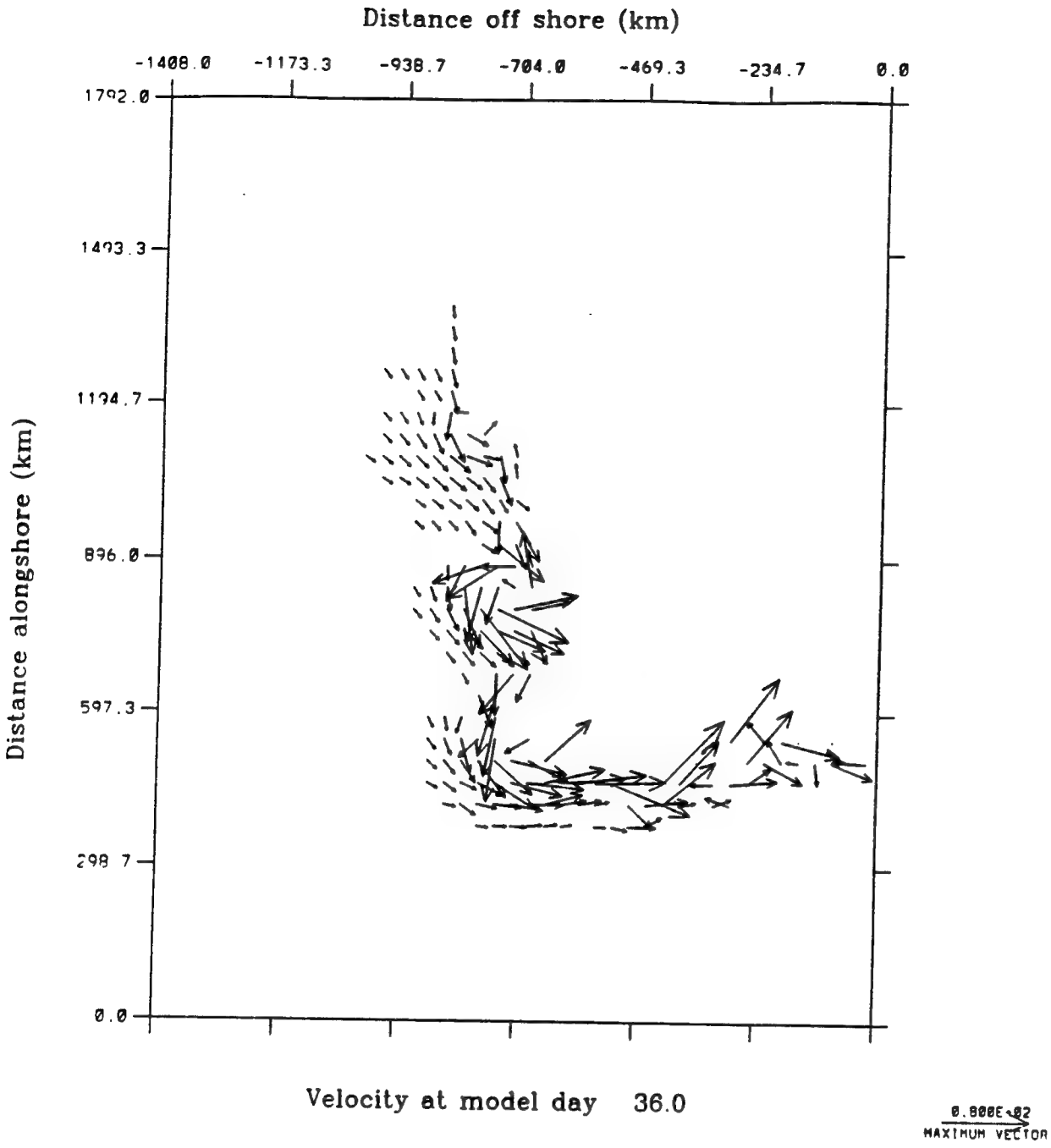

Figure 4.6a Experiment 2: Surface velocity vectors at day 36. To avoid clutter, velocity vectors are plotted at every third grid point in both the cross-shore and alongshore direction, and velocities less than 5 cm s^{-1} are not plotted. Note large undulations near the Shark Bay meander (y~1000 km) and Fremantle meander (y~850 km).

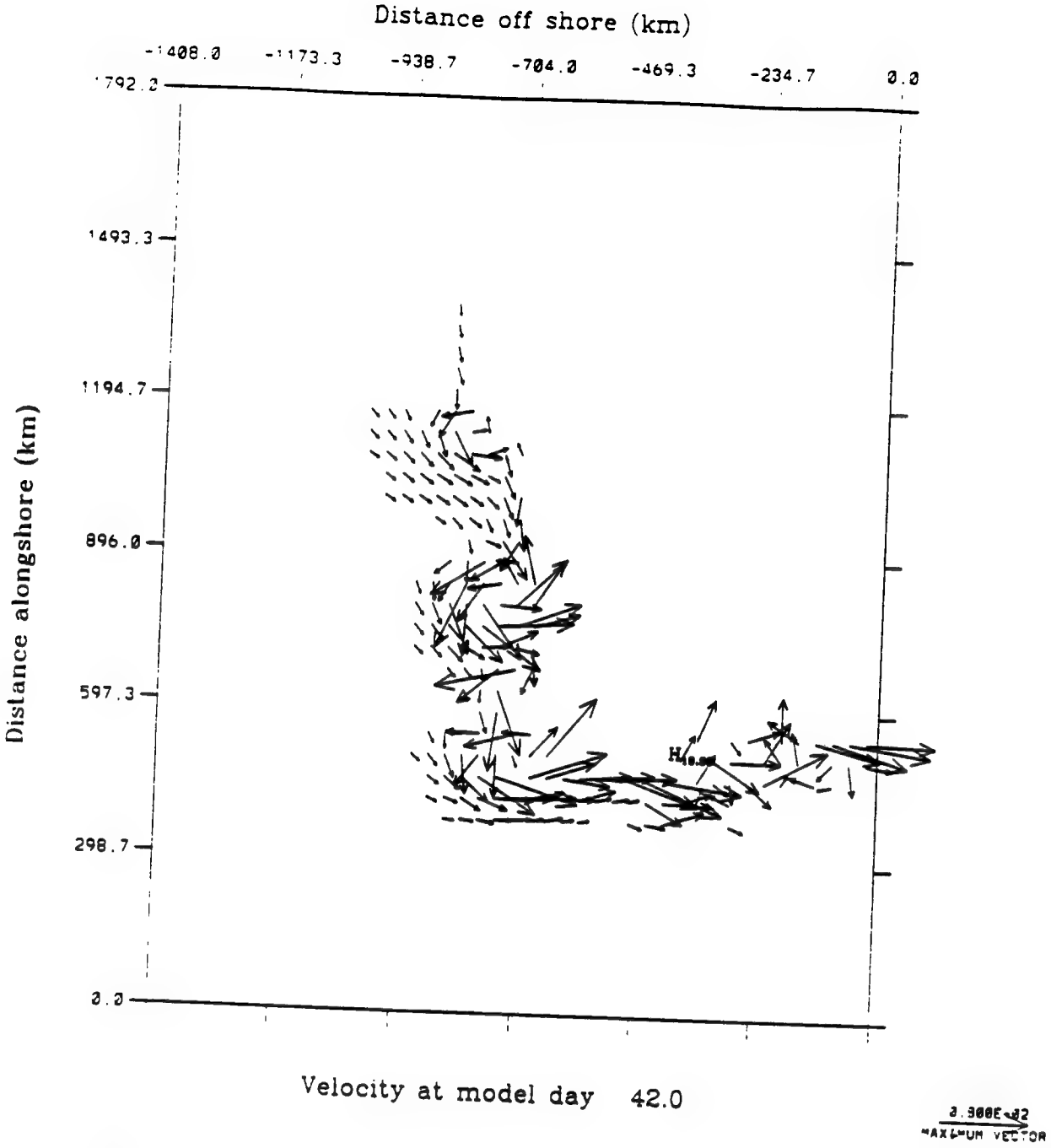

Figure 4.6b Experiment 2: Surface velocity vectors at day 42. To avoid clutter, velocity vectors are plotted at every third grid point in both the cross-shore and alongshore direction, and velocities less than 5 cm s^{-1} are not plotted. Note intensifying undulations and offshoots at Esperance (x~100 km).

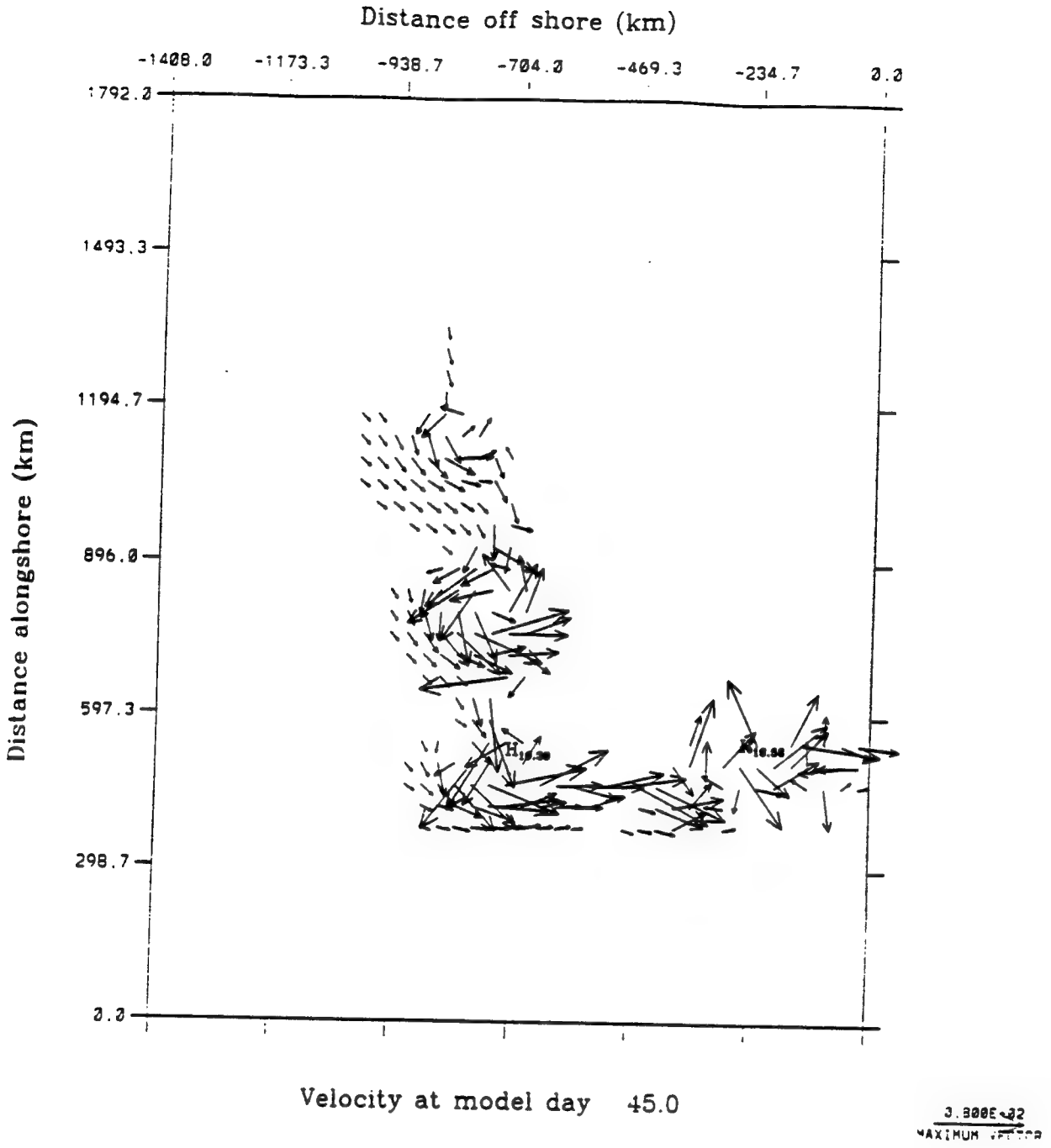

Figure 4.6c Experiment 2: Surface velocity vectors at day 45. To avoid clutter, velocity vectors are plotted at every third grid point in both the cross-shore and alongshore direction, and velocities less than 5 cm s^{-1} are not plotted. Note the formation of anticyclonic eddies at Cape Leeuwin (y~500 km), Fremantle (y~850 km) and Shark Bay (y~1000 km).

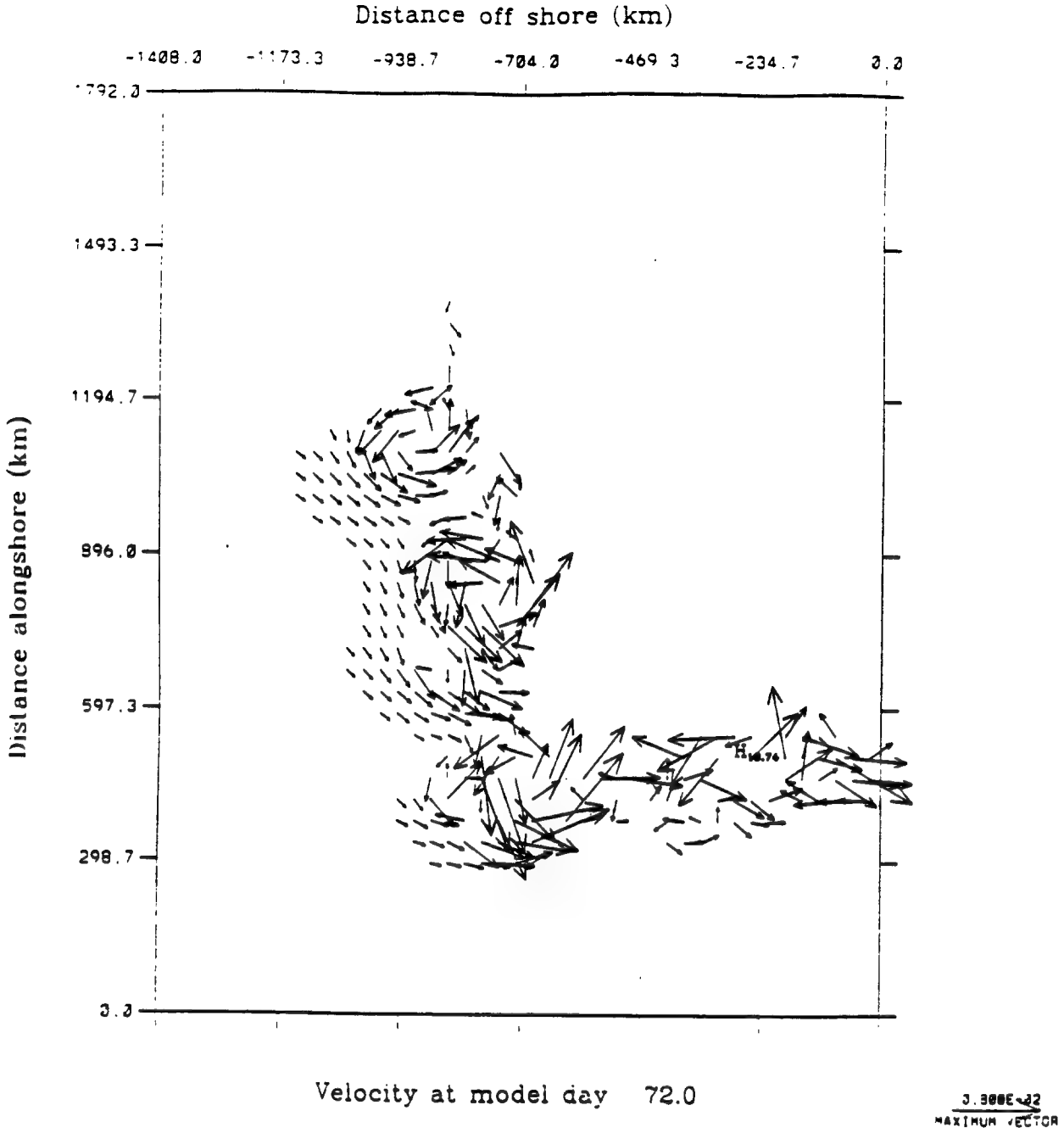

Figure 4.6d Experiment 2: Surface velocity vectors at day 72. To avoid clutter, velocity vectors are plotted at every third grid point in both the cross-shore and alongshore direction, and velocities less than 5 cm s^{-1} are not plotted. Note the formation of an anticyclonic eddy between Albany and Esperance (x~400 km).

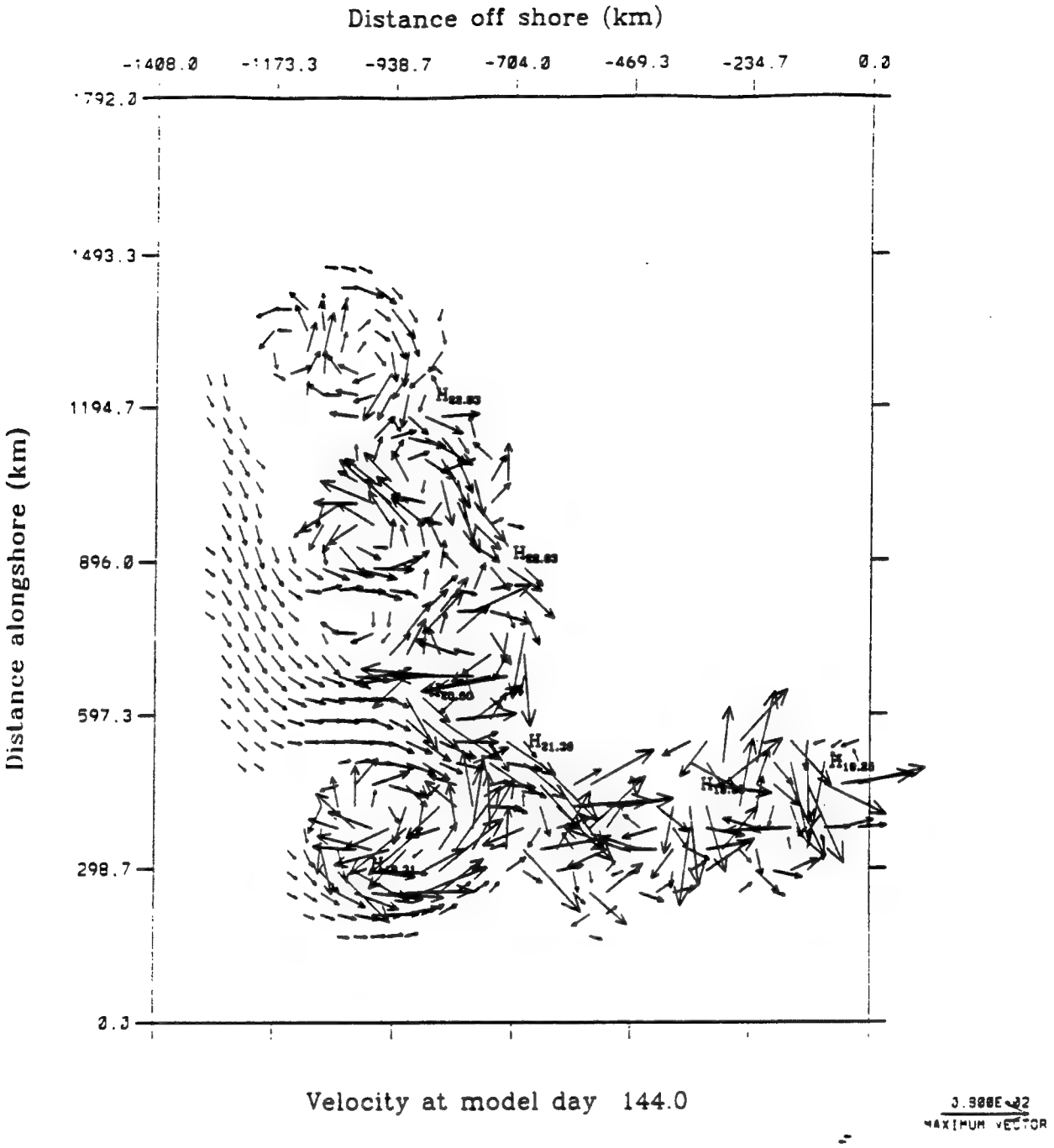

Figure 4.6e Experiment 2: Surface velocity vectors at day 144. To avoid clutter, velocity vectors are plotted at every third grid point in both the cross-shore and alongshore direction, and velocities less than 5 cm s^{-1} are not plotted. Note that the Leeuwin Current is no longer distinctly defined along the Southern Australian coast due to meanders and eddy pairs in the coastal region.

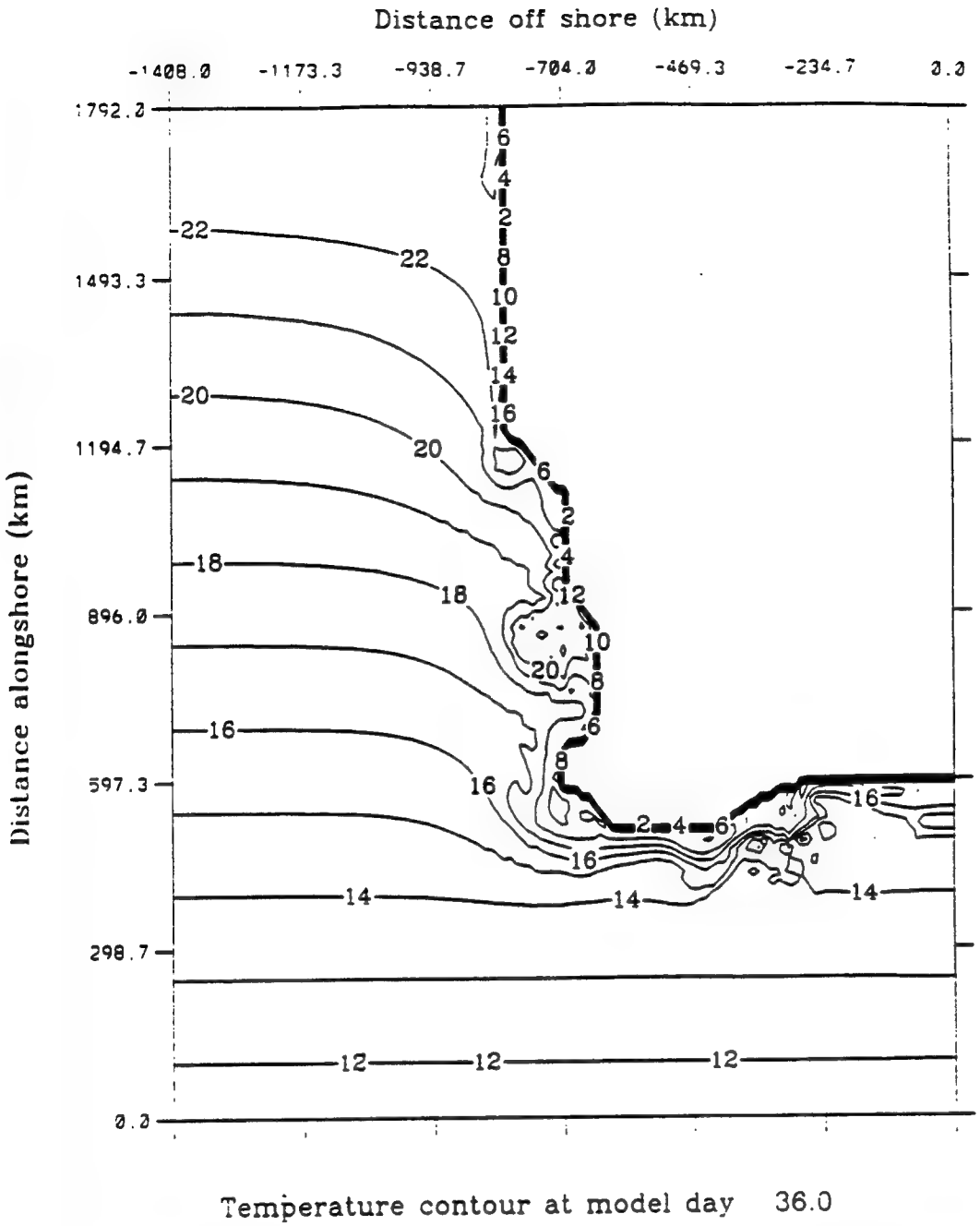

Figure 4.7 Experiment 2: Surface temperature at day 36. The contour interval is 1° C. The temperature increases towards the west coast.

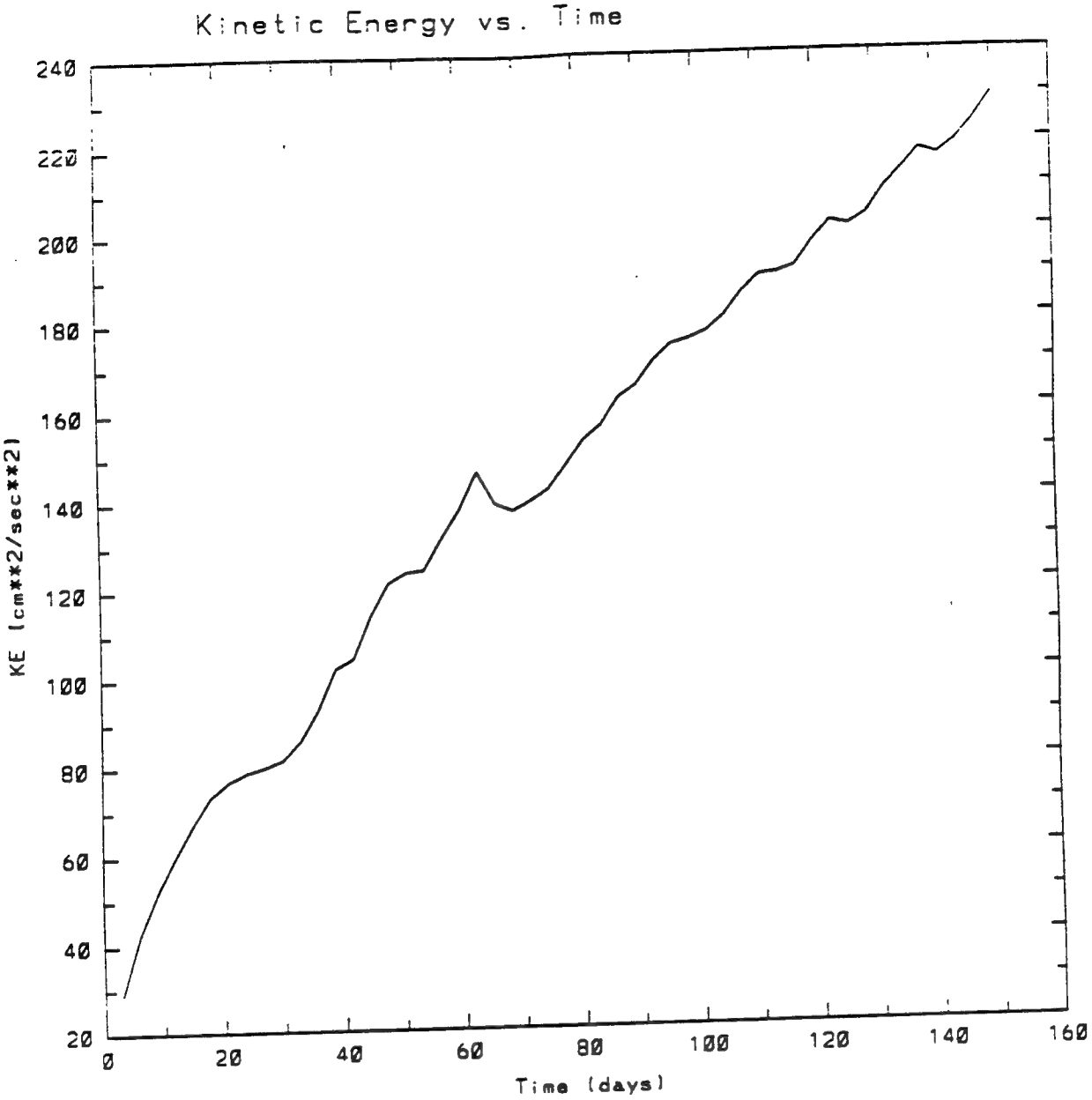

Figure 4.8 Experiment 2: Total kinetic energy per unit mass time series for the first 150 model days averaged over the entire domain (Units of the kinetic energy are cm^2s^{-2}).

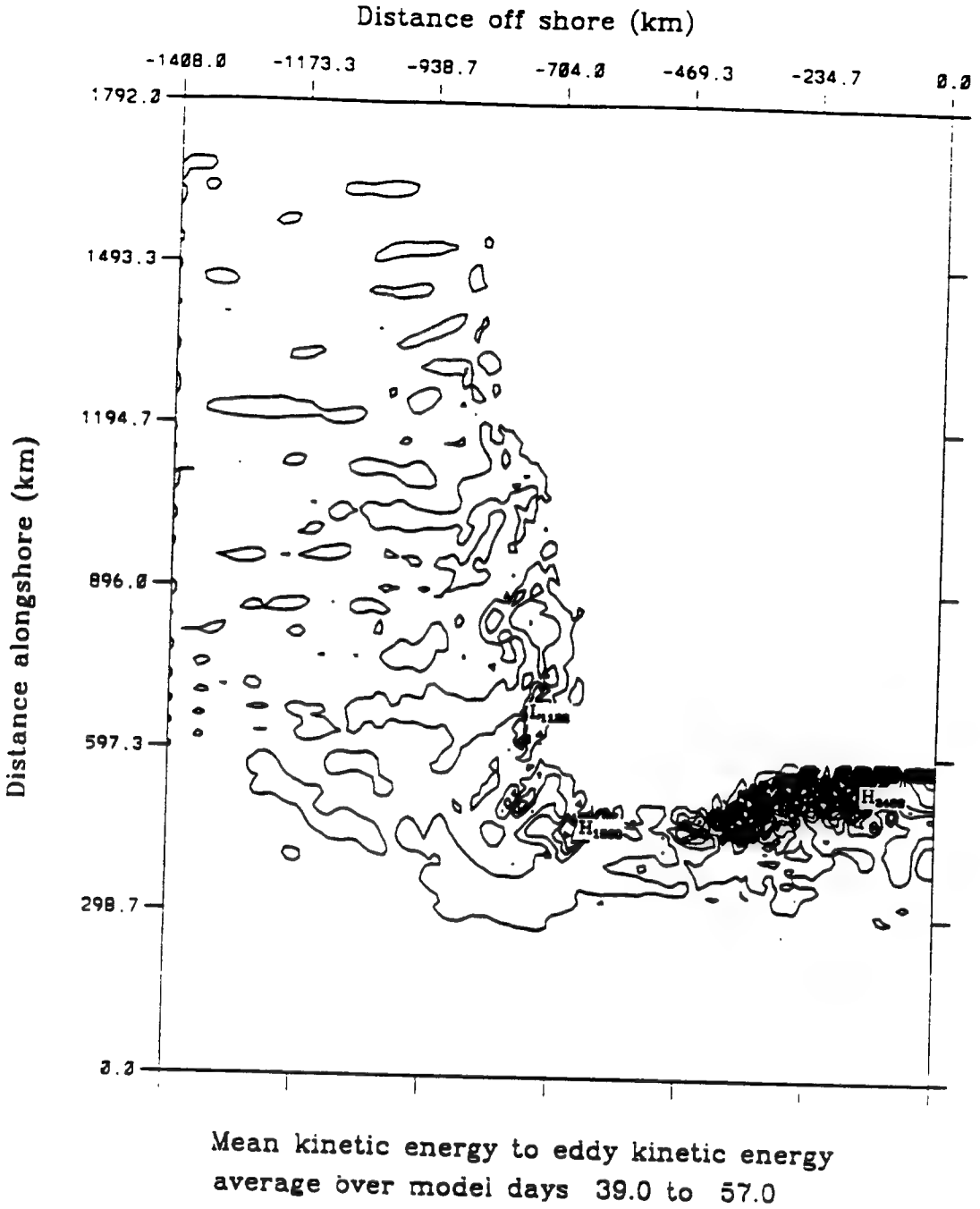

Figure 4.9a Experiment 2: Energy transfers of mean to eddy kinetic energy (i.e., barotropic energy transfer) for model days 39 to 57. The contour interval is 1 ergs cm^{-3} s^{-1}.

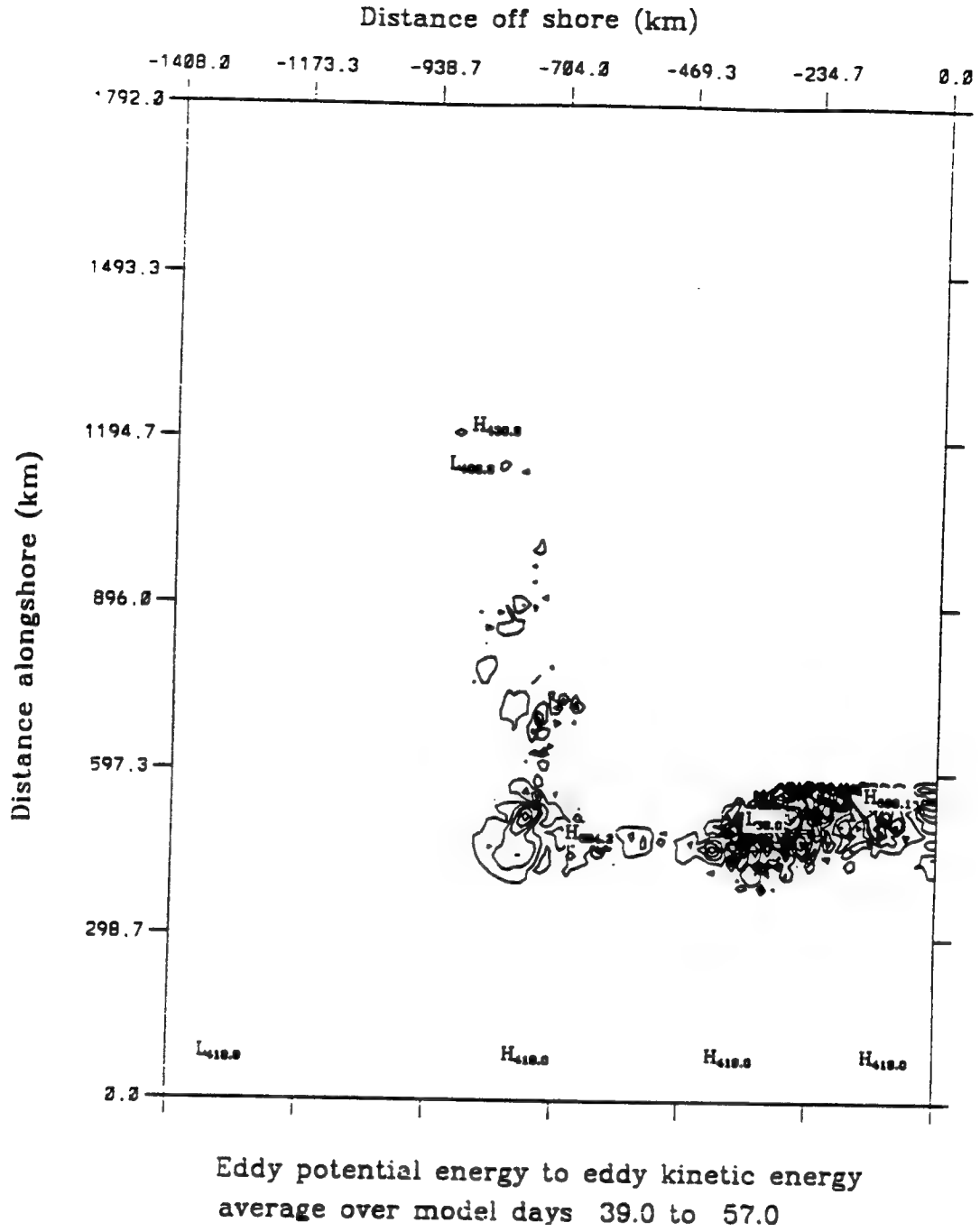

Figure 4.9b Experiment 2: Energy transfers of eddy potential to eddy kinetic energy (i.e., baroclinic energy transfer) for model days 39 to 57. The contour interval is 1 ergs cm^{-3} s^{-1}.

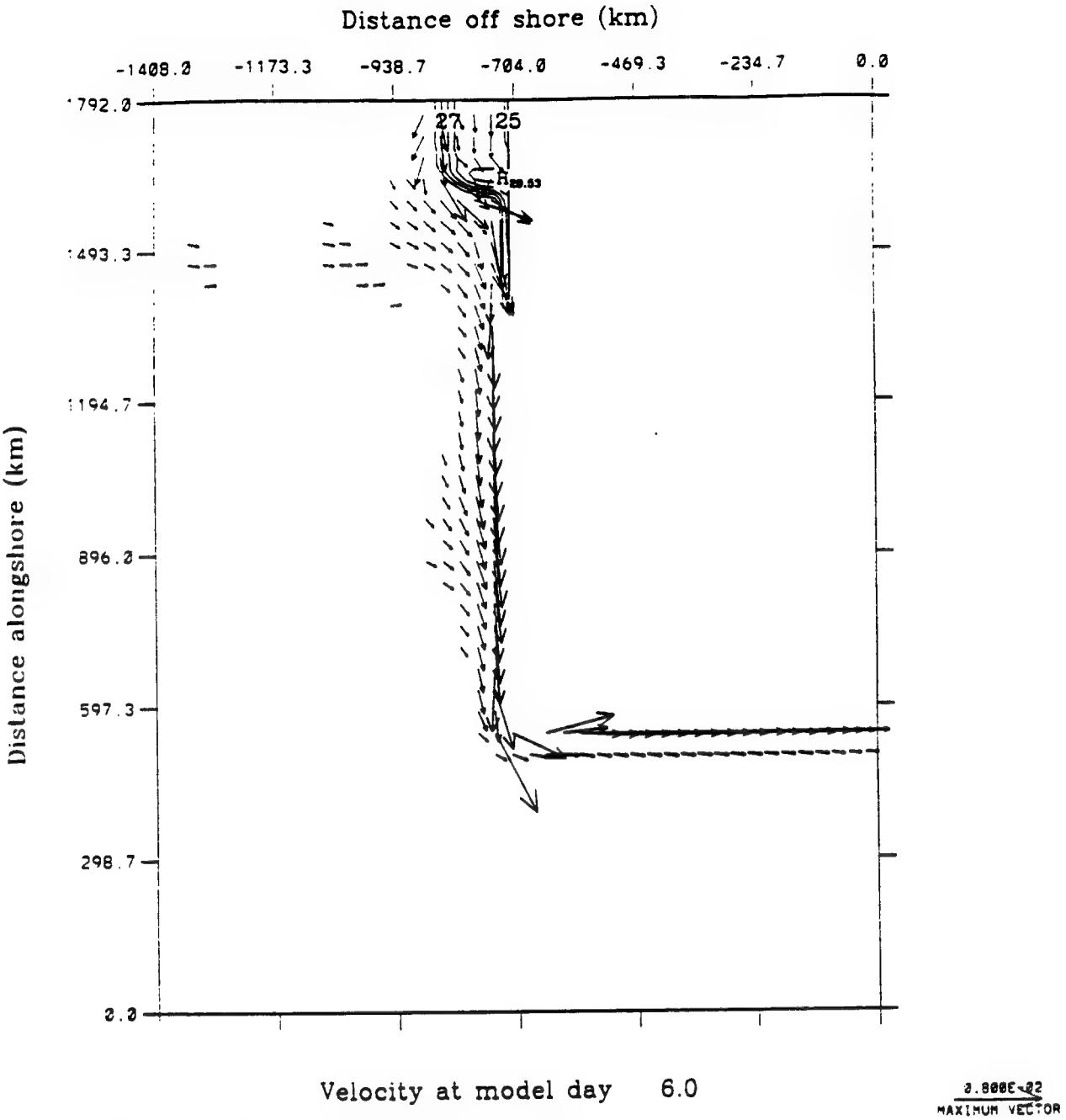

Figure 4.10a Experiment 3: Surface velocity vectors at day 6. To avoid clutter, velocity vectors are plotted at every third grid point in both the cross-shore and alongshore direction, and velocities less than 5 cm s^{-1} are not plotted. Note a small anticyclonic eddy near the NWS water source region (y~1500), and the large offshoot near Cape Leeuwin (y~500 km).

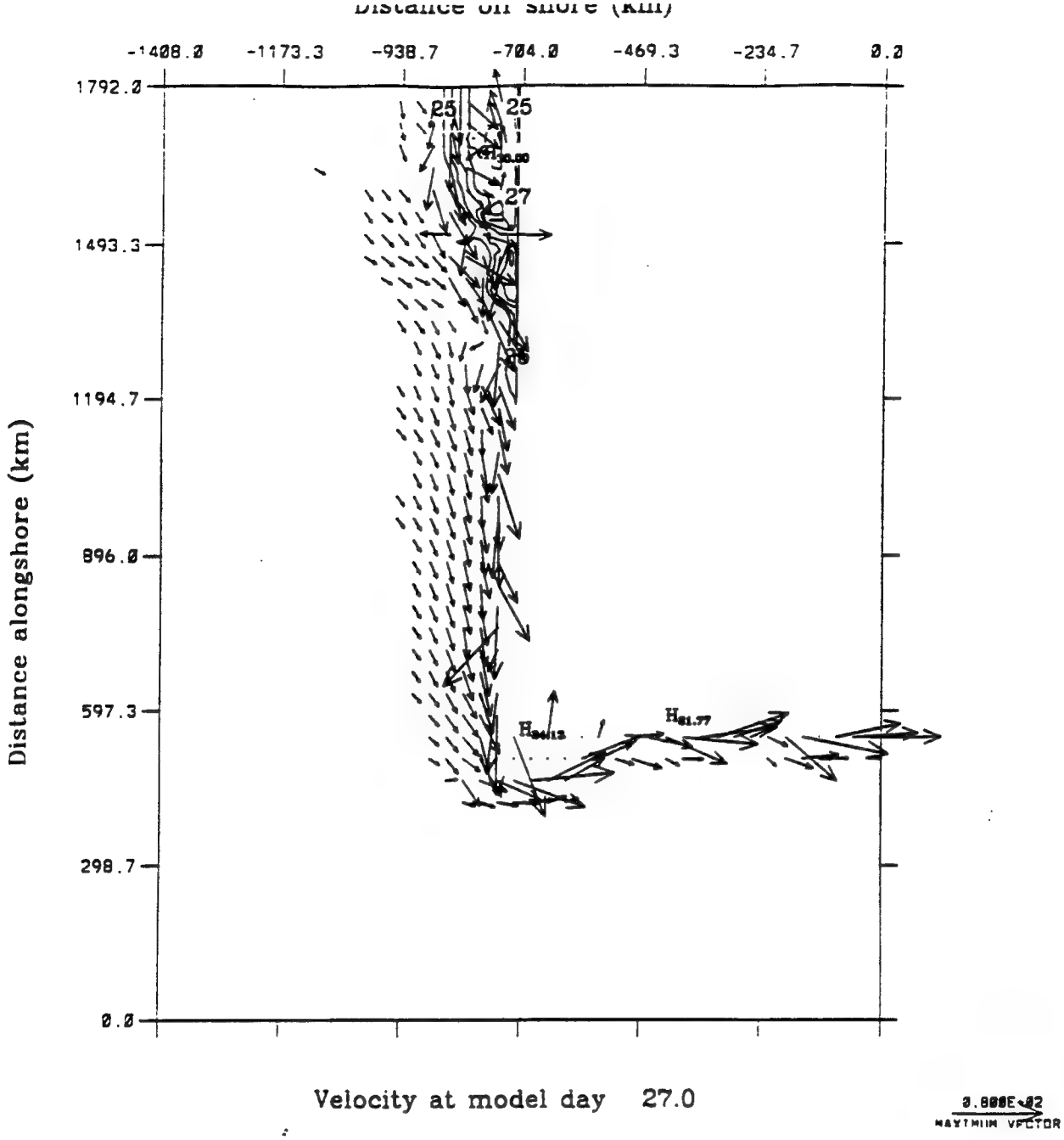

Figure 4.10b Experiment 3: Surface velocity vectors at day 27. To avoid clutter, velocity vectors are plotted at every third grid point in both the cross-shore and alongshore direction, and velocities less than 5 cm s^{-1} are not plotted. Note anticyclonic meanders, one just south of Shark Bay (y~1000 km), and one at Cape Leeuwin (y~500 km).

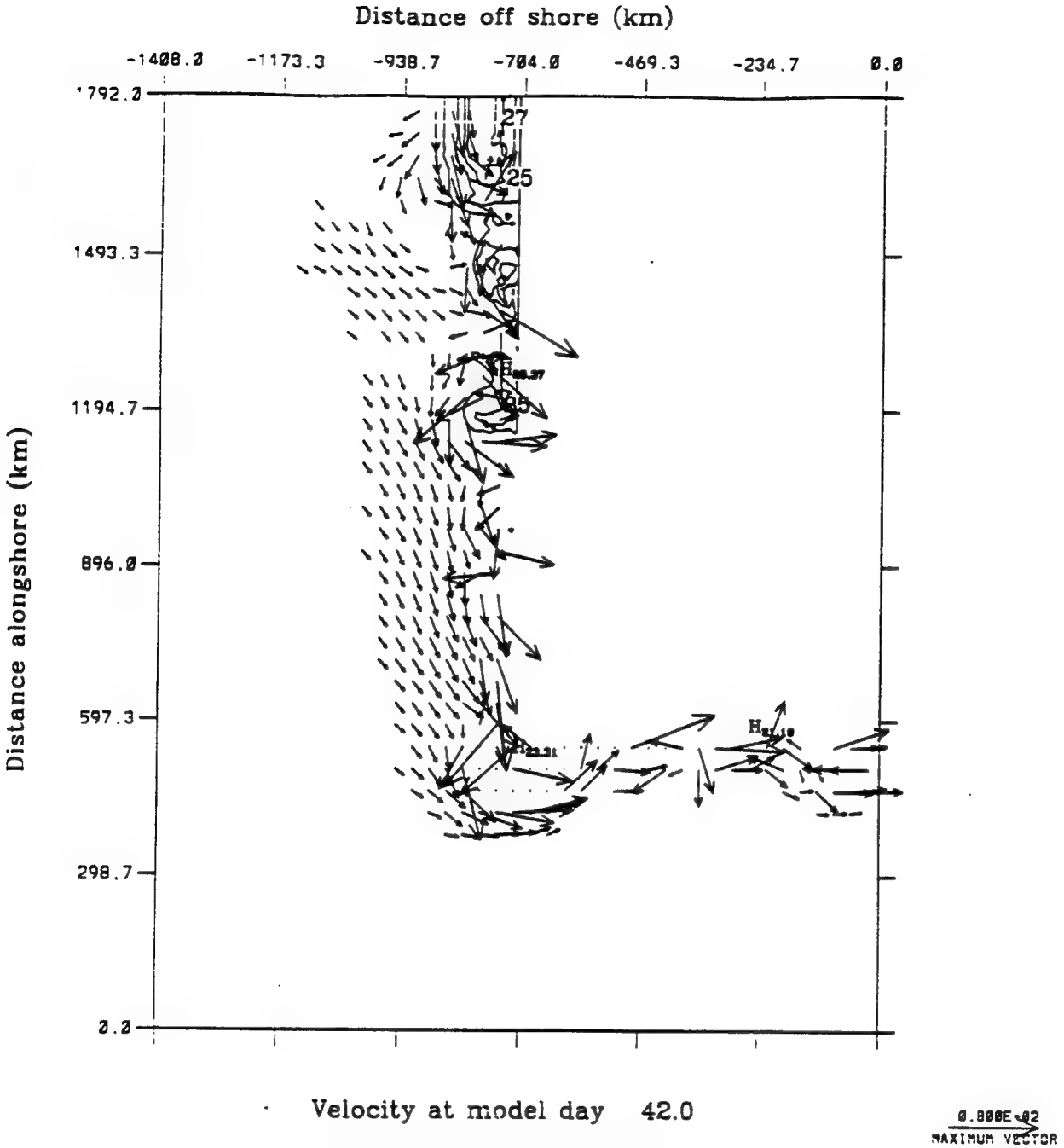

Figure 4.10c Experiment 3: Surface velocity vectors at day 42. To avoid clutter, velocity vectors are plotted at every third grid point in both the cross-shore and alongshore direction, and velocities less than 5 cm s^{-1} are not plotted. Note the formation of intense anticyclonic meanders at Cape Leeuwin (y~500 km), Fremantle (y~850 km) and Shark Bay (y~1000 km).

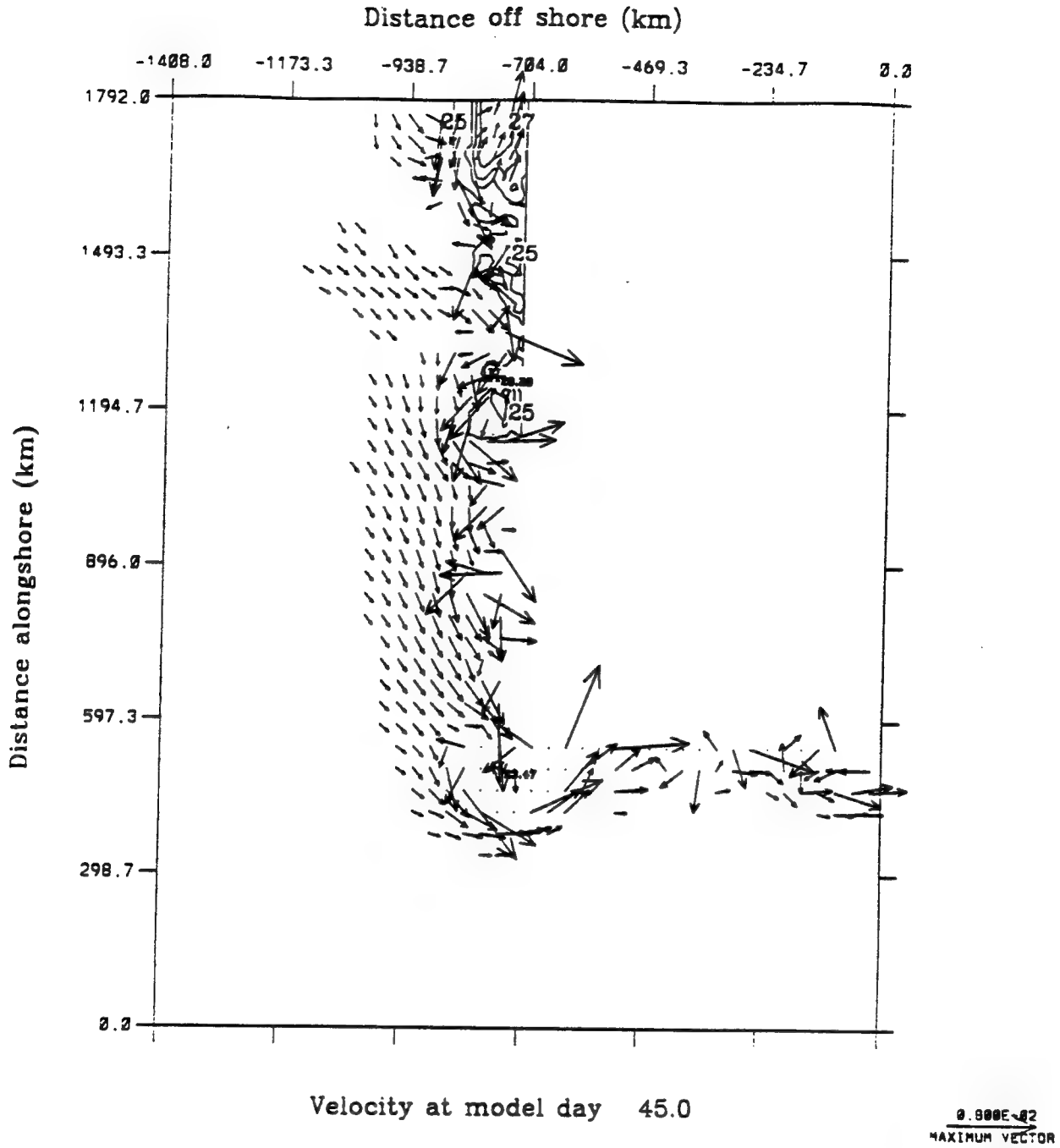

Figure 4.10d Experiment 3: Surface velocity vectors at day 45. To avoid clutter, velocity vectors are plotted at every third grid point in both the cross-shore and alongshore direction, and velocities less than 5 cm s^{-1} are not plotted. Note the anticyclonic eddies near the NWS water source region (y~1700 km), Shark Bay (y~1000 km), Fremantle (y~850 km), and Cape Leeuwin (y~500 km).

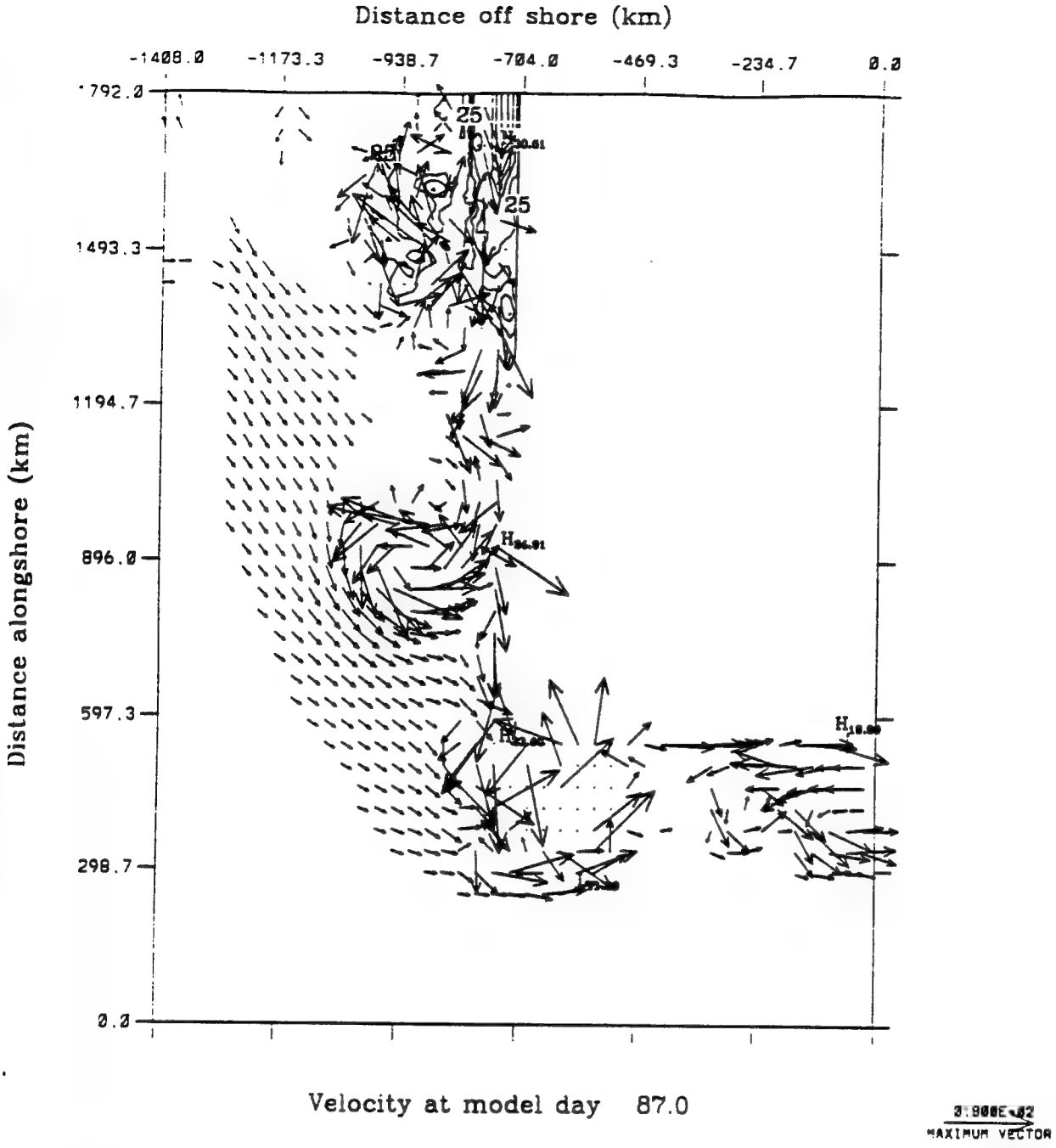

Figure 4.10e Experiment 3: Surface velocity vectors at day 87. To avoid clutter, velocity vectors are plotted at every third grid point in both the cross-shore and alongshore direction, and velocities less than 5 cm s^{-1} are not plotted. Note the formation of an anticyclonic eddy between Albany (x~500 km) and Esperance (x~50 km).

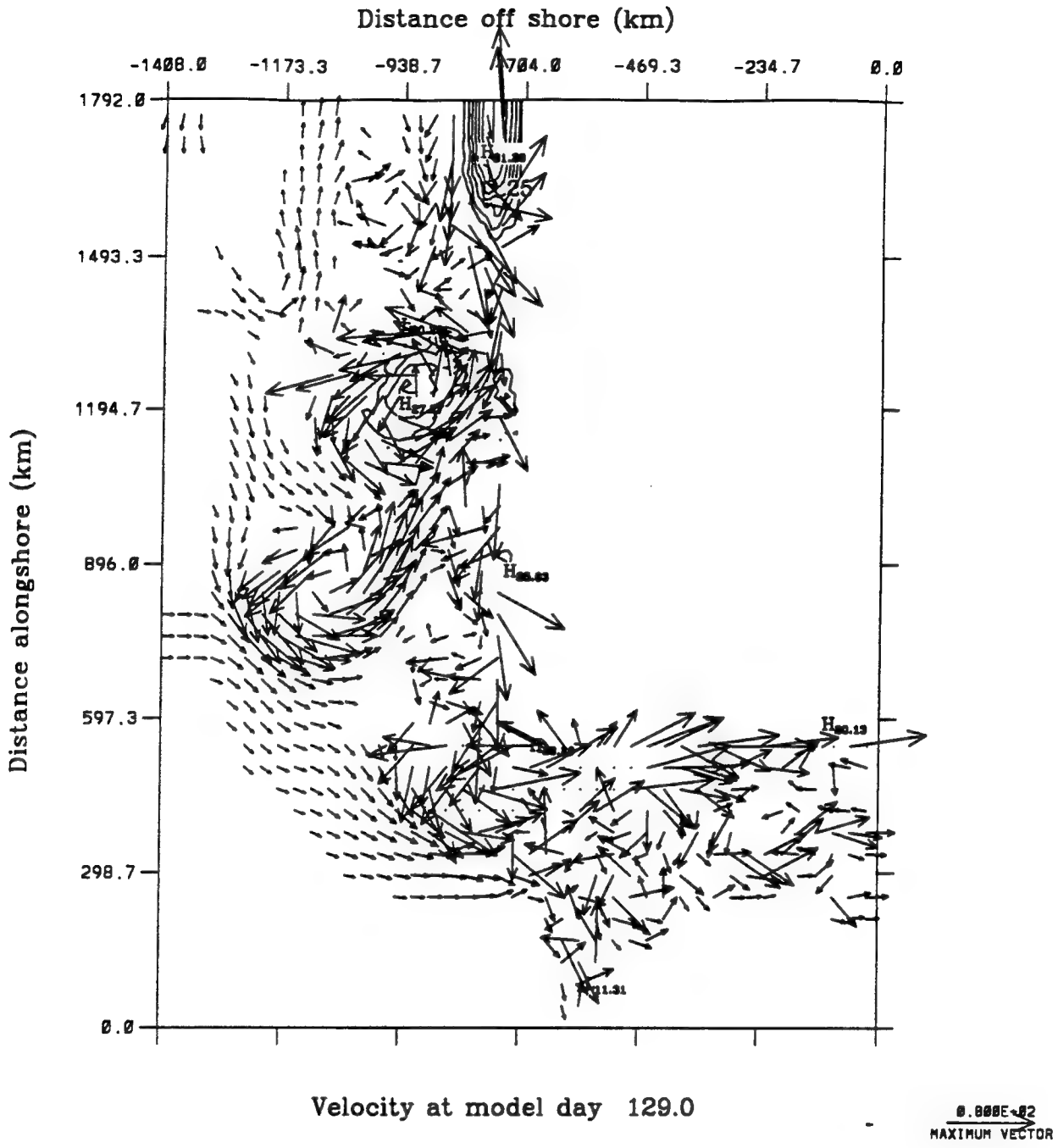

Figure 4.10f Experiment 3: Surface velocity vectors at day 129. To avoid clutter, velocity vectors are plotted at every third grid point in both the cross-shore and alongshore direction, and velocities less than 5 cm s^{-1} are not plotted. Note the westward propagation of eddies. Also, eddy pairs are visible throughout the coastal region.

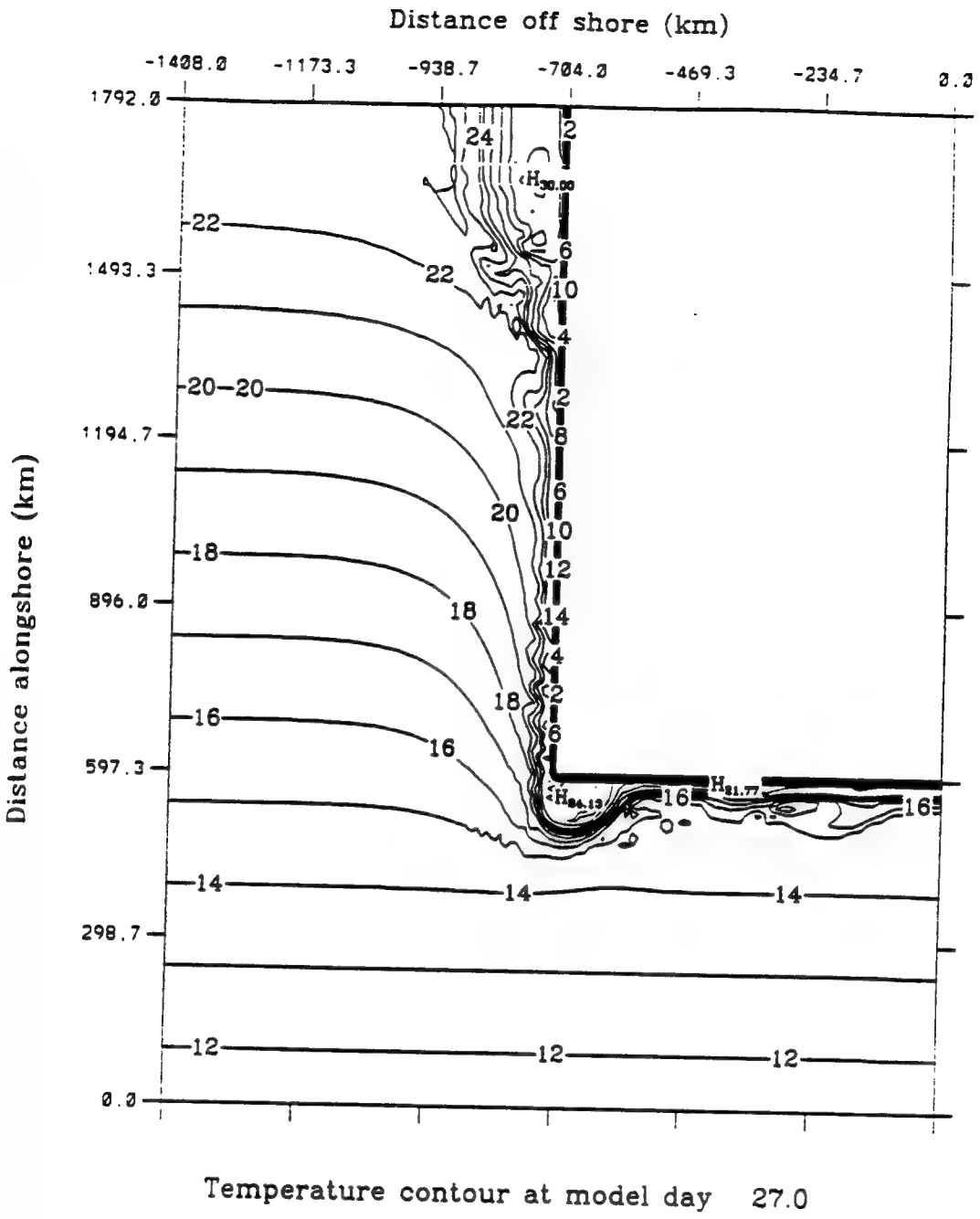

Figure 4.11a Experiment 3: Surface temperature at day 27. The contour interval is 1° C. The temperature increases towards the west coast.

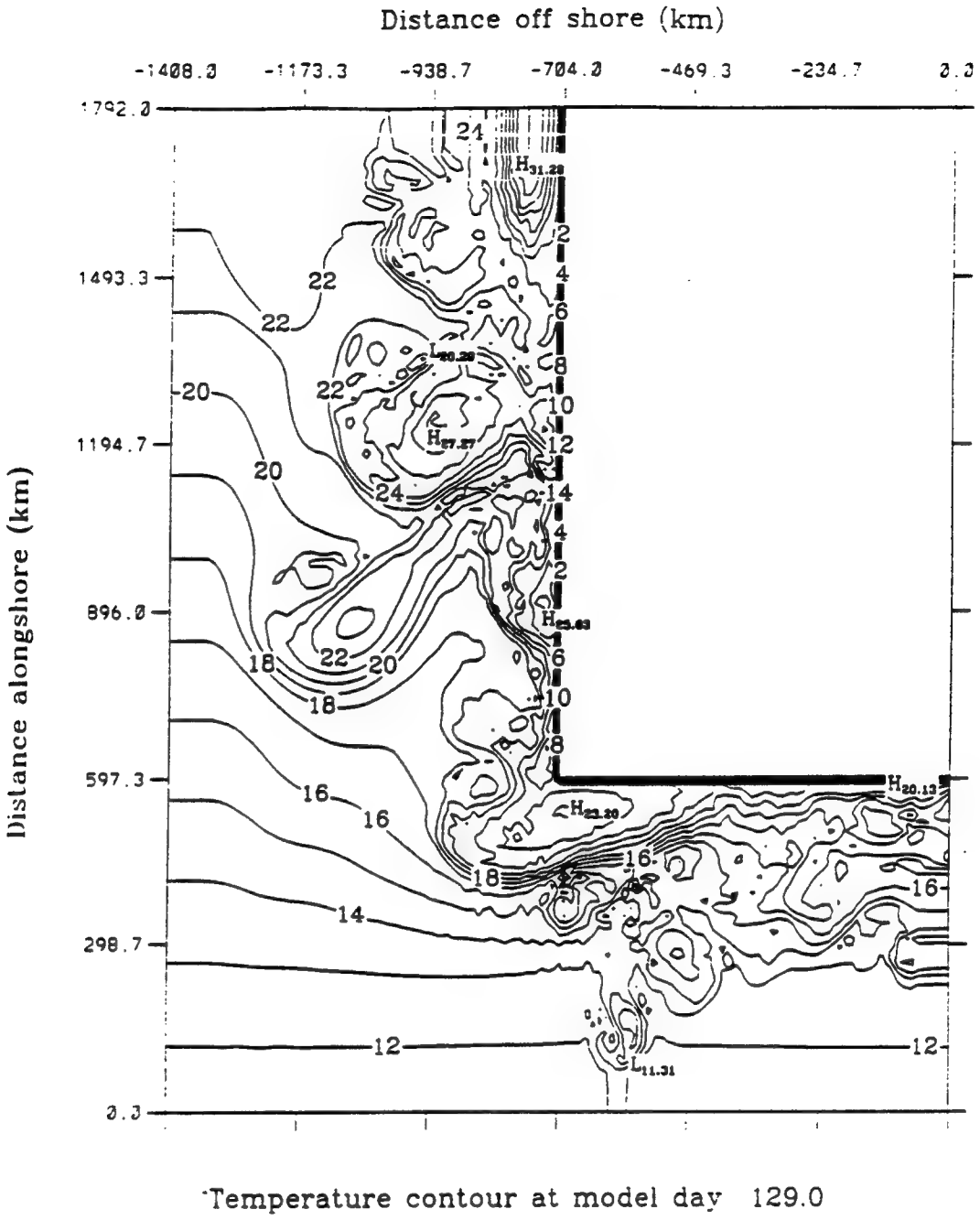

Figure 4.11b Experiment 3: Surface temperature at day 129. The contour interval is 1° C. The temperature increases towards the west coast.

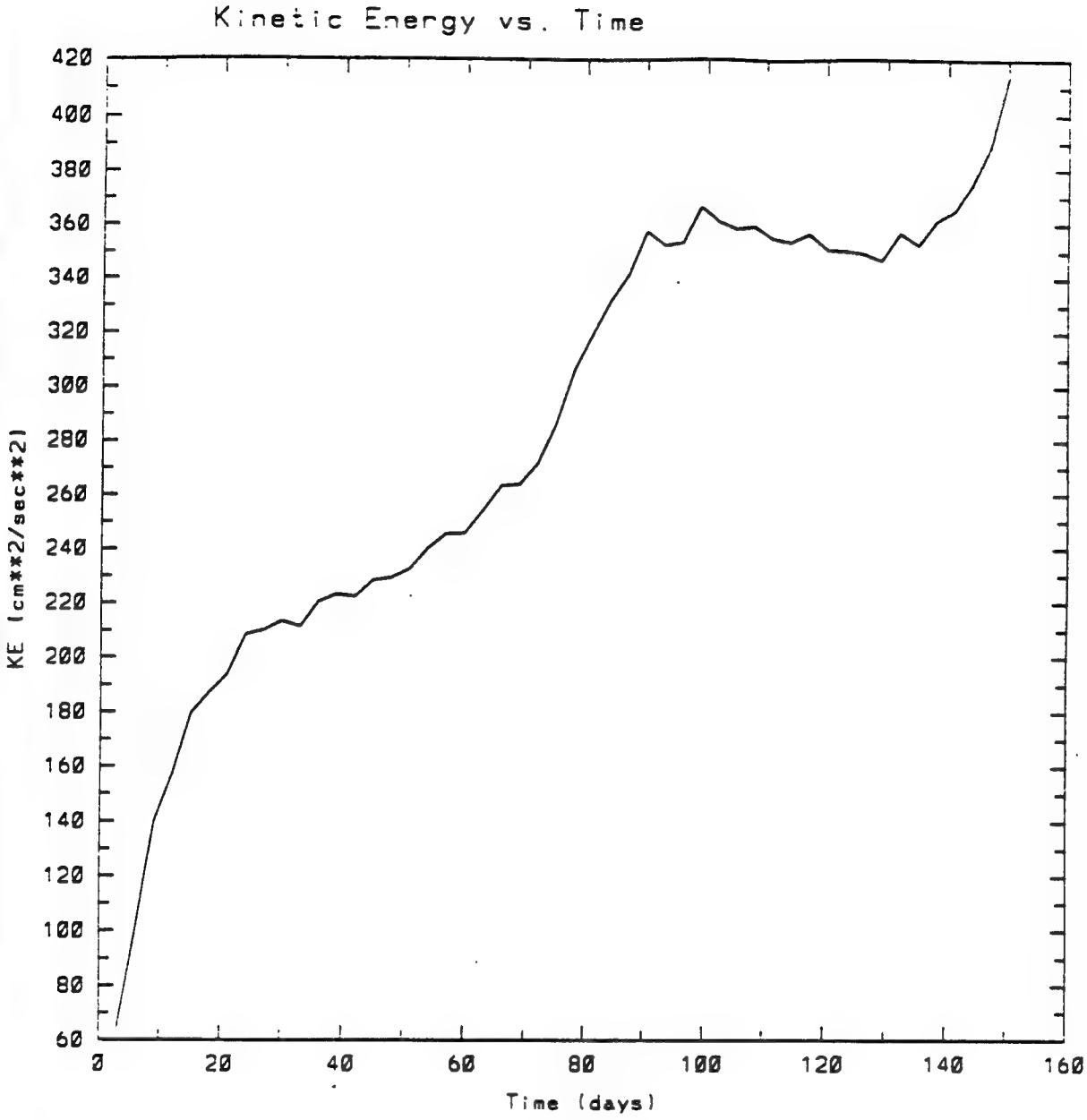

Figure 4.12 Experiment 3: Total kinetic energy per unit mass time series for the first 150 model days averaged over the entire domain (Units of the kinetic energy are cm^2s^{-2}).

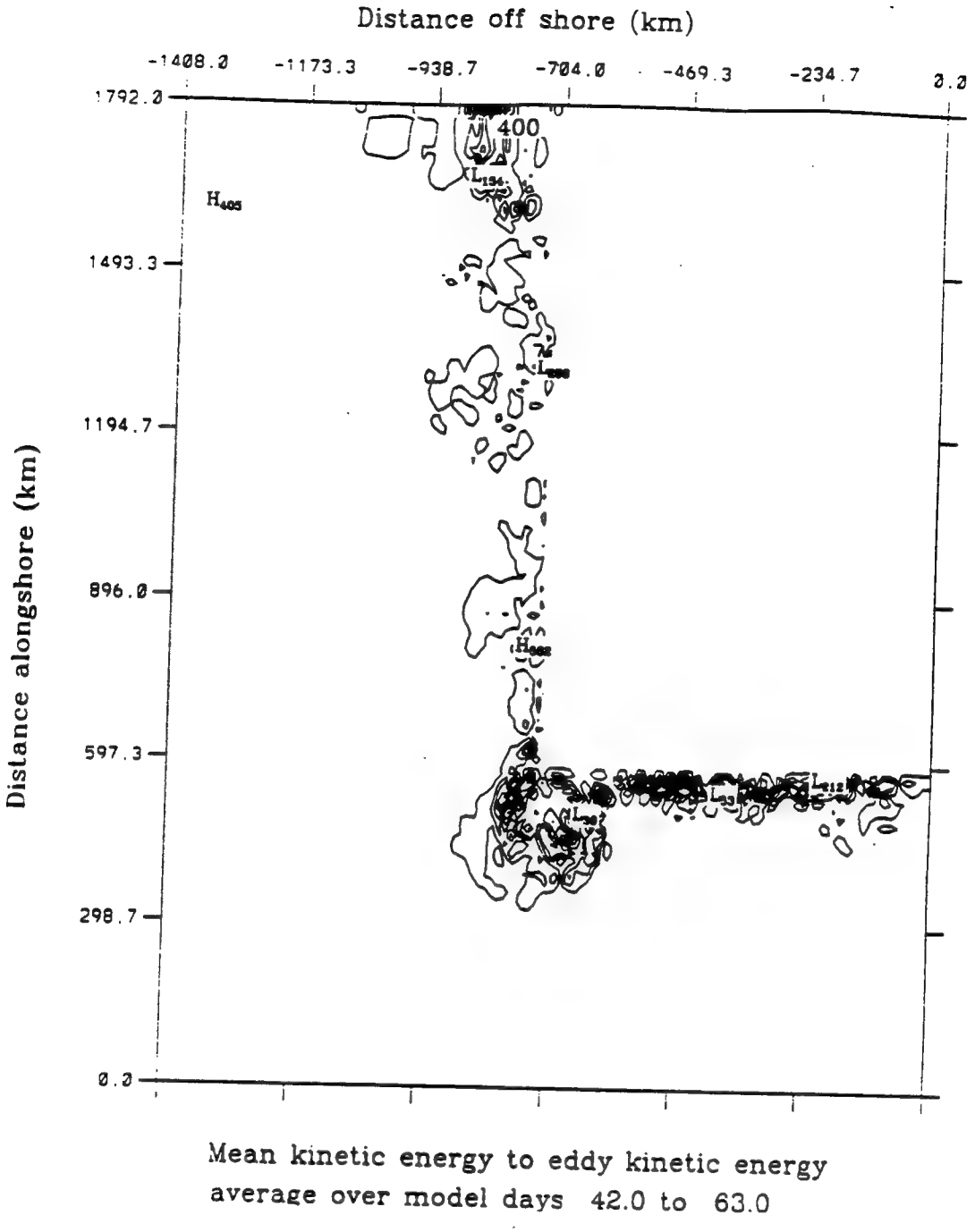

Figure 4.13a Experiment 3: Energy transfers of mean to eddy kinetic energy (i.e., barotropic energy transfer) for model days 42 to 63. The contour interval is 1 ergs cm^{-3} s^{-1}.

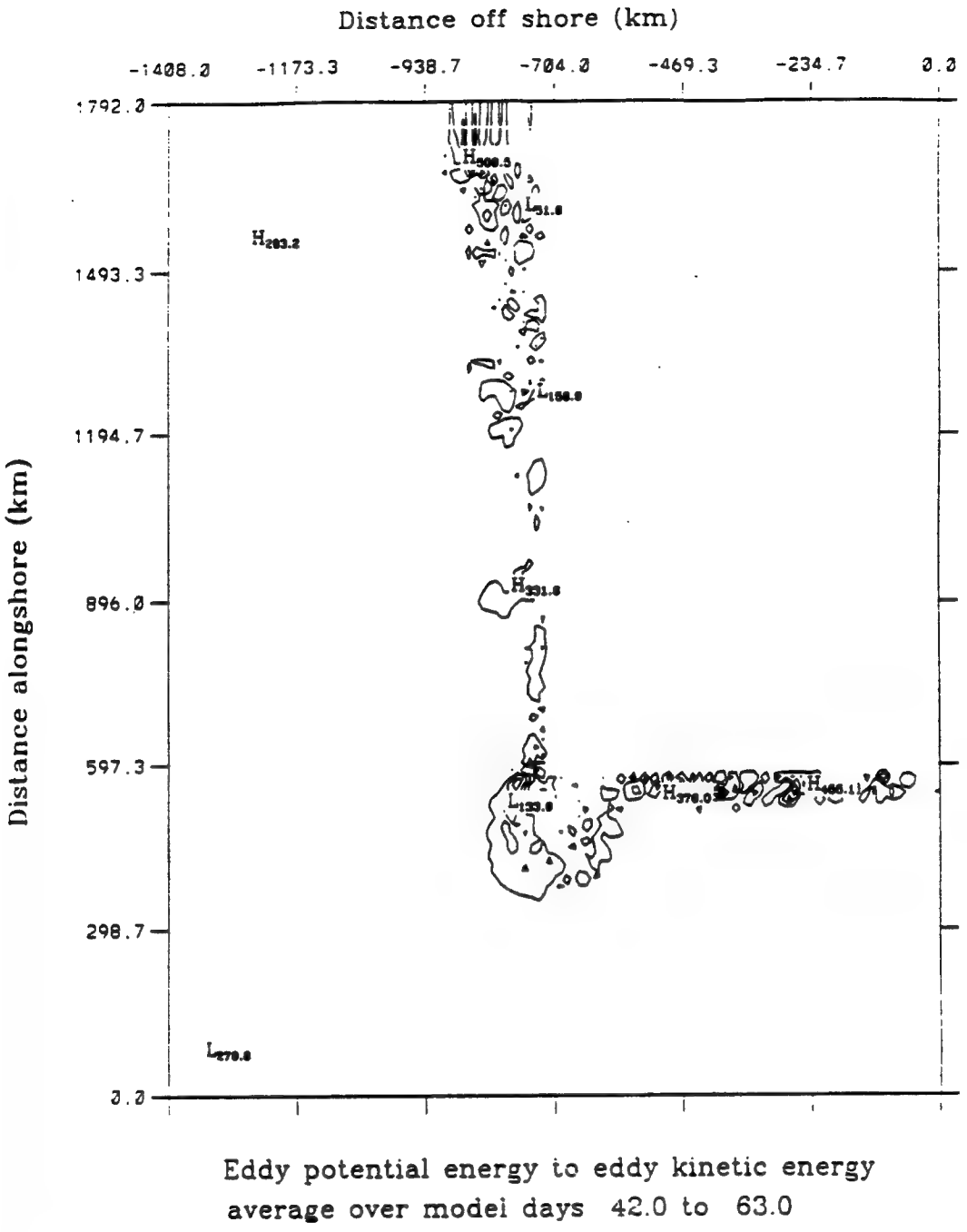

Figure 4.13b Experiment 3: Energy transfers of eddy potential to eddy kinetic energy (i.e., baroclinic energy transfer) for model days 42 to 63. The contour interval is 1 ergs cm^{-3} s^{-1}.

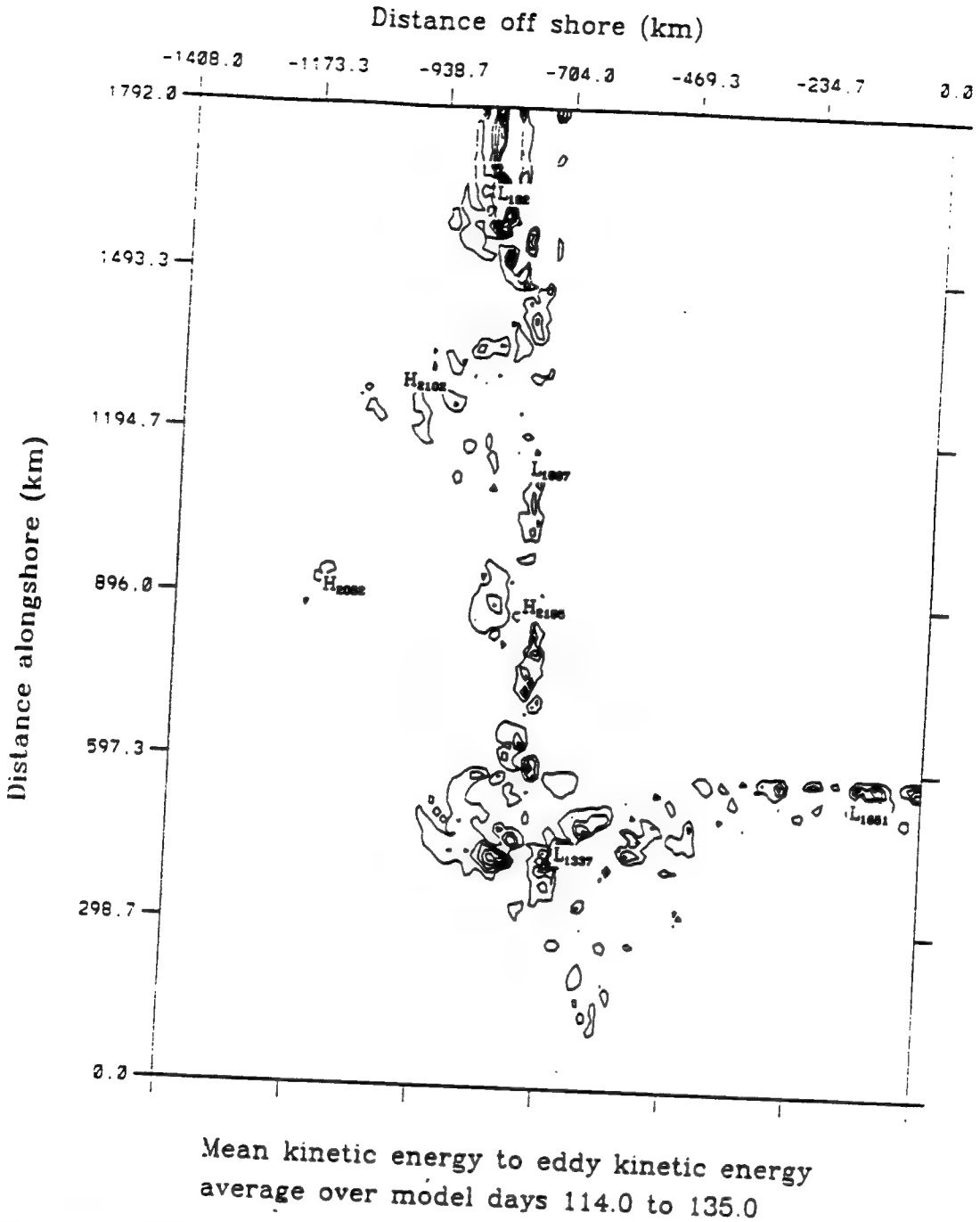

Figure 4.14a Experiment 3: Energy transfers of mean to eddy kinetic energy (i.e., barotropic energy transfer) for model days 114 to 135. The contour interval is 1 ergs cm^{-3} s^{-1}.

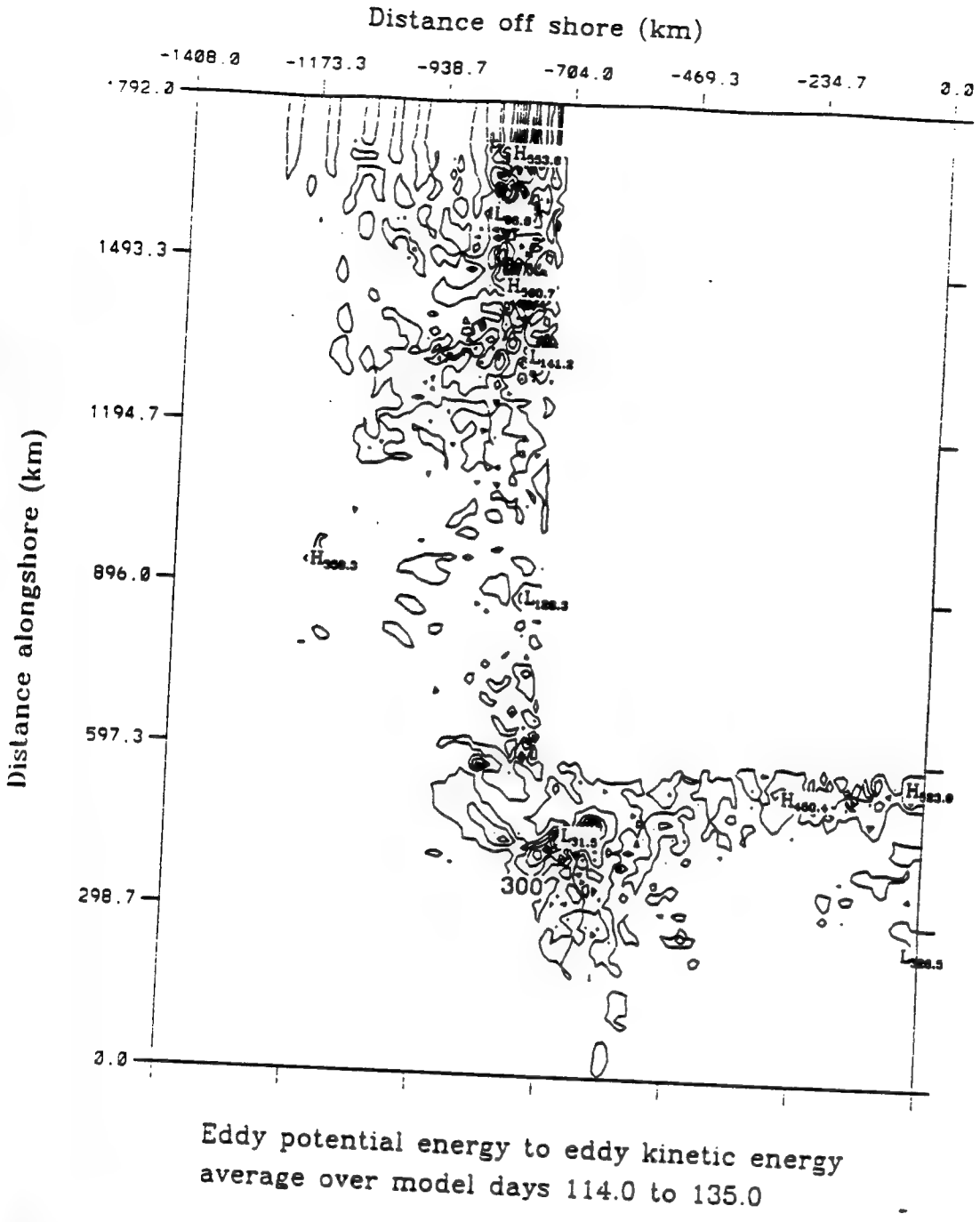

Figure 4.14b Experiment 3: Energy transfers of eddy potential to eddy kinetic energy (i.e., baroclinic energy transfer) for model days 114 to 135. The contour interval is 1 ergs cm^{-3} s^{-1}.

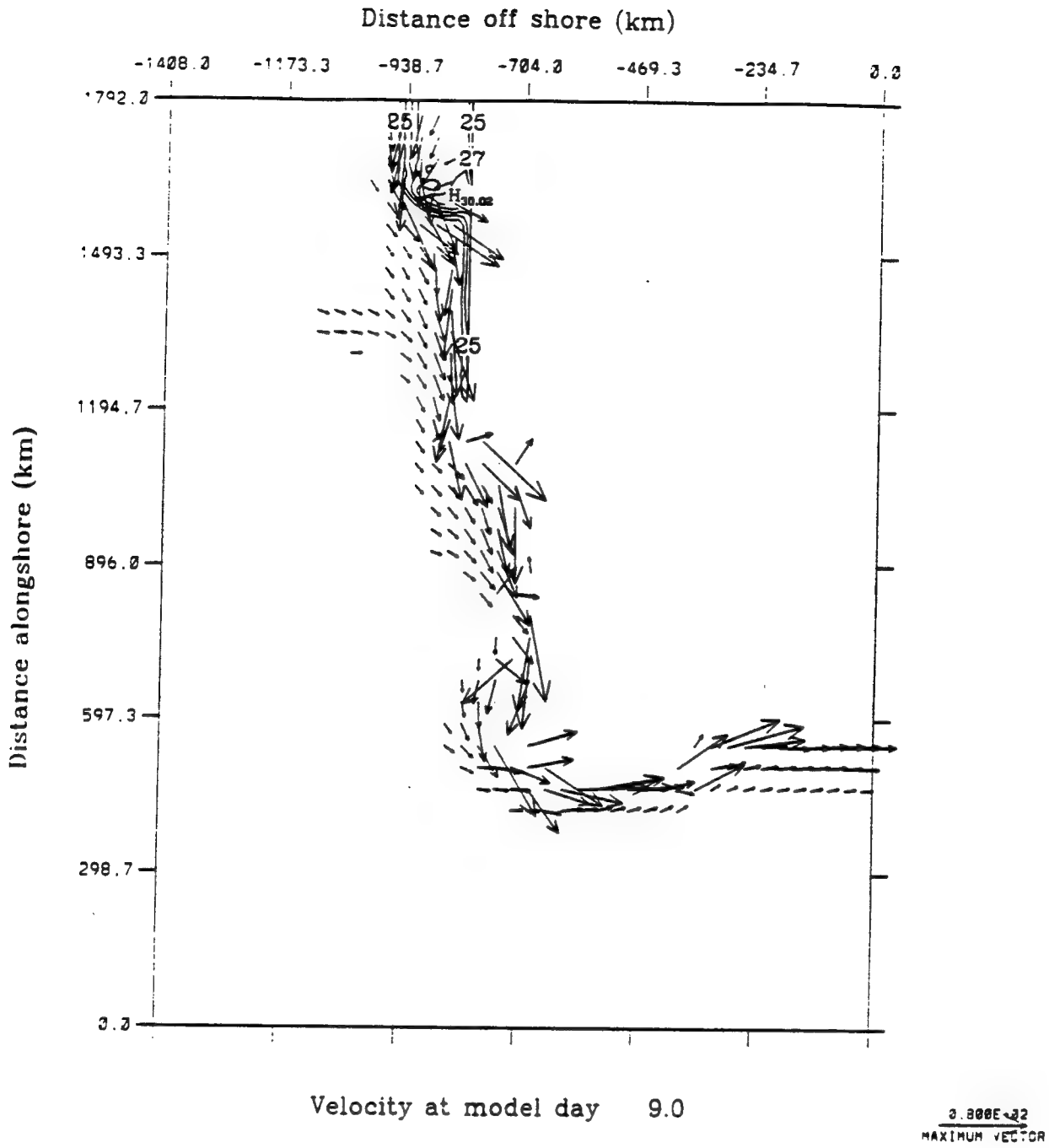

Figure 4.15a Experiment 4: Surface velocity vectors at day 9. To avoid clutter, velocity vectors are plotted at every third grid point in both the cross-shore and alongshore direction, and velocities less than 5 cm s^{-1} are not plotted. Note the large offshoots near preferred locations off the coast of Shark Bay (y~1000 km), Fremantle (y~850 km), Cape Leeuwin (y~500 km), and Albany (x~500 km).

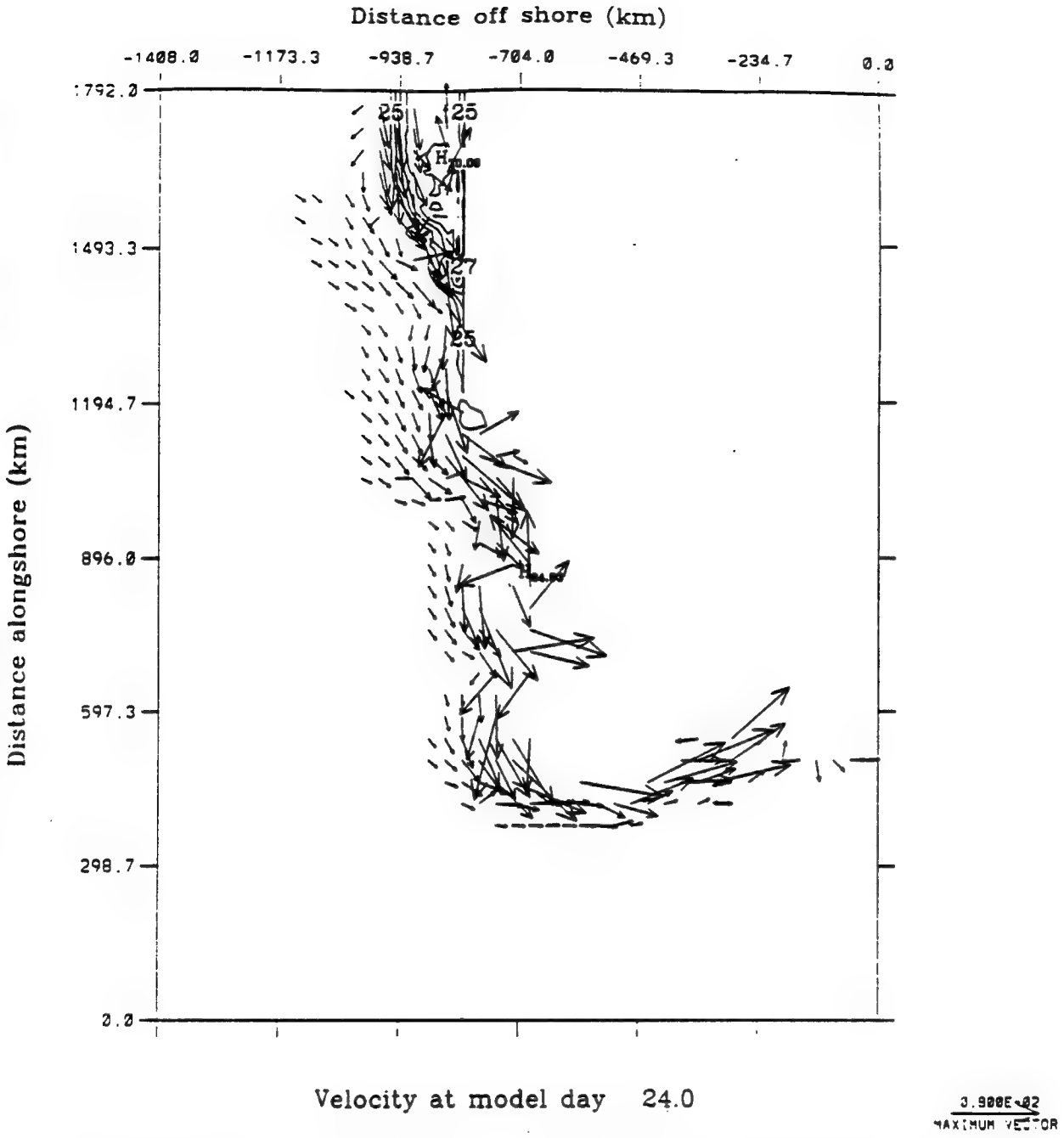

Figure 4.15b Experiment 4: Surface velocity vectors at day 24. To avoid clutter, velocity vectors are plotted at every third grid point in both the cross-shore and alongshore direction, and velocities less than 5 cm s^{-1} are not plotted. Note that the offshoots of Figure 4.15a have intensified and developed into anticyclonic meanders.

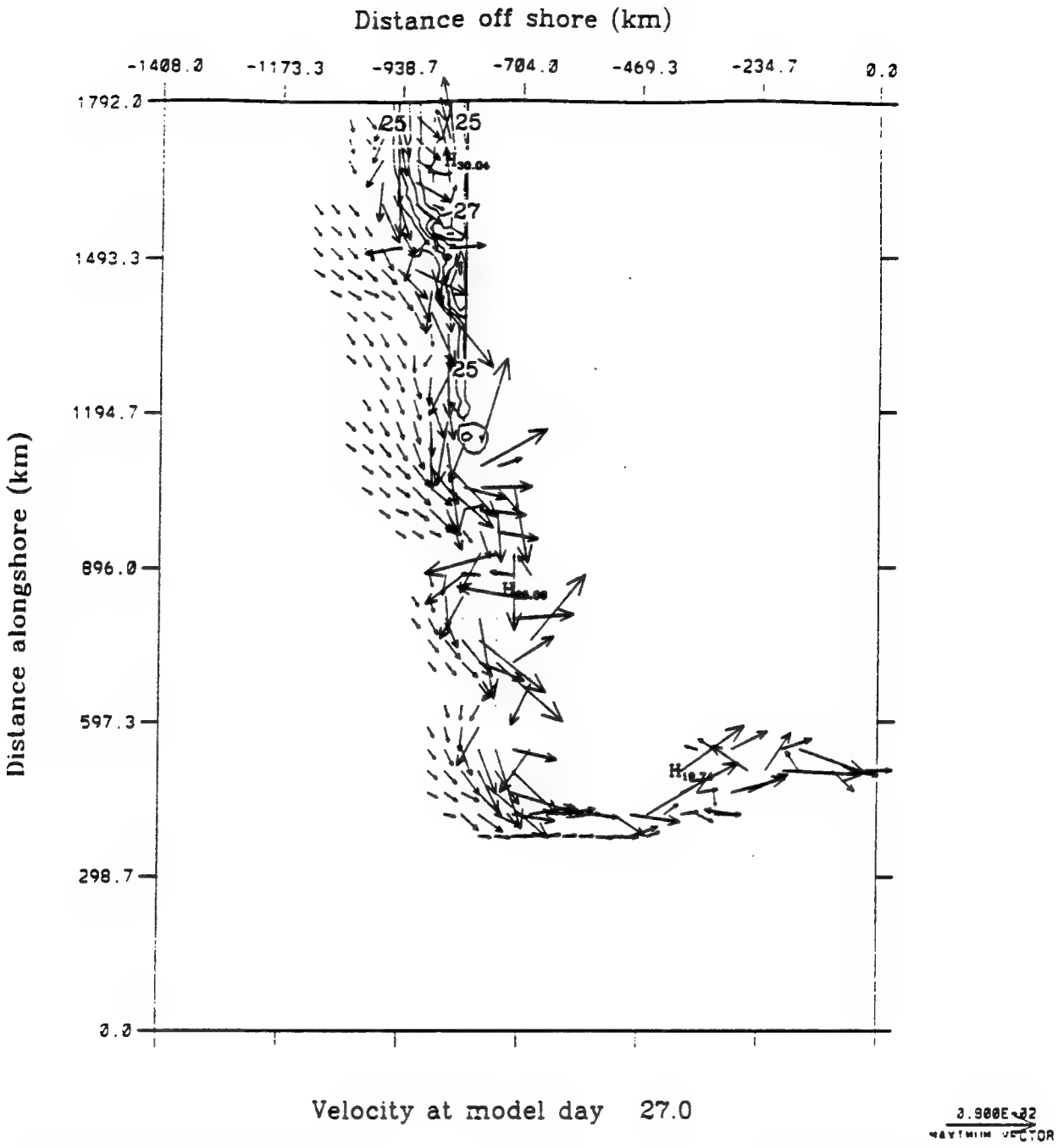

Figure 4.15c Experiment 4: Surface velocity vectors at day 27. To avoid clutter, velocity vectors are plotted at every third grid point in both the cross-shore and alongshore direction, and velocities less than 5 cm s^{-1} are not plotted. Note the formation of anticyclonic eddies at Fremantle (y~850 km), and Shark Bay (y~1000 km).

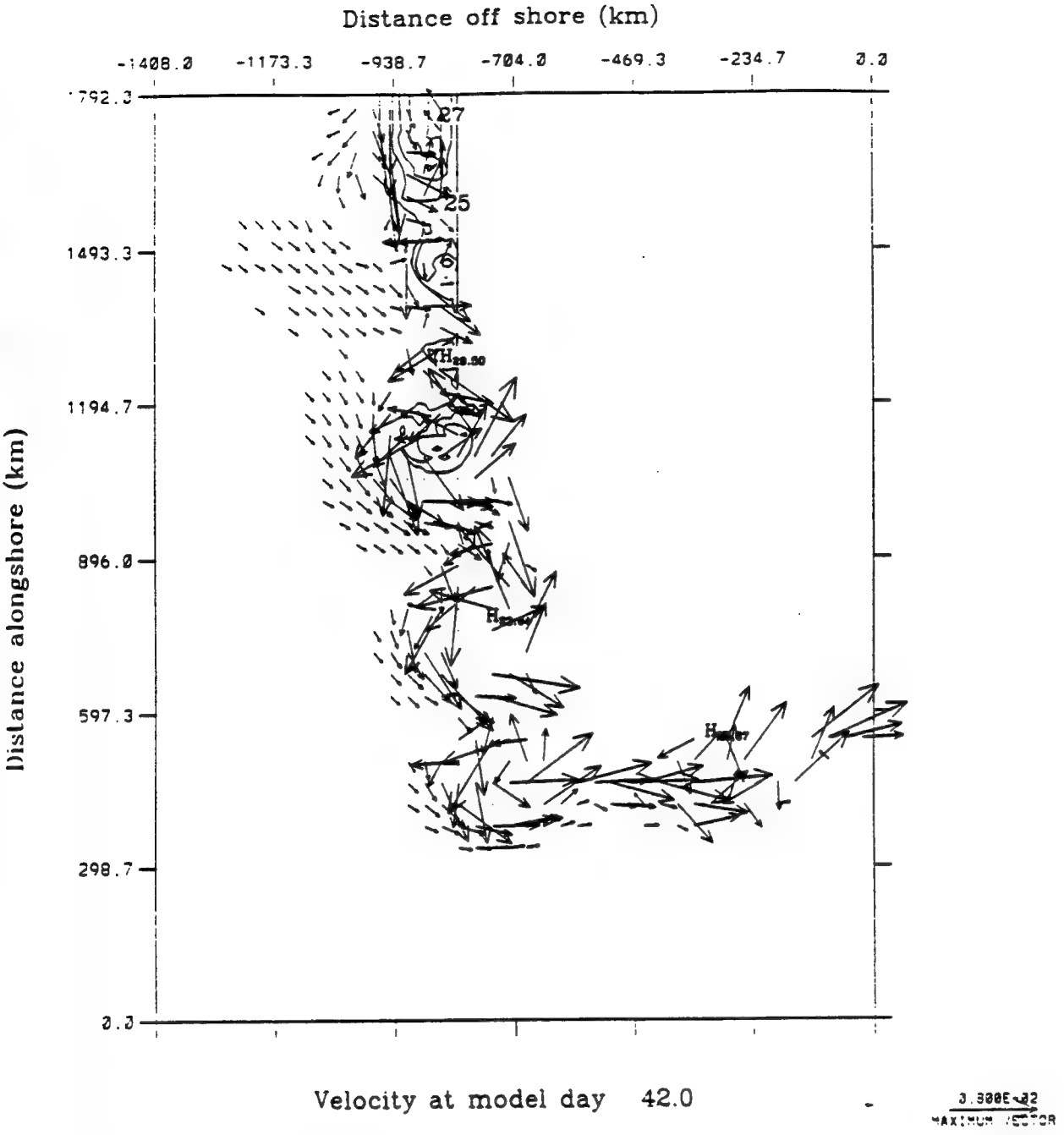

Figure 4.15d Experiment 4: Surface velocity vectors at day 42. To avoid clutter, velocity vectors are plotted at every third grid point in both the cross-shore and alongshore direction, and velocities less than 5 cm s^{-1} are not plotted. Note the anticyclonic eddies near Cape Leeuwin (y~500 km) and Cliffy Head (x~770), and off the coast of Albany (x~500 km). The Fremantle (y~850 km) eddy has begun its westward propagation.

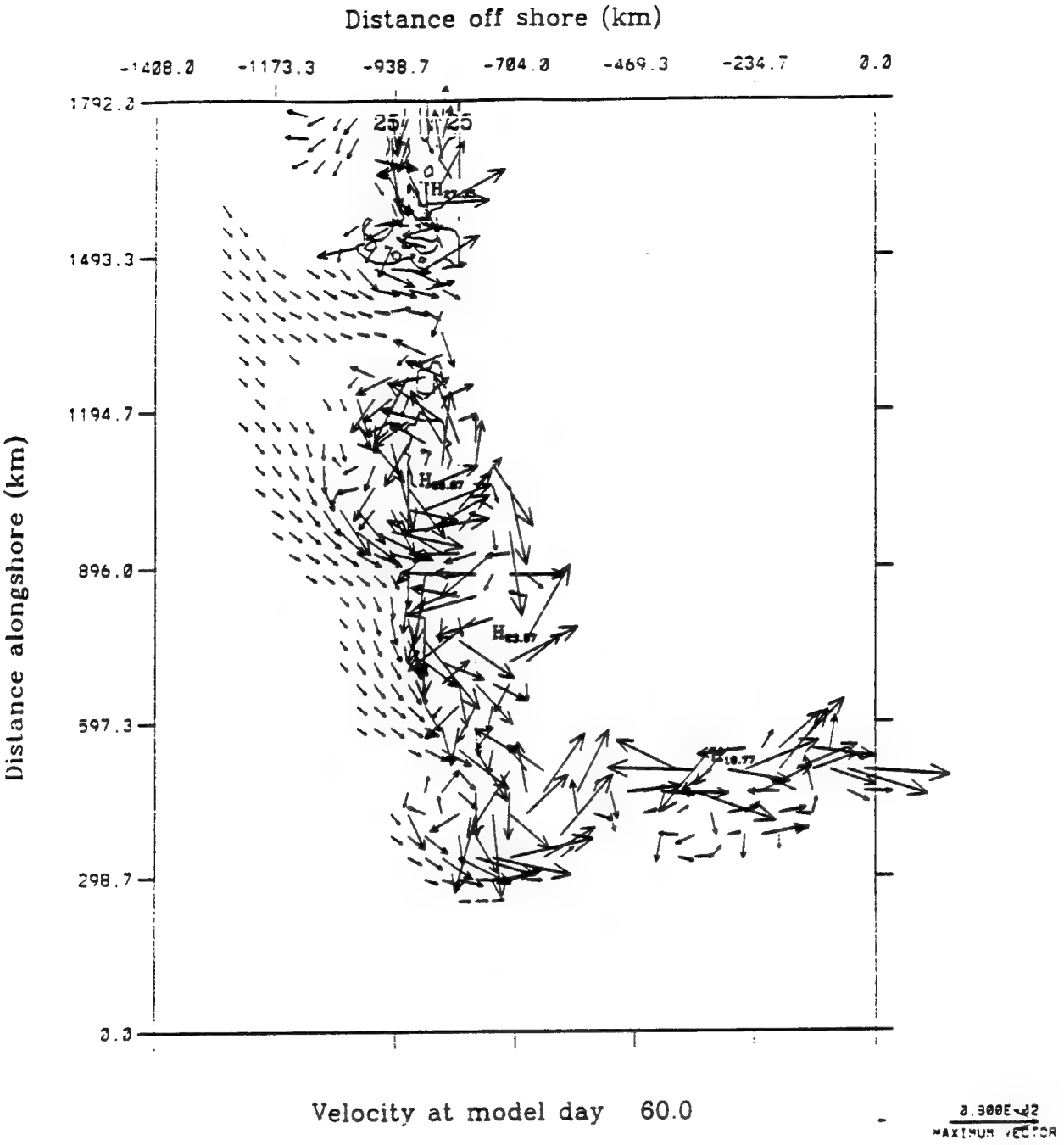

Figure 4.15e Experiment 4: Surface velocity vectors at day 60. To avoid clutter, velocity vectors are plotted at every third grid point in both the cross-shore and alongshore direction, and velocities less than 5 cm s^{-1} are not plotted. Note the formation of a second anticyclonic eddy in the NWS water source region, and the existence of eddy pairs along the entire coast.

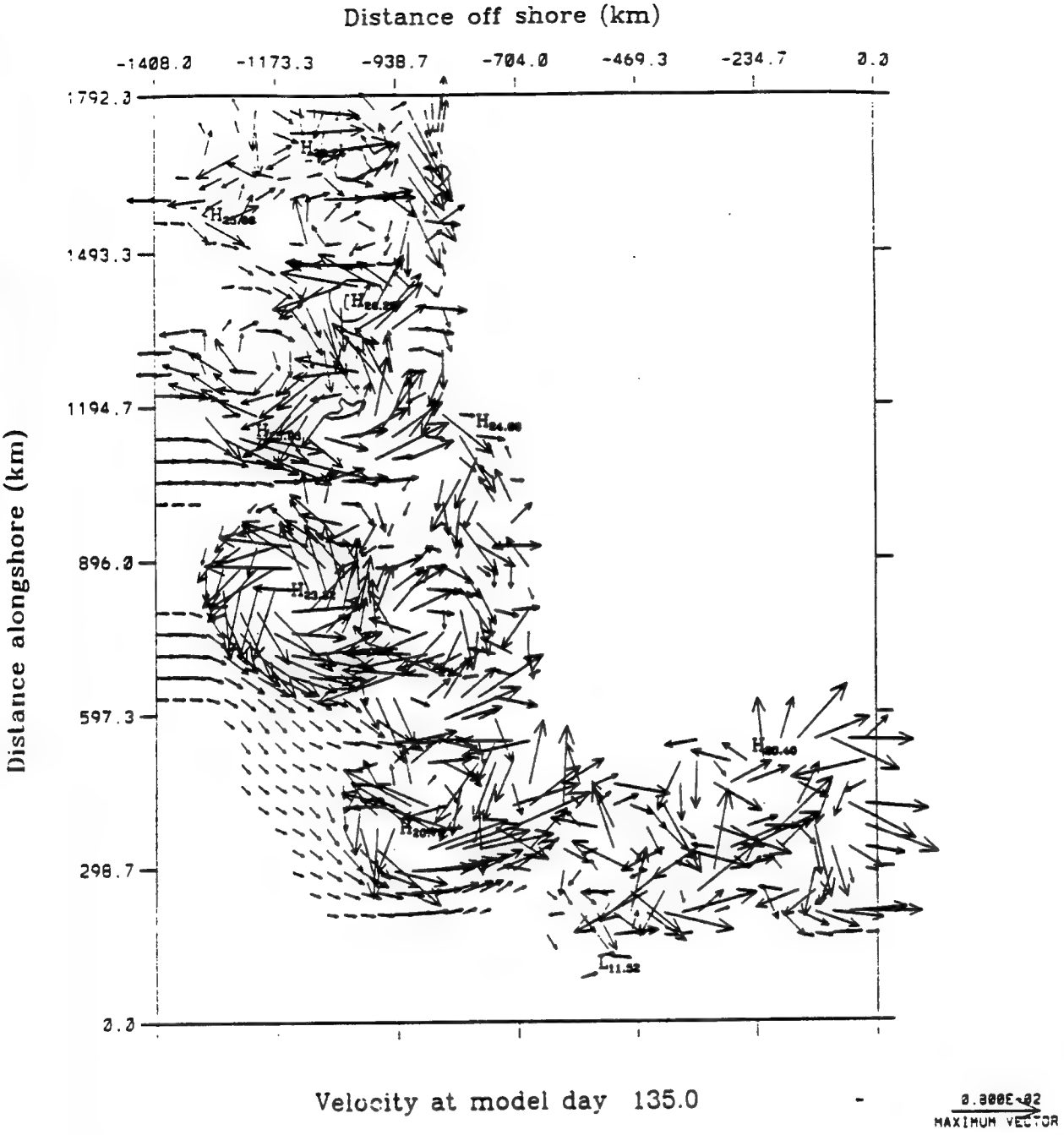

Figure 4.10f Experiment 4: Surface velocity vectors at day 135. To avoid clutter, velocity vectors are plotted at every third grid point in both the cross-shore and alongshore direction, and velocities less than 5 cm s^{-1} are not plotted. Note the formation of a new anticyclonic eddy at Dongara (y~900 km). The Leeuwin Current is forced far offshore away from the coastal regions due to westward propagation of eddies. Also, eddy pairs are visible throughout the coastal region.

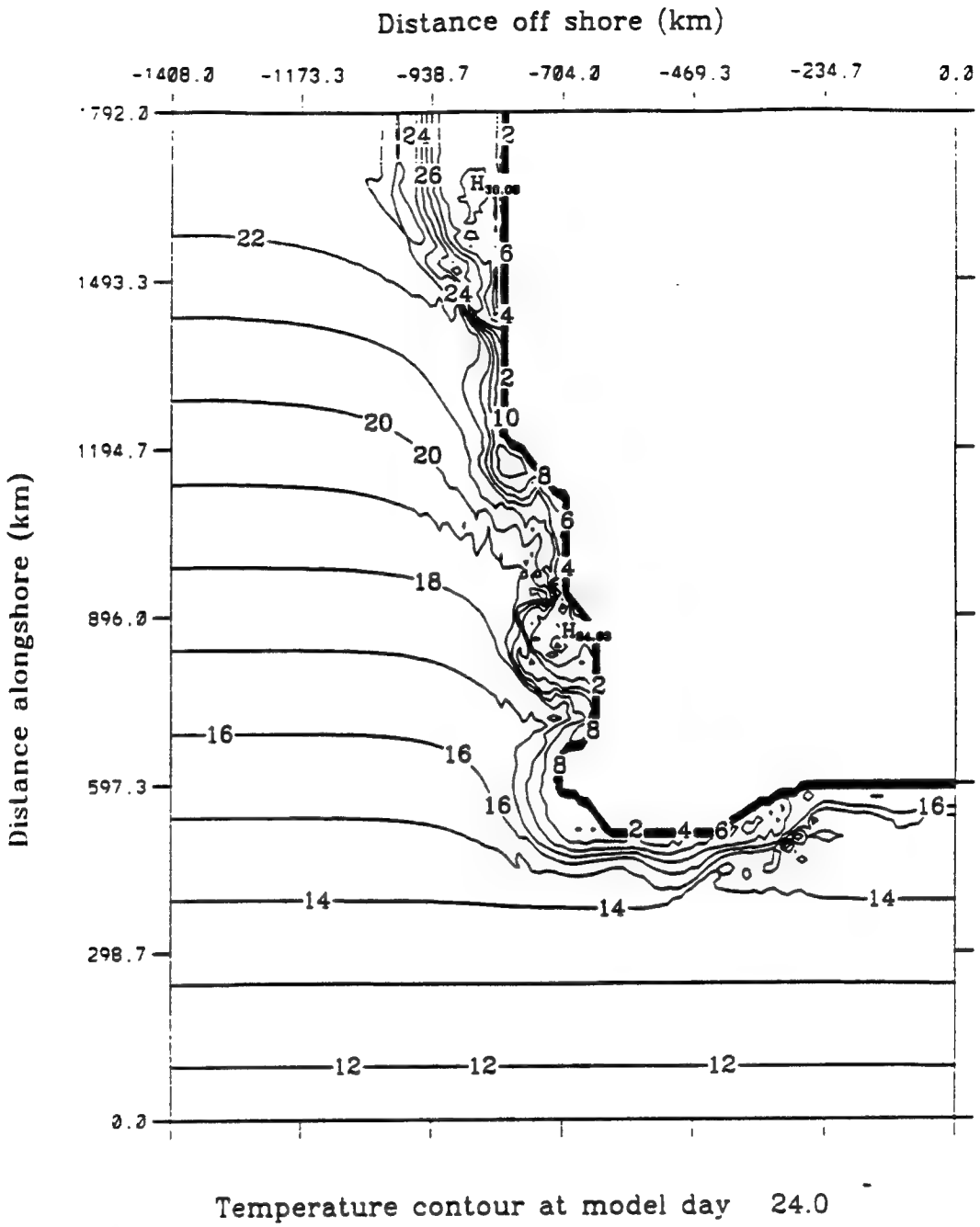

Figure 4.16 Experiment 4: Surface temperature at day 24. The contour interval is 1° C. The temperature increases towards the west coast. Note the strong temperature front established along the Southern Australian coast.

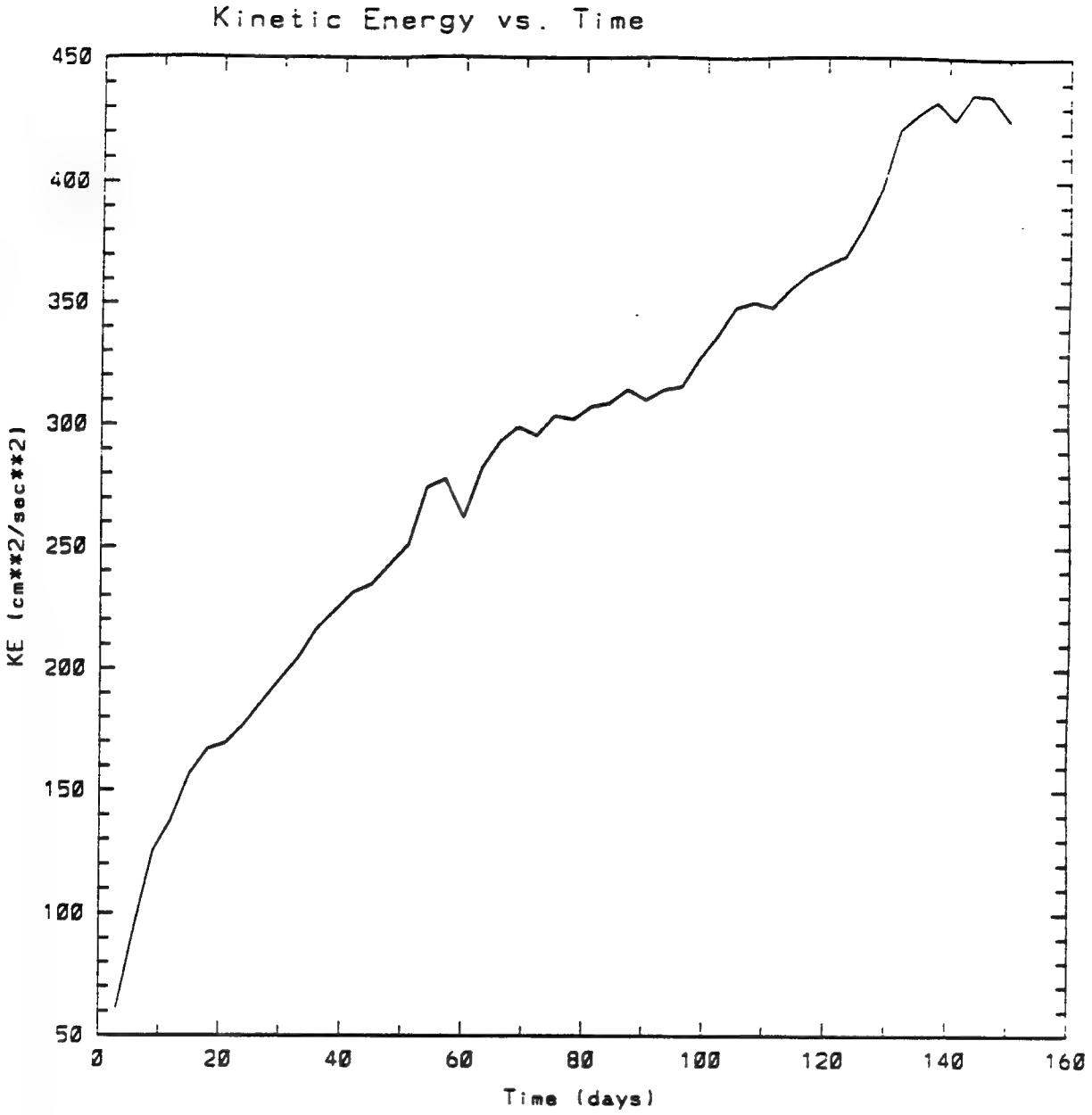

Figure 4.17 Experiment 4: Total kinetic energy per unit mass time series for the first 150 model days averaged over the entire domain (Units of the kinetic energy are cm^2s^{-2}).

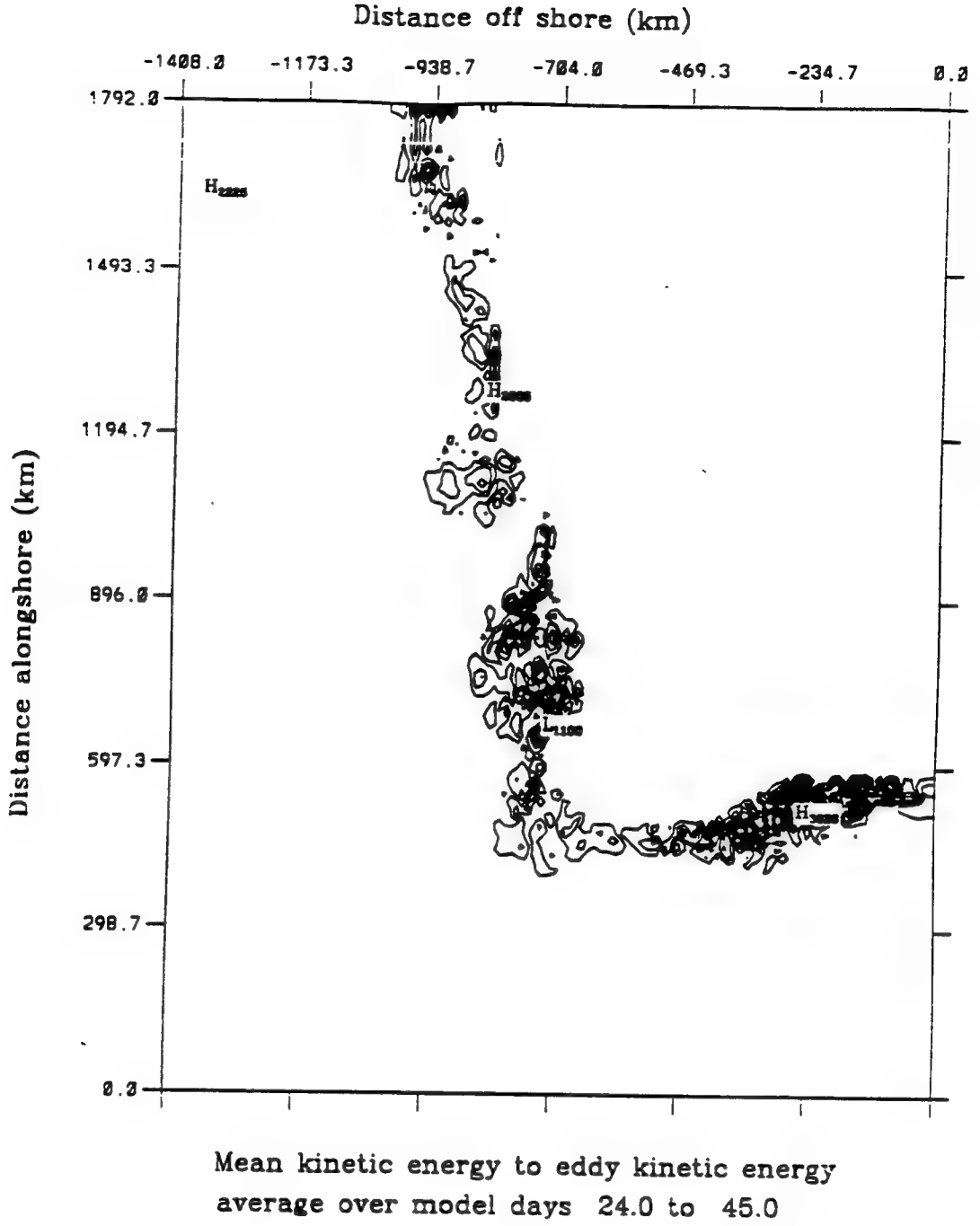

Figure 4.18a Experiment 4: Energy transfers of mean to eddy kinetic energy (i.e., barotropic energy transfer) for model days 24 to 45. The contour interval is 1 ergs cm^{-3} s^{-1}.

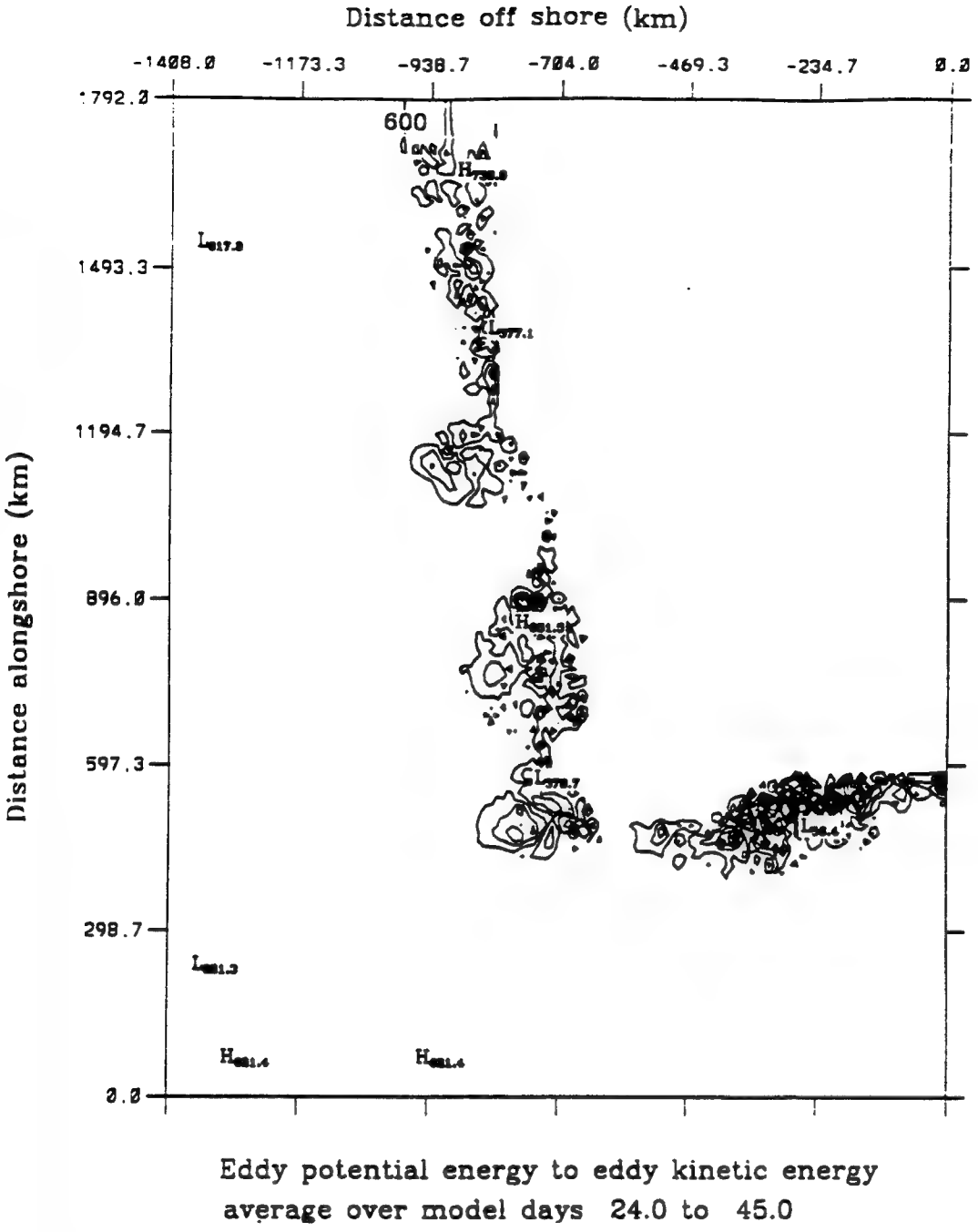

Figure 4.18b Experiment 4: Energy transfers of eddy potential to eddy kinetic energy (i.e., baroclinic energy transfer) for model days 24 to 45. The contour interval is 1 ergs cm^{-3} s^{-1}.

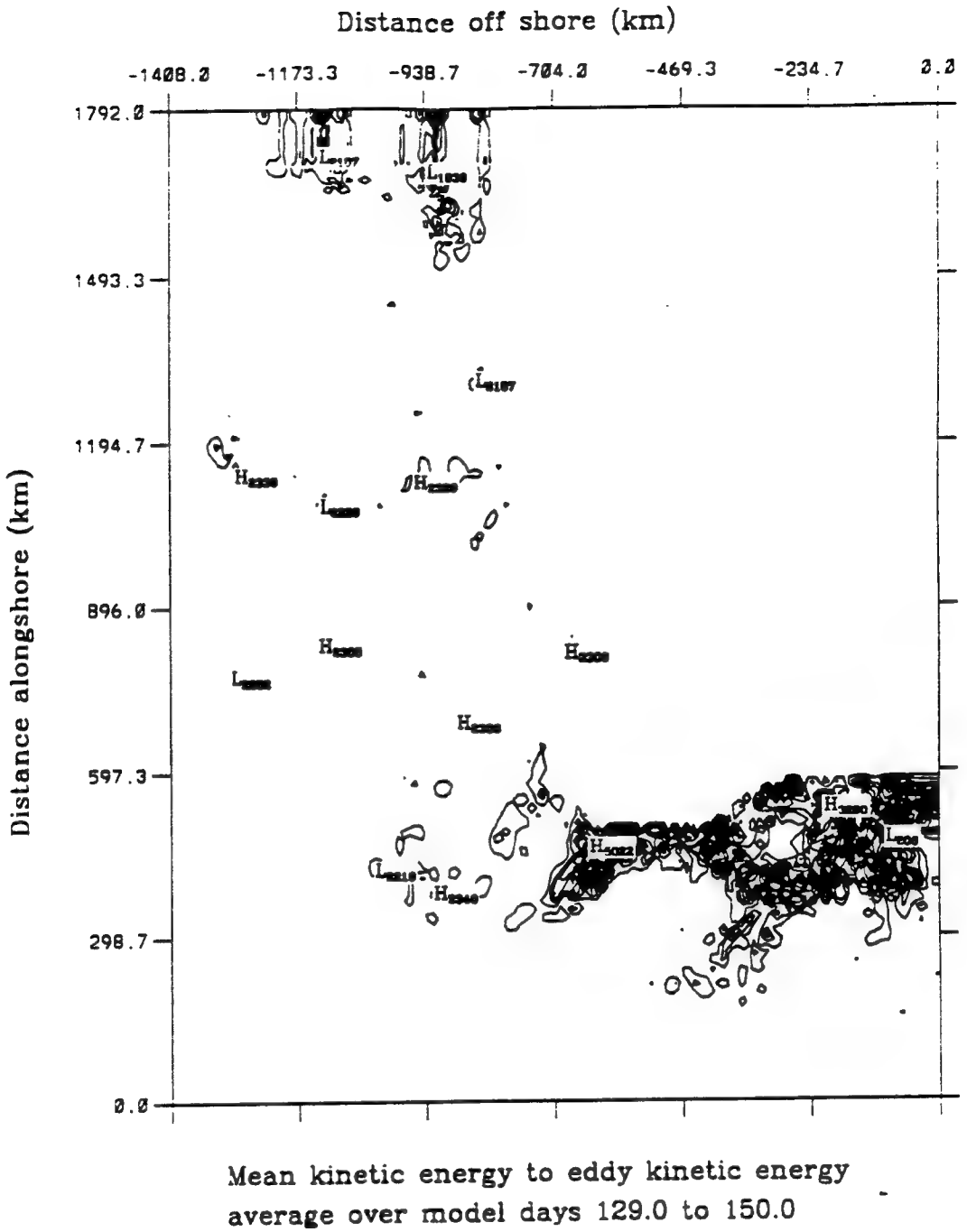

Figure 4.19a Experiment 4: Energy transfers of mean to eddy kinetic energy (i.e., barotropic energy transfer) for model days 129 to 150. The contour interval is 1 ergs cm^{-3} s^{-1}.

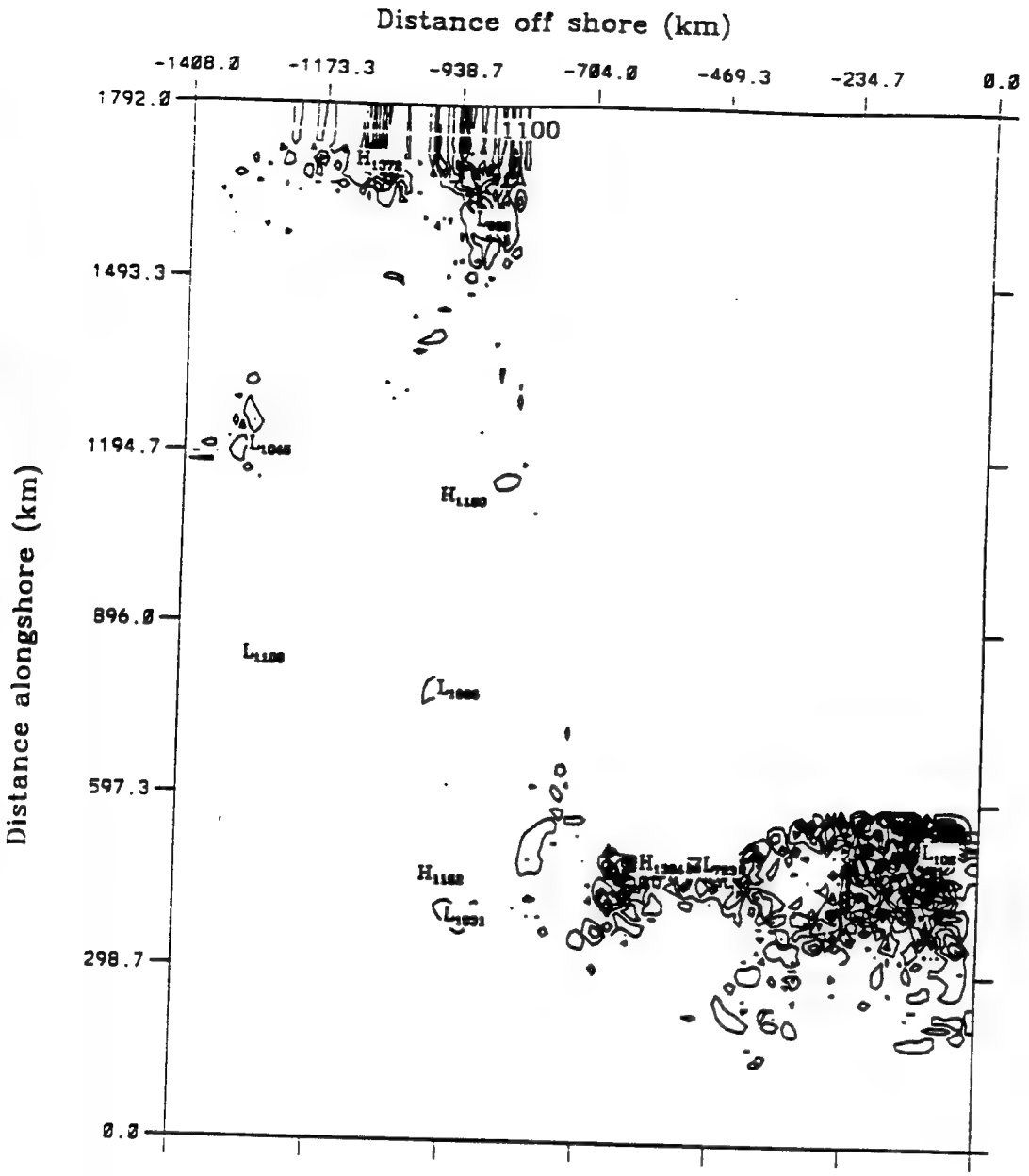

Figure 4.19b Experiment 4: Energy transfers of eddy potential to eddy kinetic energy (i.e., baroclinic energy transfer) for model days 129 to 150. The contour interval is 1 ergs cm^{-3} s^{-1}.

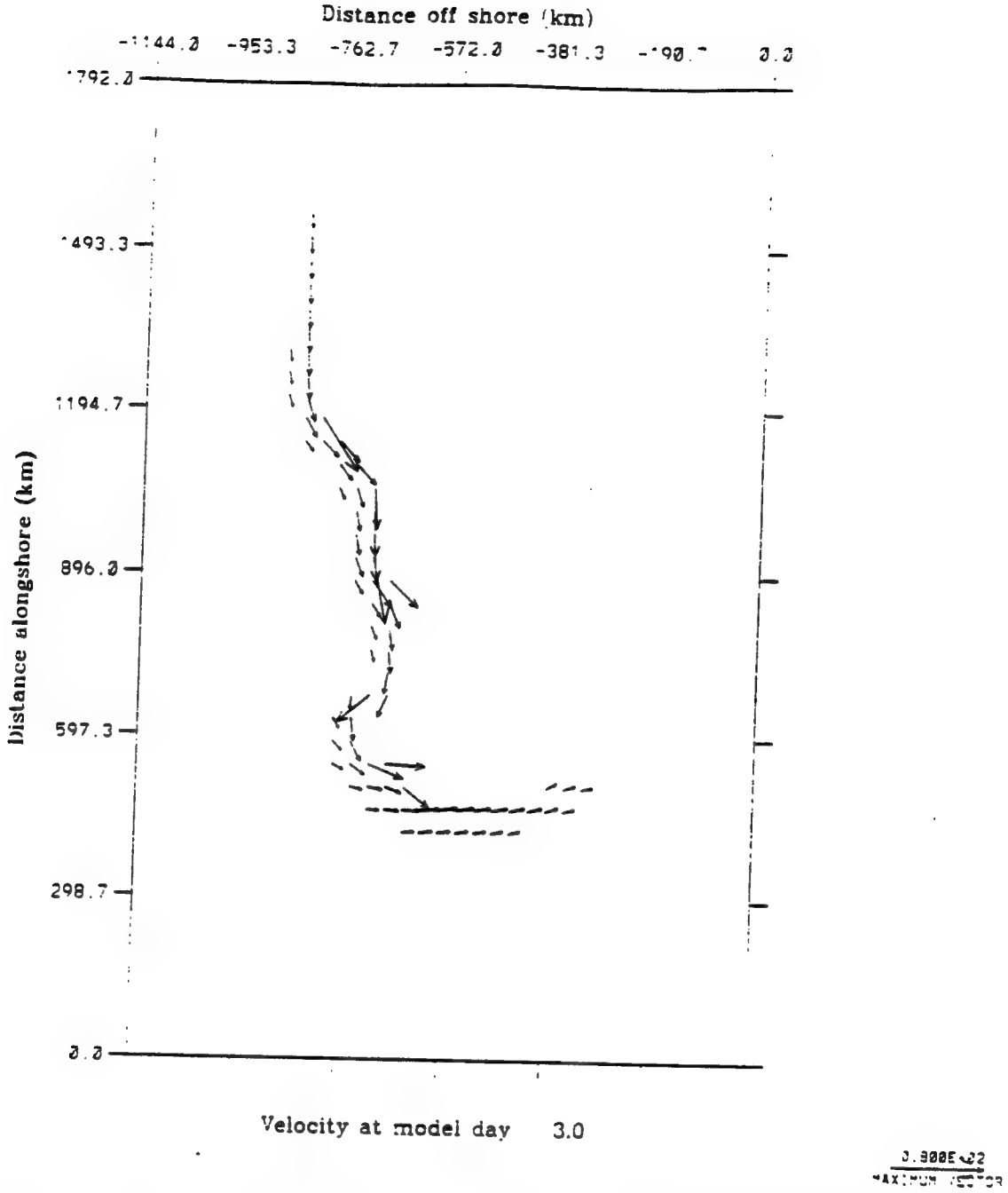

Figure 4.20a Experiment 5: Surface velocity vectors at day 3. To avoid clutter, velocity vectors are plotted at every third grid point in both the cross-shore and alongshore direction, and velocities less than 5 cm s^{-1} are not plotted.

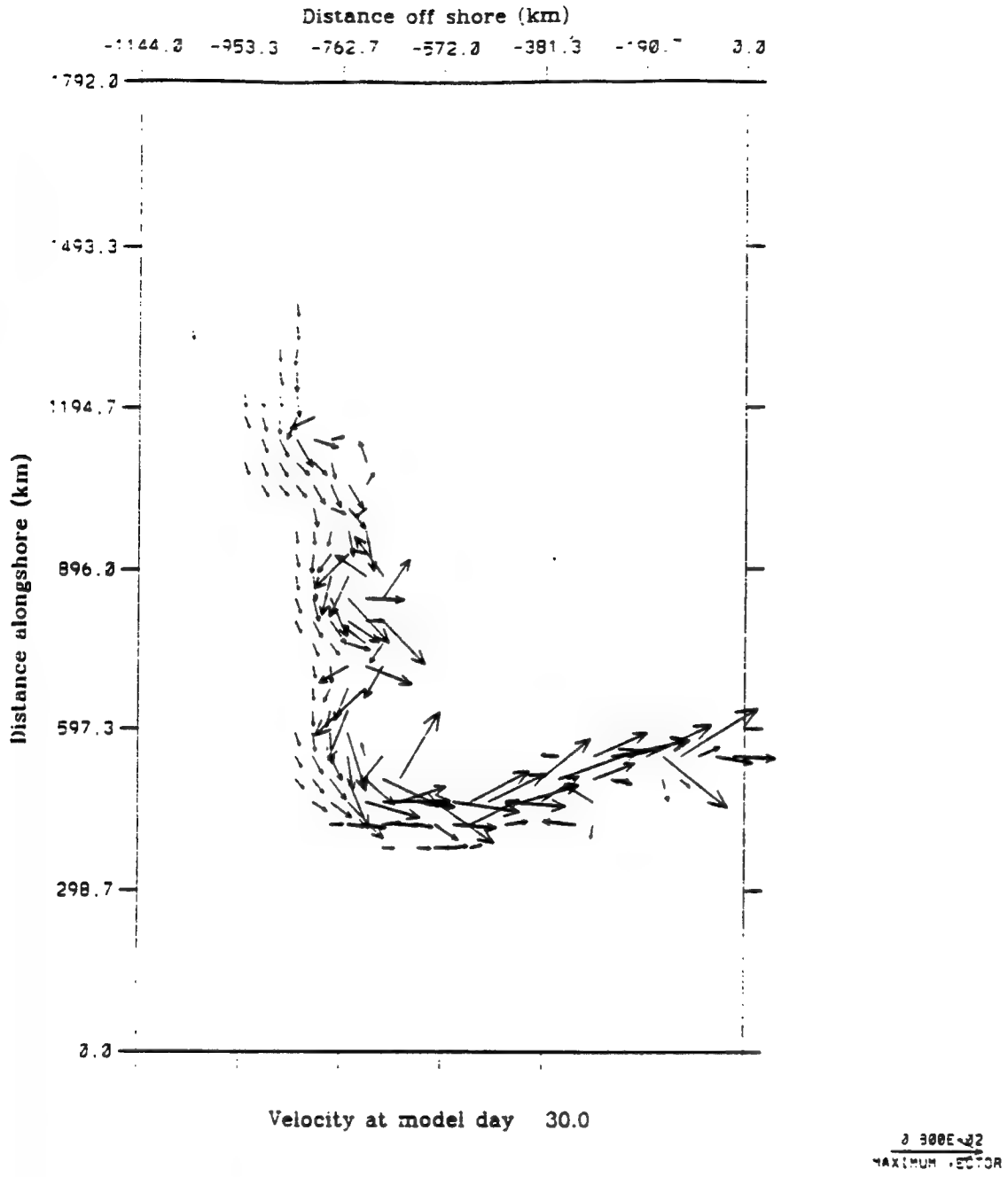

Figure 4.20b Experiment 5: Surface velocity vectors at day 30. To avoid clutter, velocity vectors are plotted at every third grid point in both the cross-shore and alongshore direction, and velocities less than 5 cm s^{-1} are not plotted. Note the presences of offshoots and meanders near Shark Bay (y~1000 km), Dongara (y~900 km), and Cape Leeuwin (y~500 km).

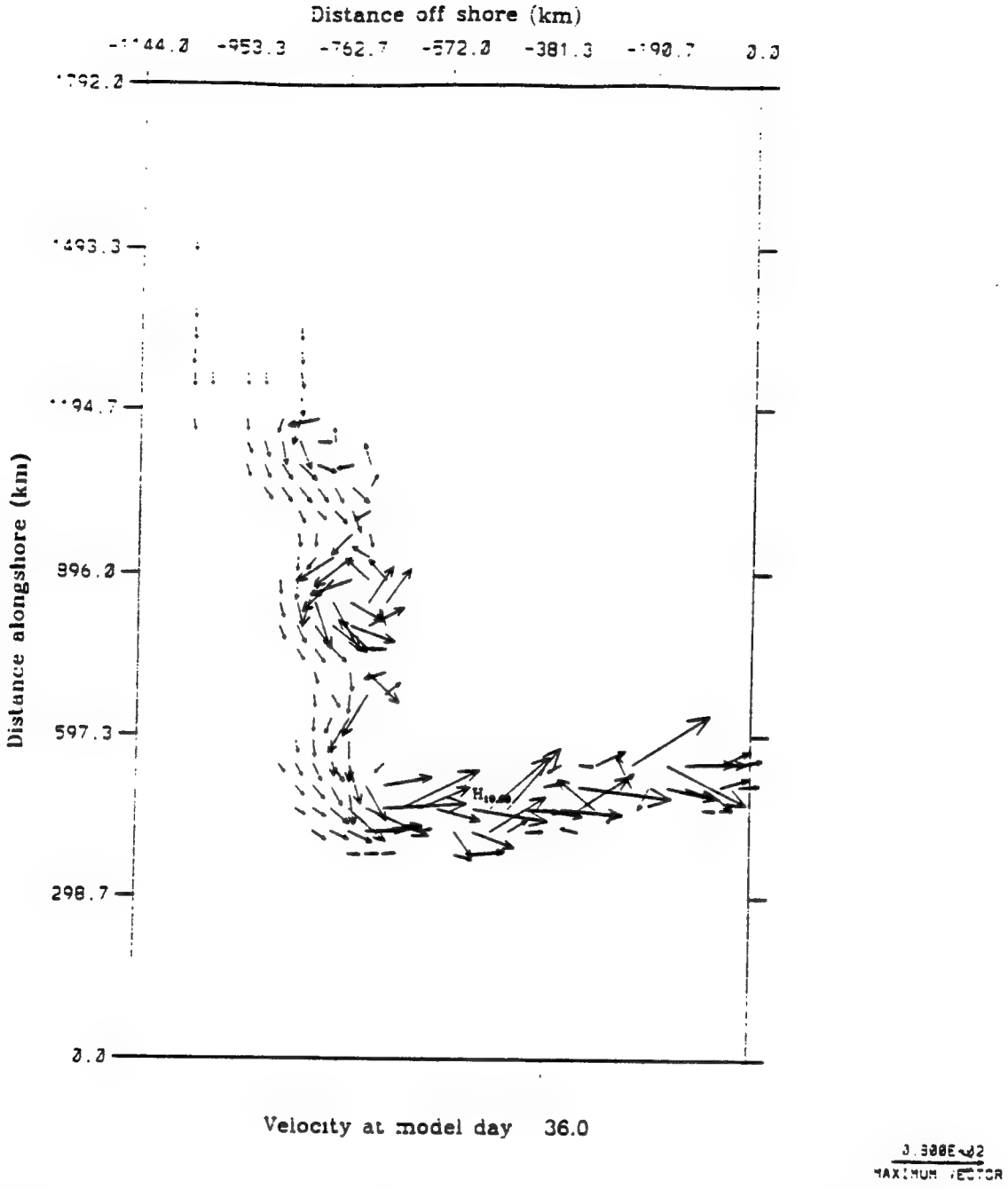

Figure 4.20c Experiment 5: Surface velocity vectors at day 36. To avoid clutter, velocity vectors are plotted at every third grid point in both the cross-shore and alongshore direction, and velocities less than 5 cm s^{-1} are not plotted. Note the formation of anticyclonic eddies at Fremantle (y~850 km), and Shark Bay (y~1000 km).

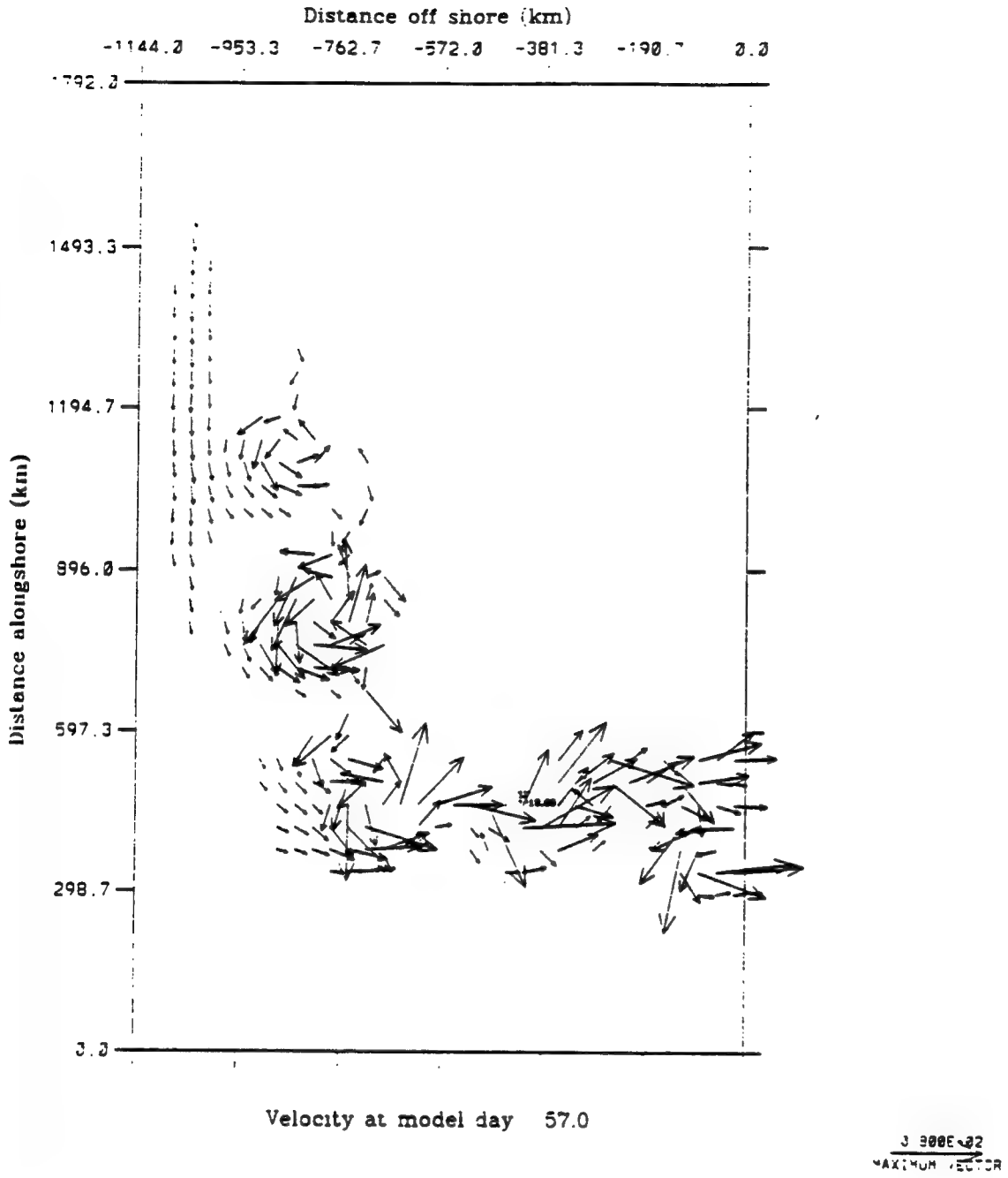

Figure 4.20d Experiment 5: Surface velocity vectors at day 57. To avoid clutter, velocity vectors are plotted at every third grid point in both the cross-shore and alongshore direction, and velocities less than 5 cm s^{-1} are not plotted. Note the anticyclonic eddies near Cape Leeuwin (y~500 km) and Cliffy Head (x~770), and off the coast of Albany (x~500 km). The appearance of an offshore poleward current has formed from a split in the geostropic inflow caused by the westward propagation of west coast eddies.

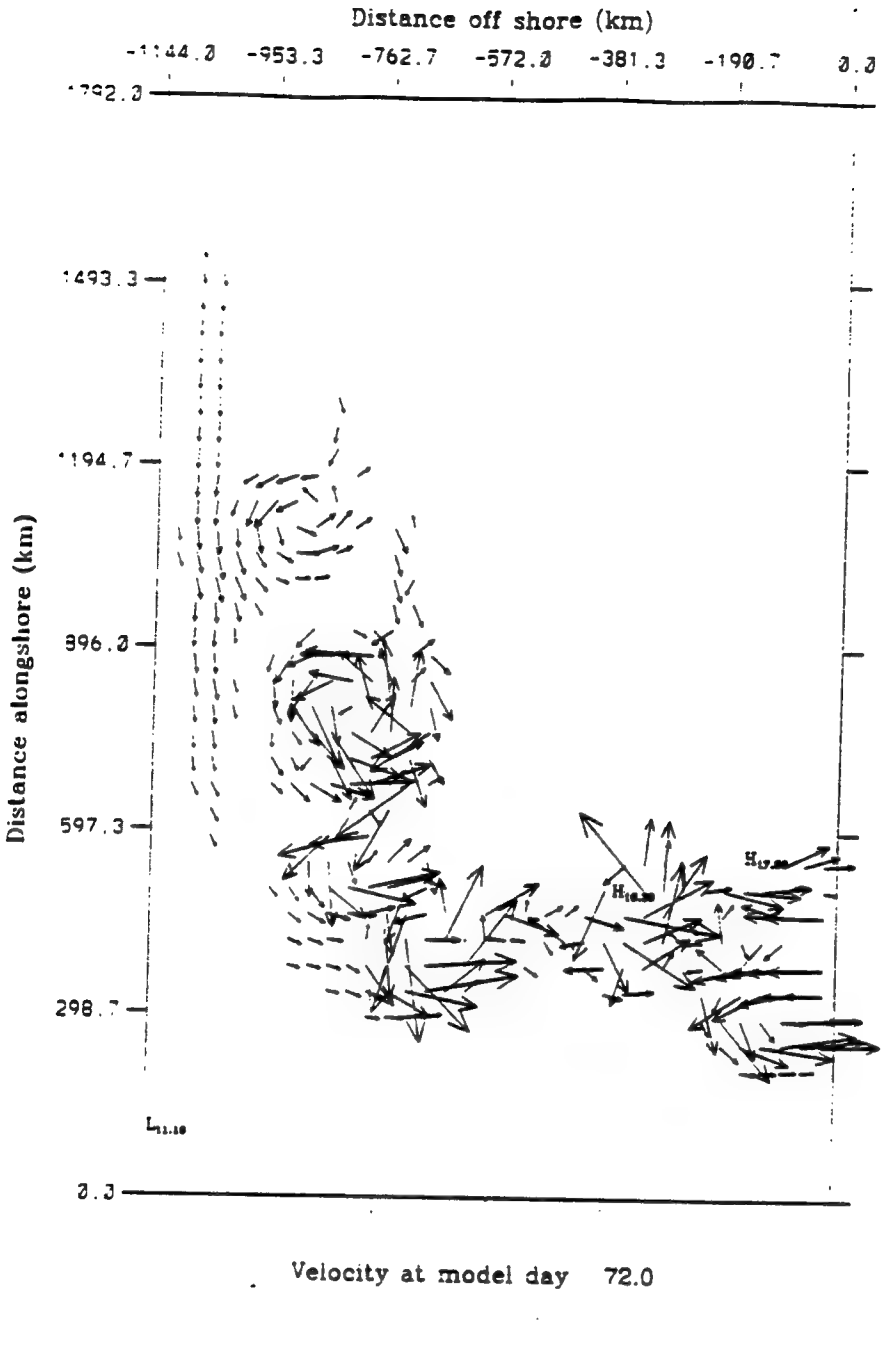

Figure 4.20e Experiment 5: Surface velocity vectors at day 72. To avoid clutter, velocity vectors are plotted at every third grid point in both the cross-shore and alongshore direction, and velocities less than 5 cm s^{-1} are not plotted. Note the formation of secondary meanders formed near Shark Bay (y~1000 km), Dongara (y~900 km), and Fremantle (y~850 km), by the influence of the NWS waters.

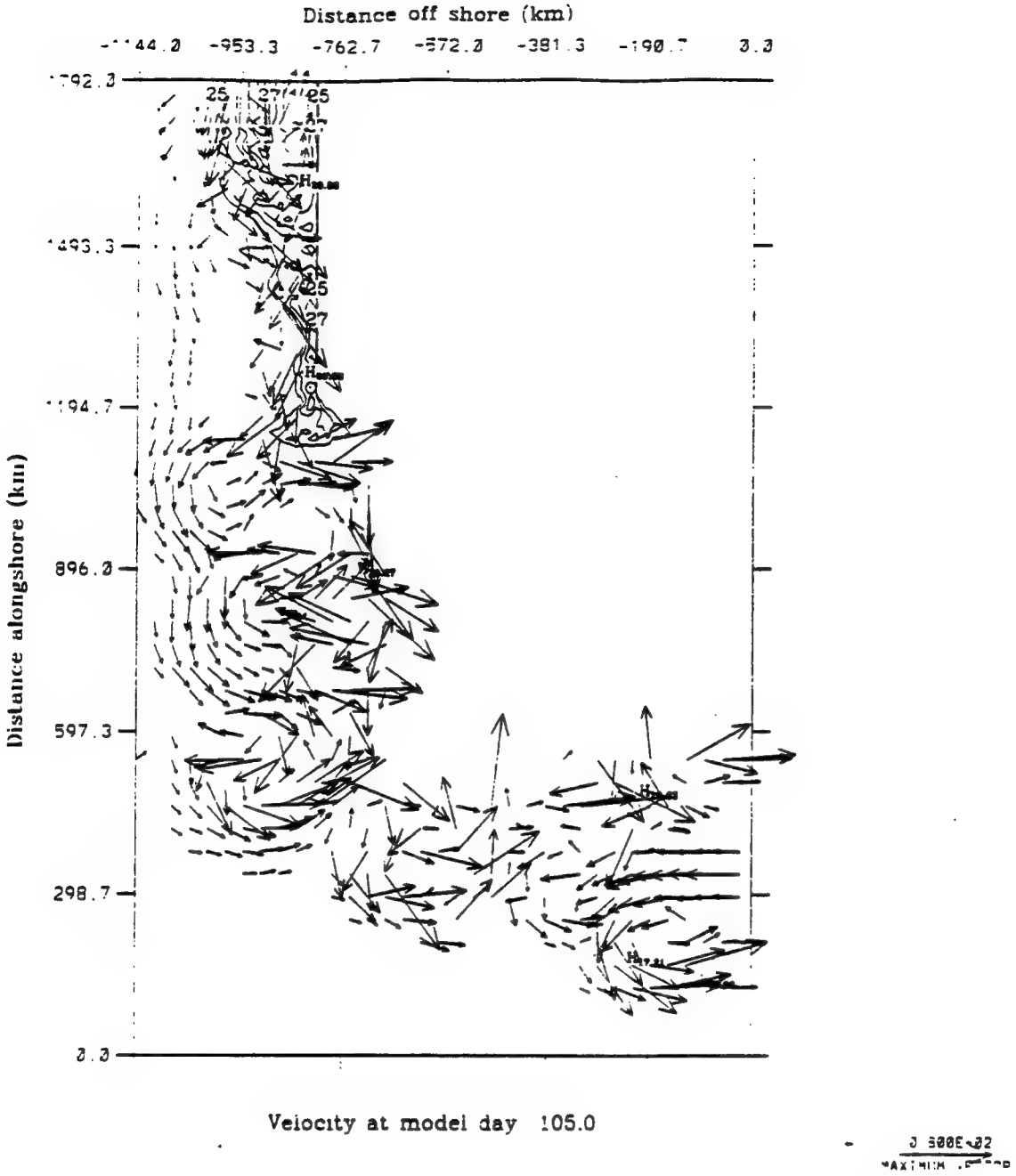

Figure 4.20f Experiment 5: Surface velocity vectors at day 105. To avoid clutter, velocity vectors are plotted at every third grid point in both the cross-shore and alongshore direction, and velocities less than 5 cm s^{-1} are not plotted. Note that the meander formed by the NWS waters "dam-break" has intensified so that anticyclonic eddies have been generated.

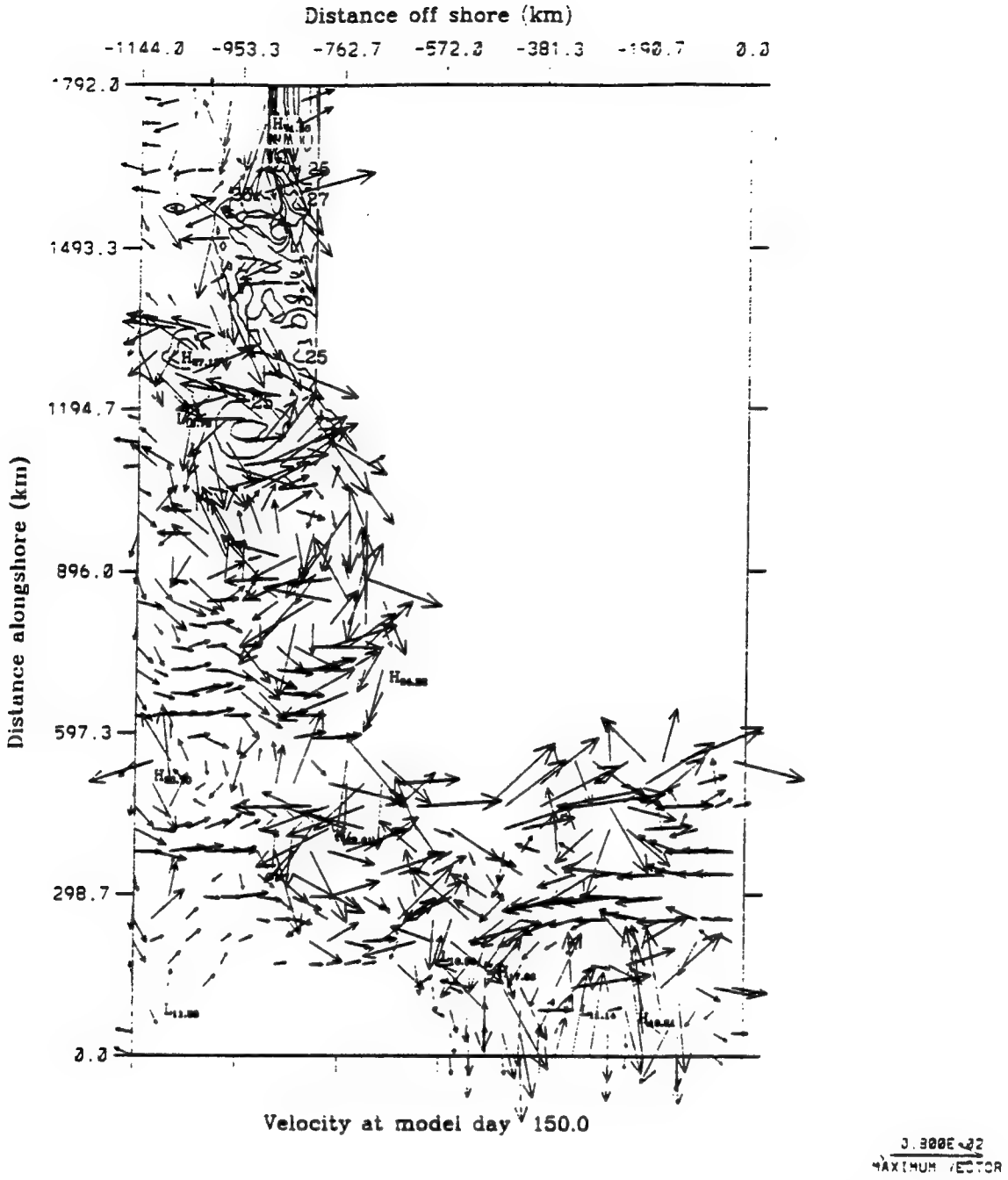

Figure 4.20g Experiment 5: Surface velocity vectors at day 150. To avoid clutter, velocity vectors are plotted at every third grid point in both the cross-shore and alongshore direction, and velocities less than 5 cm s^{-1} are not plotted. Note that the intensification of the offshore poleward current restricts the growth and propagation rate of eddies.

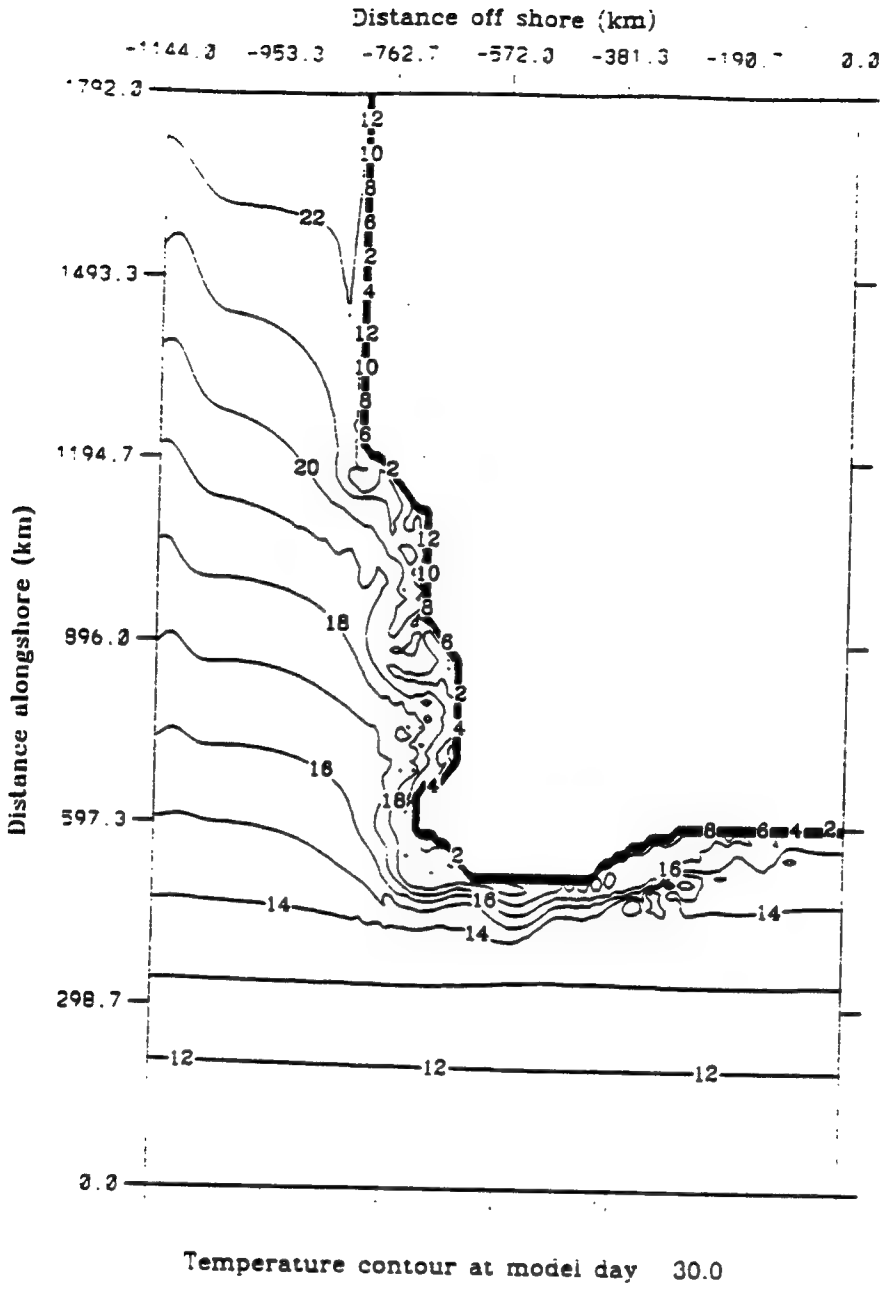

Figure 4.21a Experiment 5: Surface temperature at day 30. The contour interval is 1° C. The temperature increases towards the west coast. Note the strong temperature front established along the Southern Australian coast.

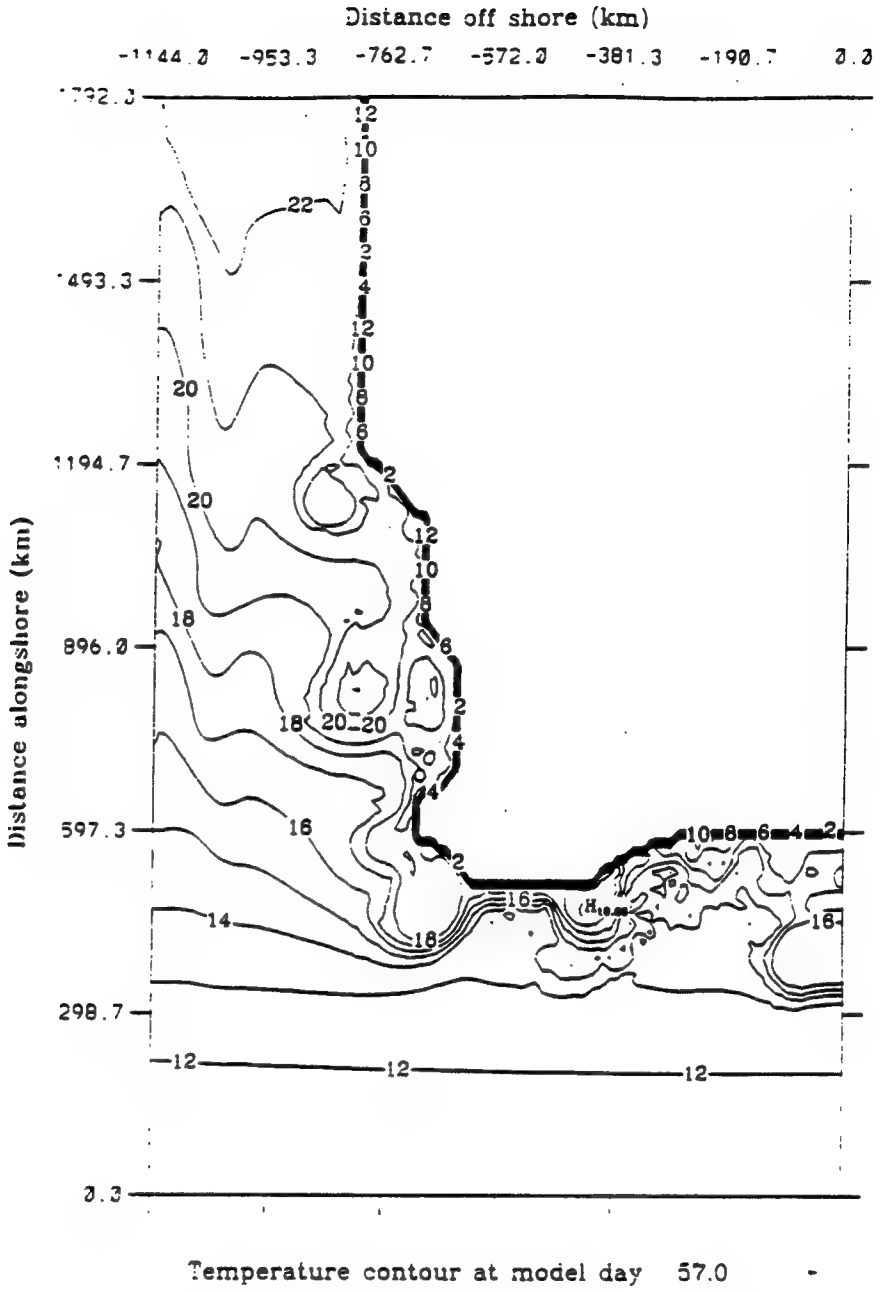

Figure 4.21b Experiment 5: Surface temperature at day 57. The contour interval is 1° C. The temperature increases towards the west coast. Note that the wind forcing has intensified the strong temperature front established along the Southern Australian coast. Cold Sub-Antarctic Waters have been entrained into the Leeuwin Current front.

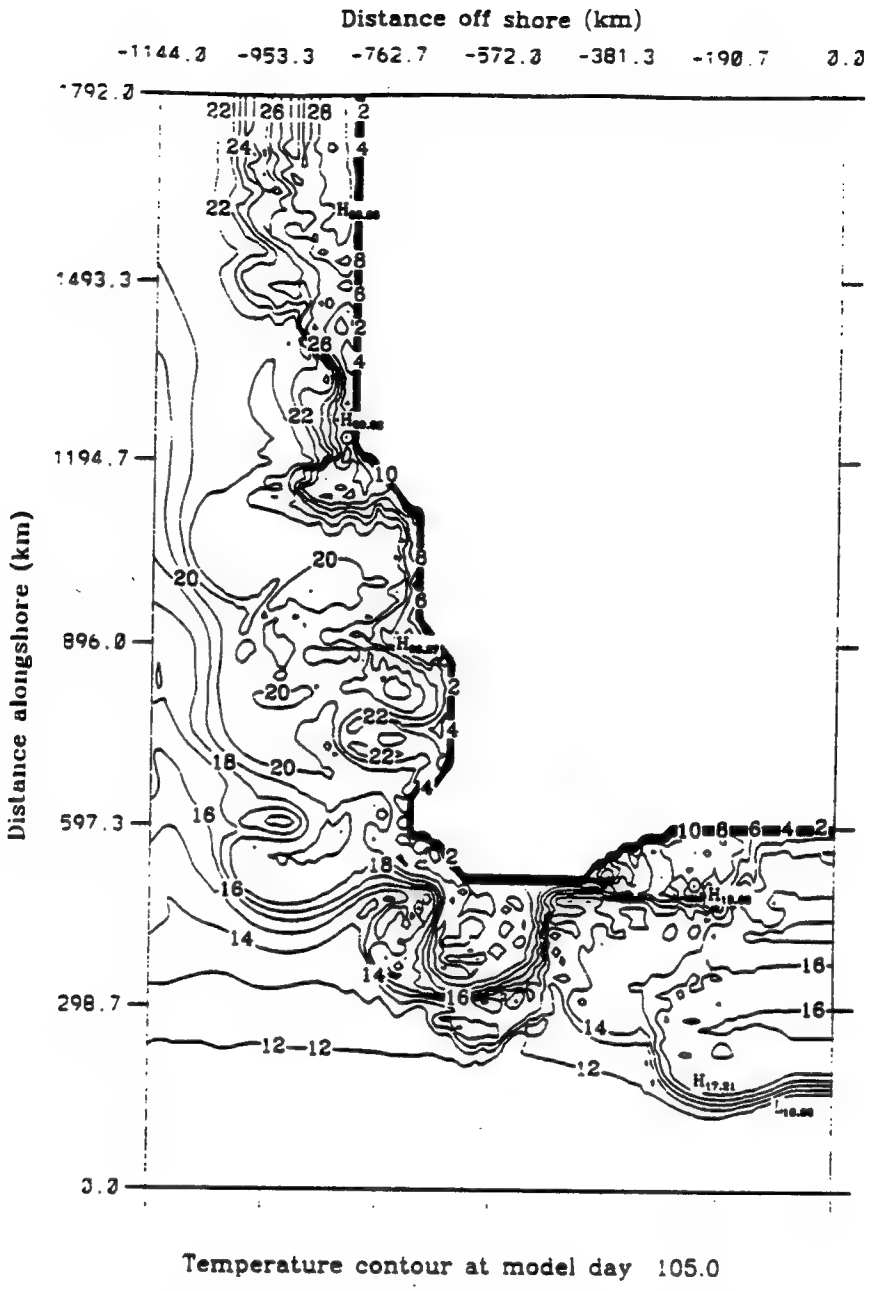

Figure 4.21c Experiment 5: Surface temperature at day 105. The contour interval is 1° C. The temperature increases towards the west coast. Note the advection of the NWS waters along the entire coast has increased the newly formed eddies temperature by ~2°C. The temperature front established along the Southern Australian coast continues to intensify.

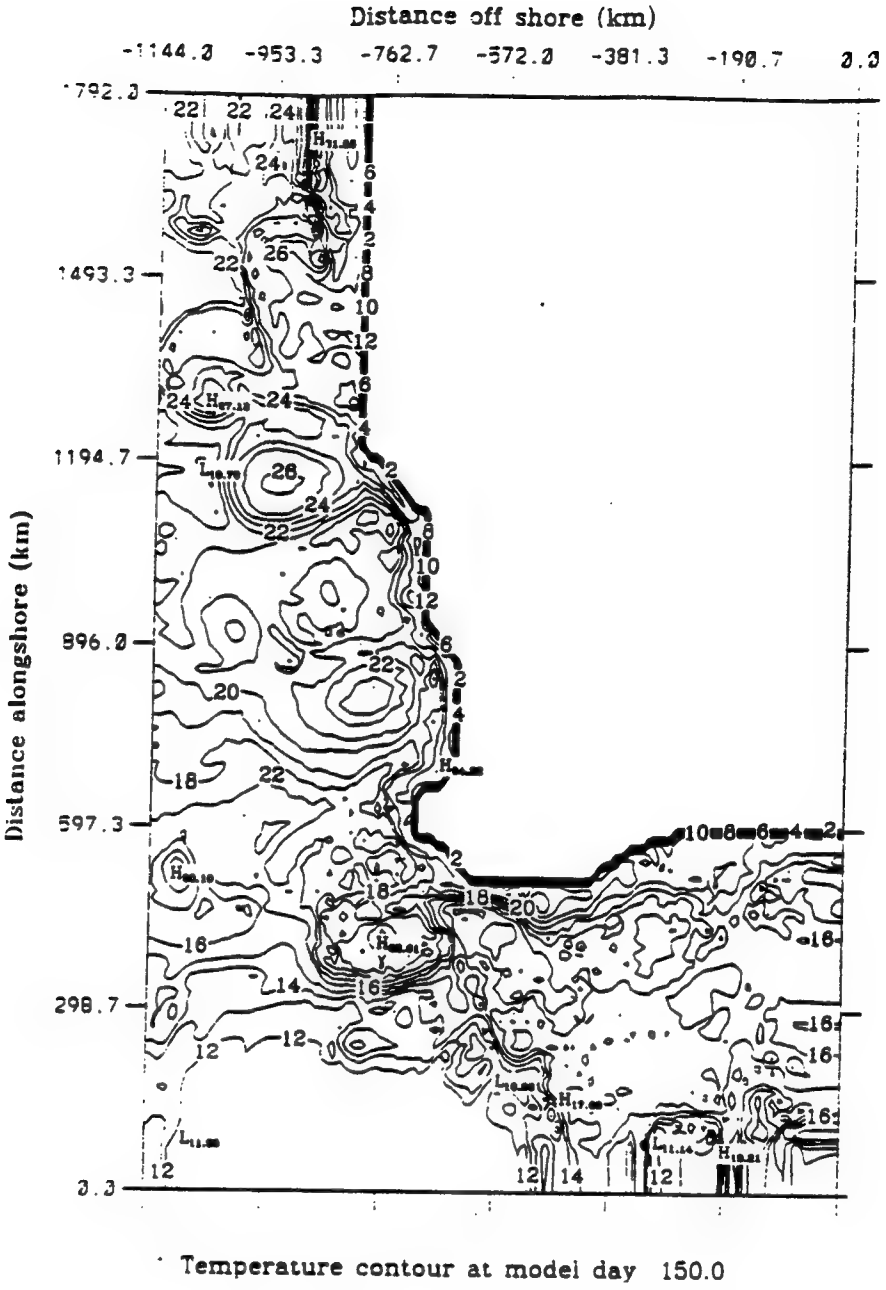

Figure 4.21d Experiment 5: Surface temperature at day 150. The contour interval is 1° C. The temperature increases towards the west coast. Note that the wind forcing acts to recede the bulk of the NWS waters to north of Shark Bay (y~1000 km), and also establishes a strong temperature front (~3°C) along the Western Australian coast.

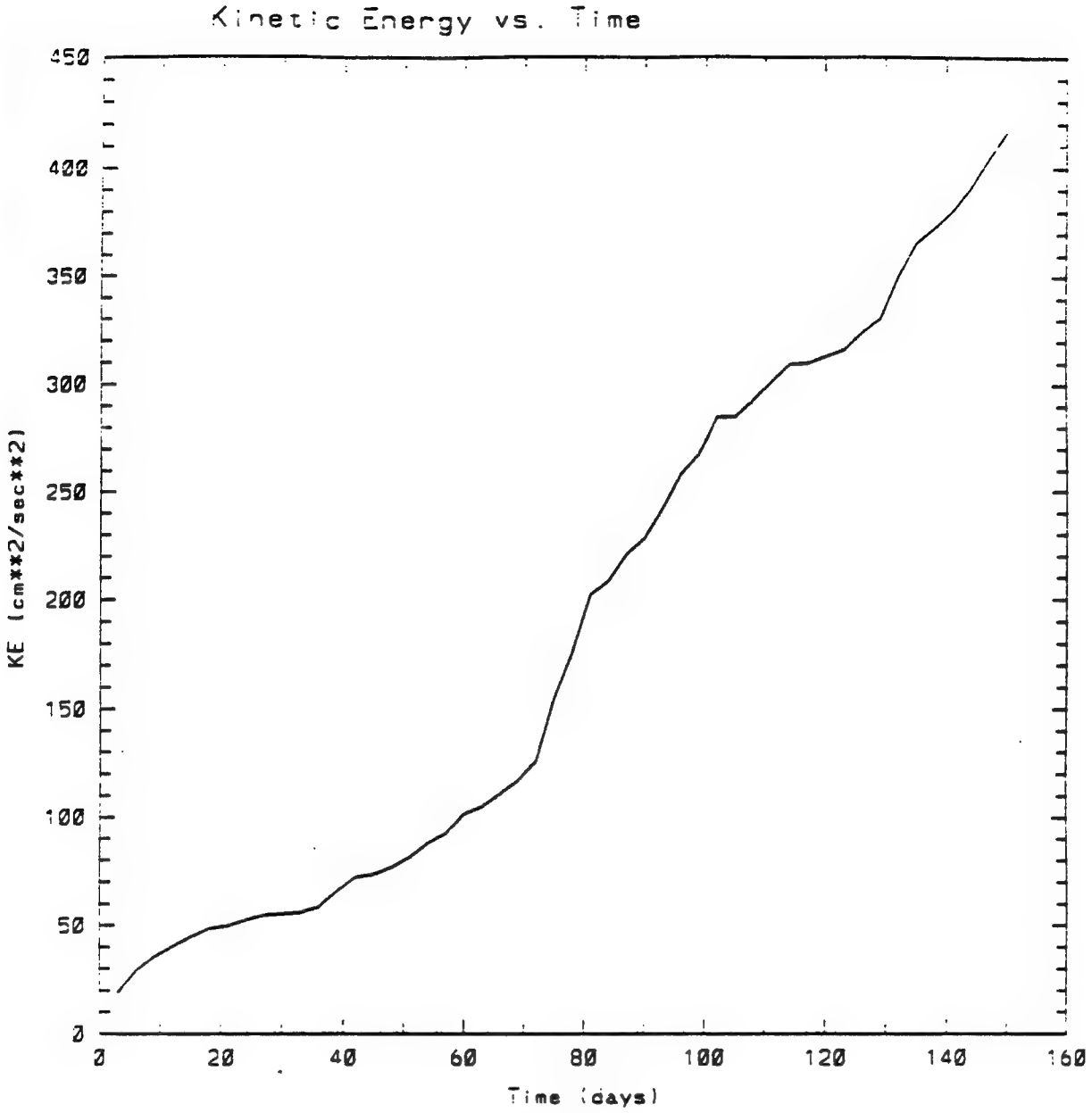

Figure 4.22 Experiment 5: Total kinetic energy per unit mass time series for the first 150 model days averaged over the entire domain (Units of the kinetic energy are cm^2s^{-2}).

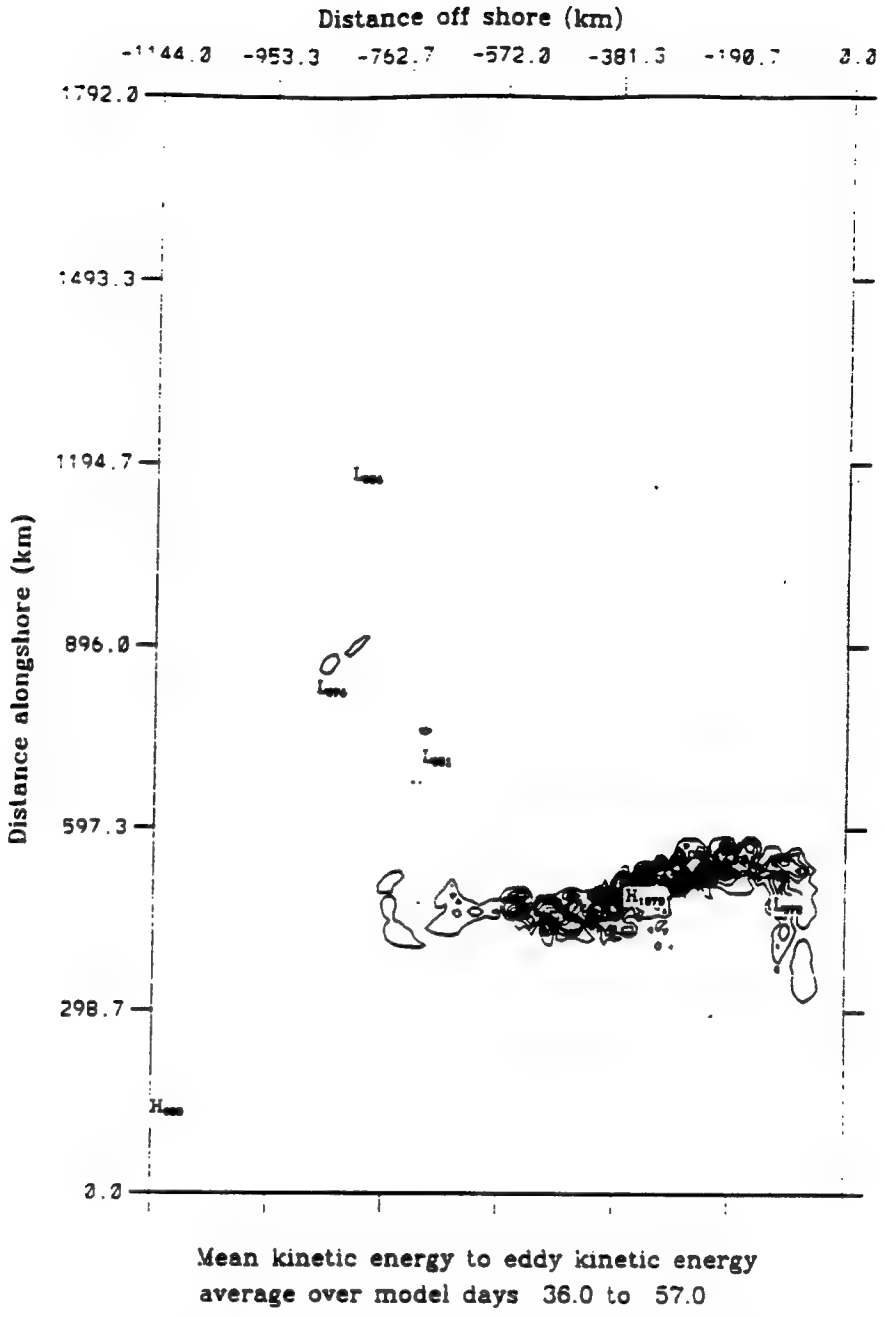

Figure 4.23a Experiment 5: Energy transfers of mean to eddy kinetic energy (i.e., barotropic energy transfer) for model days 36 to 57. The contour interval is 1 ergs cm^{-3} s^{-1}.

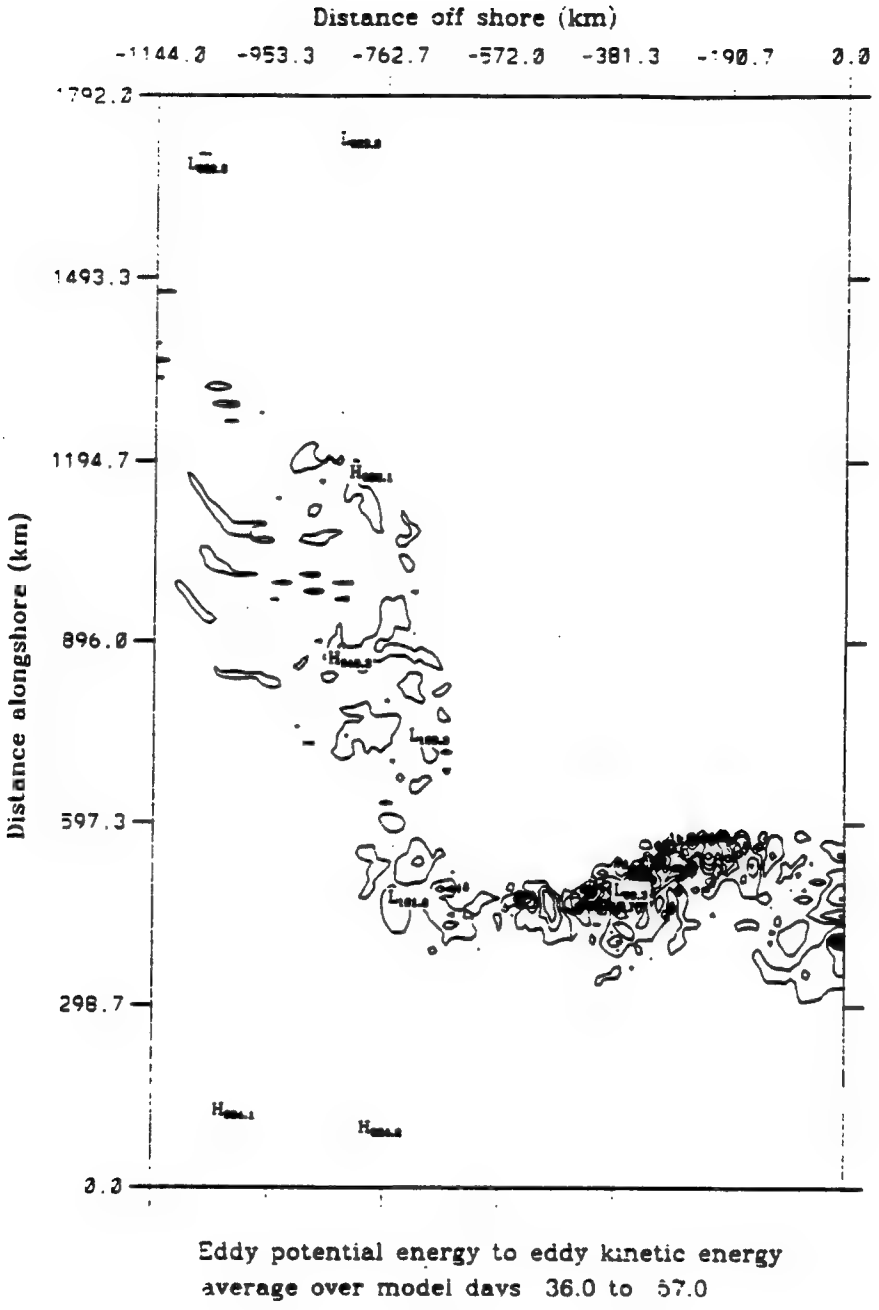

Figure 4.23b Experiment 5: Energy transfers of eddy potential to eddy kinetic energy (i.e., baroclinic energy transfer) for model days 36 to 57. The contour interval is 1 ergs cm^{-3} s^{-1}.

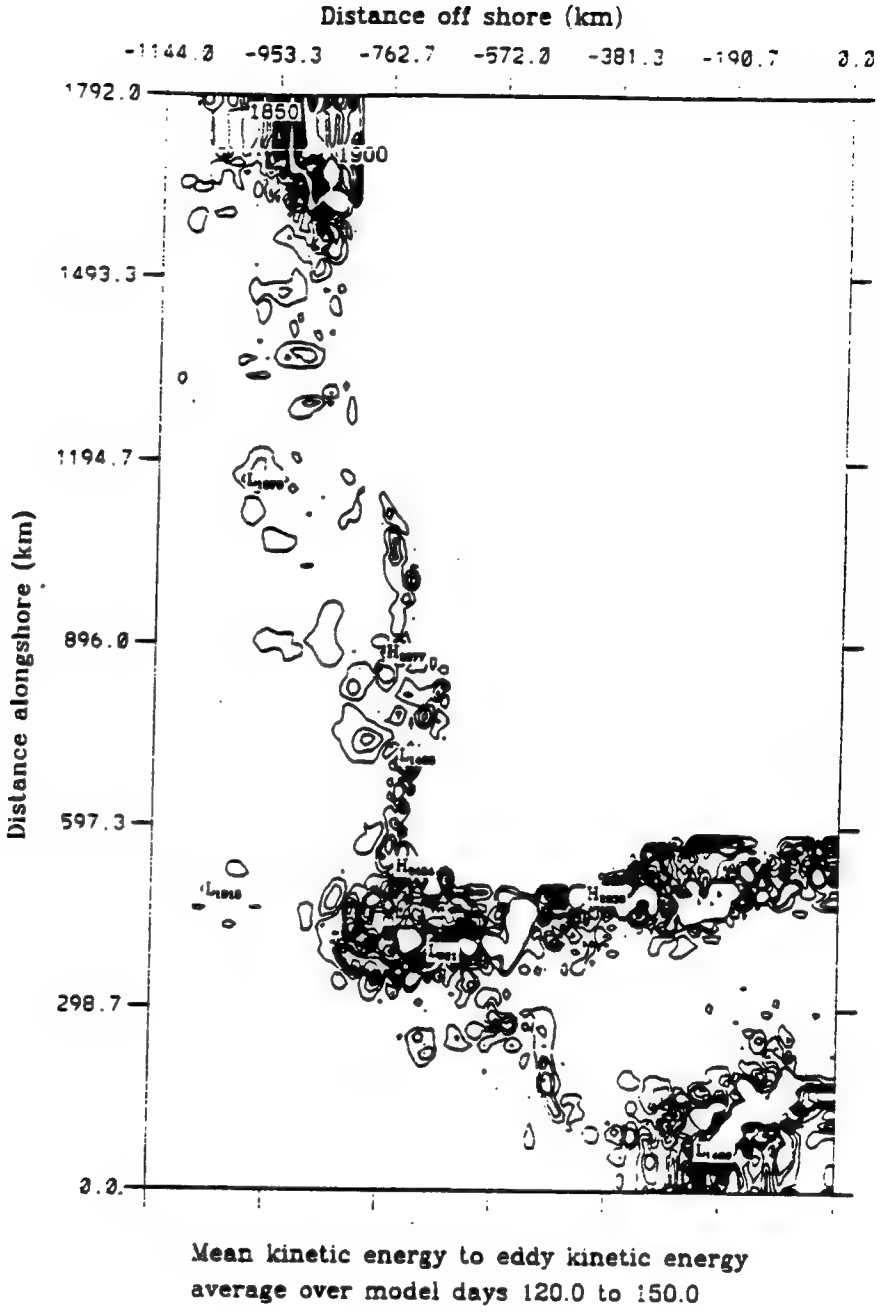

Figure 4.24a Experiment 5: Energy transfers of mean to eddy kinetic energy (i.e., barotropic energy transfer) for model days 120 to 150. The contour interval is 1 ergs cm^{-3} s^{-1}.

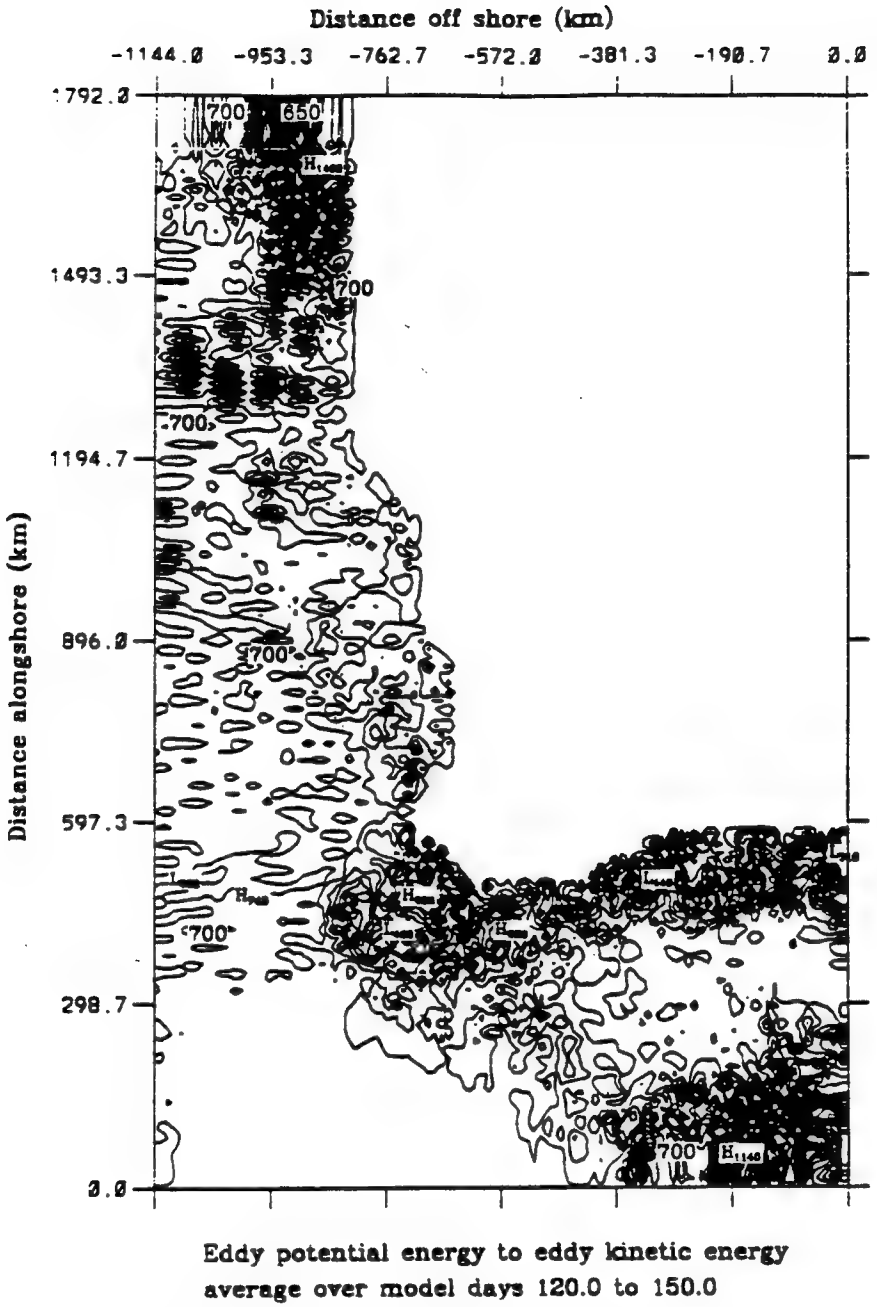

Figure 4.24b Experiment 5: Energy transfers of eddy potential to eddy kinetic energy (i.e., baroclinic energy transfer) for model days 120 to 150. The contour interval is 1 ergs cm^{-3} s^{-1}.

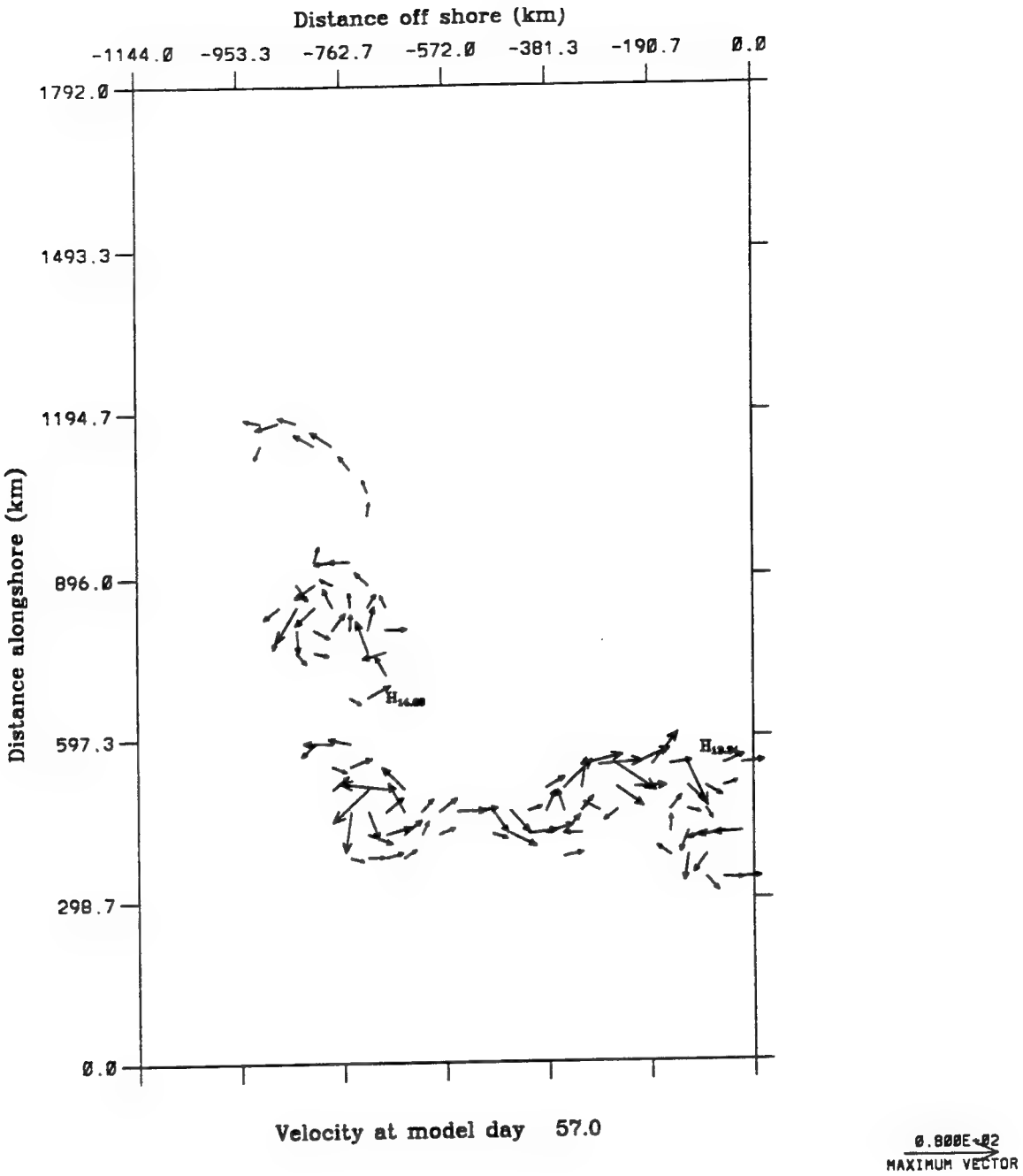

Figure 4.25 Experiment 5: Model level 5 (316 m) velocity vectors at day 57. To avoid clutter, velocity vectors are plotted at every third grid point in both the cross-shore and alongshore direction, and velocities less than 5 cm s^{-1} are not plotted. Note that the preferred locations for eddy formation are evident at model level 5. Also note the westward offshoot of the anticyclonic eddy at Cliffy Head (x~500 km).

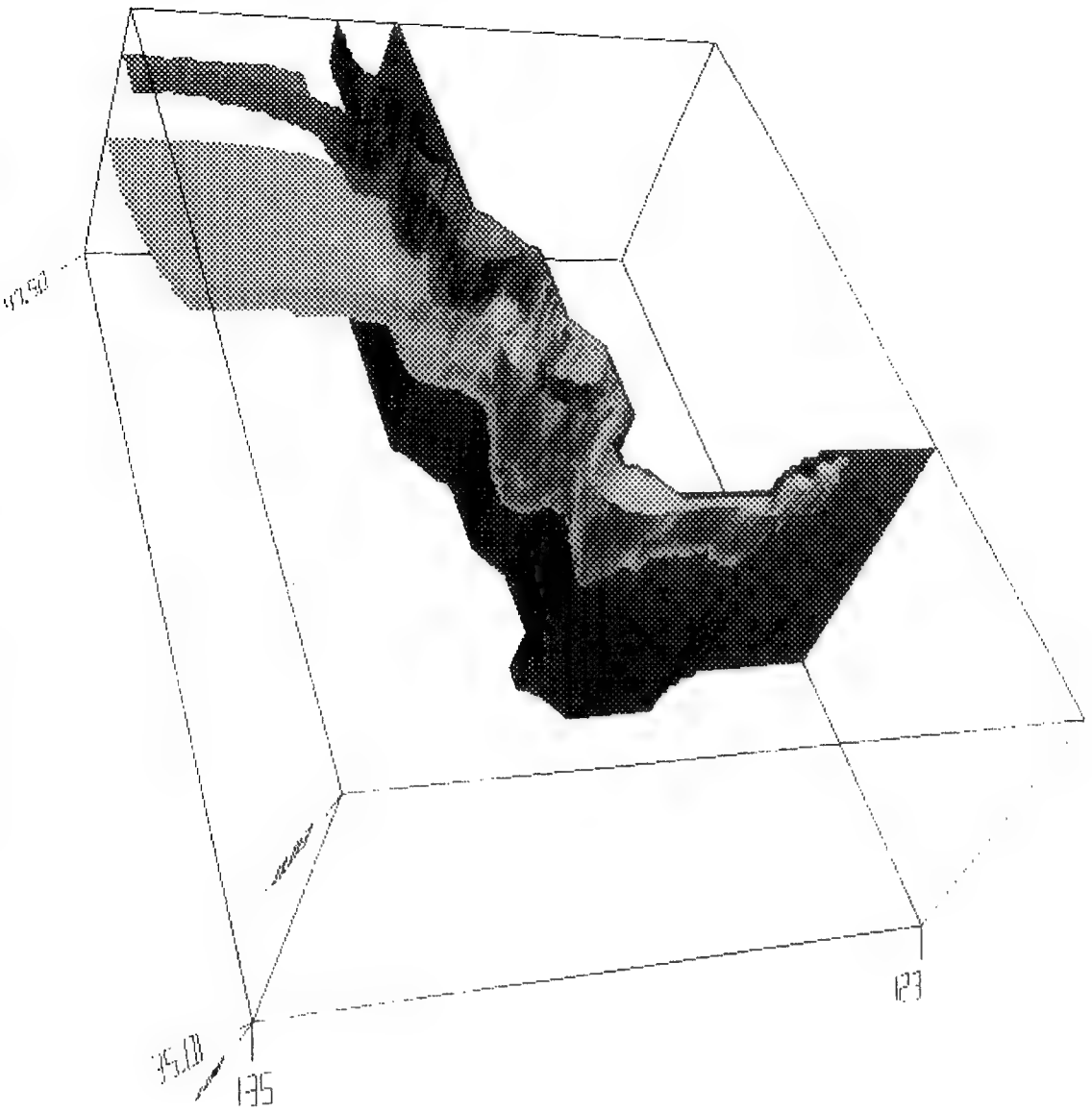

Figure 4.26a This three dimensional depiction of the model's irregular coastline shows the preferred location for the formation of mesoscale instabilities. Note the development of meanders and eddies near Shark Bay, between Dongara and Fremantle, Cape Leeuwin and off the coast of Albany.

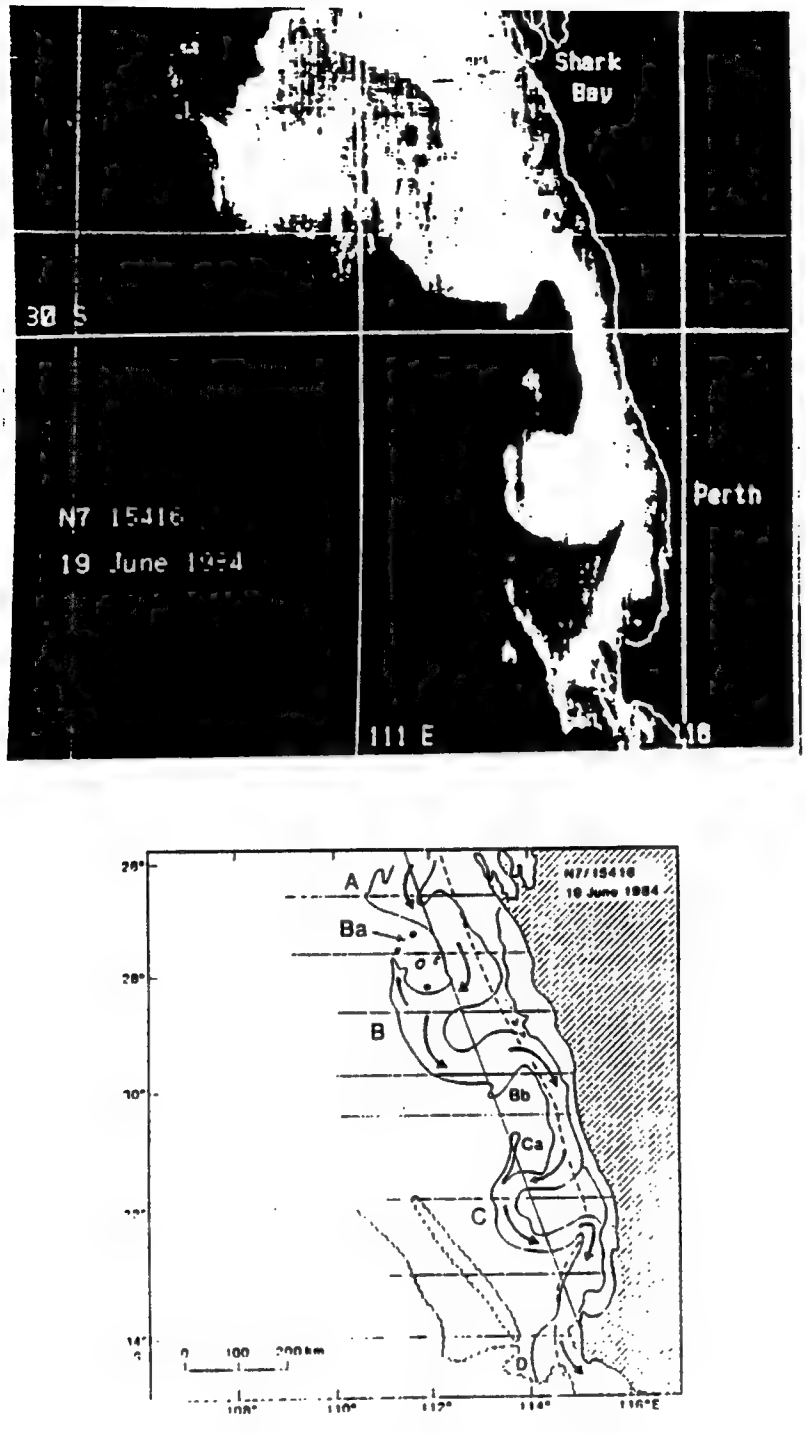

Figure 4.26b The top figure displays brightness temperature from AVHRR band 4 taken June 19, 1984. The land to the right of the image is grey, and the Leeuwin Current (warm) is in pale tones. The bottom figure is a line sketch of the AVHRR image displaying the major west coast Leeuwin Current structures (A,B,C, and D). The location of these major structures are consistent with the preferred location of mesoscale instabilities along the model's irregular coastline (from Pearce and Griffiths, 1991)

Figure 4.26c Surface temperature images from the NOAA11 satellite. Warmer water appear as red with the coolest water a dark blue. Both the top image (16 April 1991), and the bottom image (28 July 1991) display the major south coast Leeuwin Current structures in the vicinity of Cape Leeuwin, Cliffy Head, and Albany. These locations are consistent with the preferred locations of mesoscale instabilities along the model's irregular coastline (Images courtesy of Allen Pearce and Angela Way).

V. SUMMARY AND RECOMMENDATIONS

A. SUMMARY

The use of process-oriented modeling studies of the Leeuwin Current System off Western and Southern Australia have been instrumental in providing insight into the development of unique current characteristics and mesoscale features. In all experiments, a poleward and eastward surface current, an equatorward and westward undercurrent, meanders, and eddies were generated. With the addition of the Southern Australian coast to the model domain, a significant amount of horizontal and vertical shear was added to the region. The maximum current (and undercurrent) velocities occurred at Cape Leeuwin. The eddies that formed had time scales of months, with some eddies appearing as semi-permanent features. The eddy length scales were consistent with the Rossby radius of deformation. The wavelengths for the west coast eddies were larger than the south coast eddies. The south coast eddies also propagated westward at a slower rate than the west coast eddies. These effects were likely due to the ongoing geostropic inflow which acted to deform the eddy shape, to inhibit the growth rate of eddies, and to impede the westward Rossby propagation of eddies.

Experiment 1 (ideal coastline) revealed how the current dynamics around Cape Leeuwin increase instability by inducing anticyclonic vorticity into the system. This anticyclonic vorticity is likely a result of the current shifting from poleward to eastward via the Coriolis and geostrophic forces acting on the current. The 90° corner (Cape Leeuwin) was the preferred location for the development of initial mesoscale features. Subsequent mesoscale features developed upstream (off Fremantle) and downstream (off Albany) of Cape Leeuwin.

In Experiment 2, the significance of adding an irregular (realistic) coastline, revealed a greater increased barotropic

instability, and a reduced baroclinic instability for eddy generation. The irregular coastline established a more energetic and dynamic surface current, but effectively decreased the magnitudes of the undercurrents (both equatorward and westward). It also limited the extent of advection of warmer equatorial waters along the entire coast. Initial eddy development occurred much earlier, and developed in preferred locations: at Shark Bay, between Dongara and Fremantle, and at Cape Leeuwin (in the vicinity of coastal indentations along Western Australia, and Cape Leeuwin).

In the follow-on experiments 3 and 4, North West Shelf (NWS) water added a significant amount of horizontal shear near the equatorial source region. The influence of the NWS waters diminished away from the source region but contributed significantly to downstream current characteristics. The overall current baroclinicity increased significantly. Greater current velocities were observed all along the coastal regions. The observed undercurrents were significantly higher than in previous experiments. The warmer NWS waters were advected further south which resulted in warmer 2-3°C increases in temperature for waters along the coast and into the Great Australian Bight region. This led to the establishment of strong temperature fronts along Southern Australia as cooler Sub-Antarctic Water was entrained into the southern branch of the current system. Mesoscale features formed earlier in the equatorial region of the model domain. The NWS waters increased the scale at which the dominant eddy growth occurred by modifying the thermal structure in the inshore region. The dominant scale of eddy generation for the west coast eddies in the current was ~180 km. As in experiments 1 and 2, eddies off the south coast were generally smaller (~120 km) than eddies off Western Australia.

Experiment 5 produced a model Leeuwin Current which had a complex flow regime due to the presence of the three major

forcing mechanisms. The wind forcing effects were strongest in the equatorial and the interior ocean regions of the model domain, and dominated the regional characteristics in the pre-NWS water time period. The winds along the irregular coastline increased the current baroclinicity via upwelling along the west coast, and produced an intensified current front along the south coast. The winds opposed the thermal forcing along the west coast, which effectively decreased the magnitude of the poleward current (and undercurrent). Near Cape Leeuwin, easterly climatological winds augmented the thermal forcing effect and significantly enhanced the current flow around Cape Leeuwin. Poleward and eastward current velocities were reduced from those of previous experiments in the pre-NWS water time period.

The formation of eddies and their subsequent westward propagation resulted in a division of the onshore geostrophic inflow. The establishment of an offshore poleward current in addition to a narrow inshore poleward current decreased the westward Rossby wave propagation rate and limited the growth rate of the west coast eddies. The two poleward currents reunited at Cape Leeuwin, which greatly increased regional horizontal and vertical shears.

When NWS waters were added to the model, they initially dominated the source region, with the wind forcing only having second order effects. This effectively eliminated regional upwelling and surged warm waters (previously held abate by the wind force) along the entire coastline. The regeneration of west coast eddies followed by their subsequent westward Rossby propagation intensified the offshore poleward current, and further increased regional shear forces. The mesoscale features generated by the NWS water subsequently propagated away from the west coast, diminishing in their dominant influence over the wind. The wind forcing along the west coast refined the narrow poleward current from Dongara to Cape

Leeuwin and intensified the coastal temperature and velocity front. This established a strong west coast baroclinic zone. The wind force additionally acted to recede the bulk of the warmer NWS water to north of Carnarvon.

Eddies formed in response to the three forcing mechanisms. Different instability mechanisms dominated different regions of the model domain. Although the eddies were generated by mixed instabilities, baroclinic instability dominated in the west coast eddy formation regions, while barotropic instability dominated in the south coast eddy formation regions. The dominant length scale for the west coast eddies in the current was ~180-300 km, while the dominant length scale for the south coast eddies was only ~140 km. Most of the eddies had time scale of months; the eddies near the dynamic region of Cape Leeuwin seem to be semi-permanent features. This is possibly due to the combined effects of easterly climatological winds, intensified geostropic inflow (from continuous thermal forcing), and shear forces that occurred as a result of the mergence of the two poleward currents.

Based on these results, it can be concluded that process-oriented modeling studies of the Leeuwin Current System off Western and Southern Australia have been instrumental in providing insight into the development of unique current characteristics and of mesoscale features. The model results from Experiment 5, which has the most realistic features, agree well with available observations off Western and Southern Australia. These findings are also generally consistent with previous model studies (e.g., Batteen et al., 1992; Weaver and Middleton, 1989,1990). These results support the hypothesis that the Leeuwin Current is a thermally driven current maintained by the equatorward surface heating and poleward surface cooling, with characteristics governed by the variation of daily thermal and wind forces.

B. NAVAL RELEVANCE AND RECOMMENDATIONS

1. Naval Relevance

Since the focus on littoral regions is an accelerated research initiative of the Office of Naval Research, obtaining an understanding of the impact of the three contributing forces driving the Leeuwin Current, as well as the preferred locations of the formation of mesoscale features, is a step in the right direction. However, further research is required in order to accurately predict the long term maintenance, location and intensity of mesoscale features. Nevertheless, the finding in this thesis can be applied to enhance Naval operations off the coast of Western and Southern Australia.

The anomalous Leeuwin Current is one of the world's strongest eastern boundary currents, with seasonal peak velocities on the order of some western boundary currents. The current's sharp velocity and temperature fronts, as well as its semi-permanent warm core eddies, can be applied tactically in the defense of the Australian Continent. Submarine, Anti-Submarine, and Mine Warfare elements can achieve a tactical advantage by properly utilizing the current system characteristics (i.e., the placement of acoustic arrays; the laying, known position, and removal of mines; and the convert deployment of drivers). This knowledge is also instrumental in planning the ingress and egress of Naval Vessels to and from a port visit in the friendly town of Fremantle, the major shipping site for Western Australia.

2. Recommendations

Future studies should extend the model runs to multiple year runs. This would help to identify seasonal characteristics (i.e., regeneration and maintenance) of the Leeuwin Current System.

There are also specific questions to address regarding the characteristics of the Leeuwin Current System: Will a

continental shelf effect the generation and intensity of the split geostropic inflow, and the formation of the offshore poleward current by impeding westward Rossby propagation of mesoscale features? Will the addition of bottom topography into the model enhance baroclinic instability even more such that it becomes the dominant instability mechanism for the entire model domain? Are the smaller scale eddies off Southern Australia a product of barotropic instability as proposed by the model, or baroclinic instability as proposed by Griffiths and Pearce (1985)? Do preferred locations for meanders and eddies actually exist? Pearce and Griffiths (1991) examined satellite images from 1982-1986 from which they tentatively concluded that no preferred location existed for meander and eddy formations. They also concluded that bottom topography did not seem to play an important role in meander and eddy formation.

It is also recommended that Experiment 5 be repeated with an even more detailed coastline (including bottom topography in the model) in an extended model run to investigate seasonal effects and the maintenance of the current over a number of years. Does the westward undercurrent actually exist, or is it just a westward offshoot of an anticyclonic eddy? A cross sectional area of the east-west velocity component area near Cliffy Head revealed a model undercurrent (e.g. 4.2b); however, the velocity plot (Figure 4.25) fails to show a sustained undercurrent with magnitudes on the same order as the cross- section plot. Figure 4.25 does show an anticyclonic eddy with a westward offshoot near Cliffy Head. To date, only the observations of RV Franklin's survey of this region have revealed a westward undercurrent (Cresswell and Peterson 1993). This anticyclonic eddy offshoot may be the source of the Cresswell and Peterson (1993) undercurrent observation.

What is the seasonal extent of the Leeuwin Current into the Great Australian Bight? The model Leeuwin Current extended into the Great Australian Bight throughout the entire model run. This was contrary to Cresswell and Peterson's (1993) 6 March 1987 observation that the Leeuwin Current recedes from the southern coast and is arrested near 34°S along the western coast. Rochford (1986) also identified a recession of the Leeuwin Current out of the Great Australia Bight region. Multiple-year model runs should provide insight and answers to the above questions, as well as insight into the seasonality of the Leeuwin Current System.

LIST OF REFERENCES

Arakawa, A., and V.R. Lamb, 1977: Computational design of the basic dynamical processes of the UCLA general circulation model. In, *Methods in Computational Physics*, J. Chang, ed., Academic Press, 17, 173-265.

Andrews, J.C., 1977: Eddy Structure and the West Australian Current. *Deep-Sea Research*, 24, 1133-48.

Bayler, E.J., and M.L. Batteen, 1991: Seasonal wind and ocean thermal forcing influences on the generation of the Leeuwin Current and its eddies. Naval Postgraduate School Technical Report, NPS OC-91-003, 194pp.

Batteen, M.L., 1989: Model simulations of a coastal jet and undercurrent in the presence of eddies and jets in the California Current System. In, *Poleward Flows Along Eastern Ocean Boundaries*, S.J. Neshyba, C.N.K. Mooers, R.L. Smith and R.T. Barber, eds., Springer-Verlag, 263-279.

Batteen, M.L., and Y.-J. Han, 1981: On the computational noise of finite-difference schemes used in ocean models. *Tellus*, 33, 387-396.

Batteen, M.L., R.L. Haney, T.A. Tielking, and P.G. Renaud, 1989: A numerical study of wind forcing of eddies and jets in the California Current System. *J. Mar. Res.*, 47, 493-523.

Batteen, M.L., M.J. Rutherford, 1990: Modeling studies of eddies in the Leeuwin Current: The role of thermal forcing. *J. Phys. Oceanogr.*, 20, 1484-1520.

Batteen, M.L., M.J. Rutherford, and E.J. Bayler, 1992: A numerical study of wind- and thermal-forcing effects on the ocean circulation off Western Australia. *J. Phys. Oceanogr.*, 22, 1406-1433.

Boland, F.M., J.A. Church, A.M.G. Forbes, J.S. Godfrey, a. Huyer, R.L. Smith and N.J. White, 1988: Current-meter data from the Leeuwin Current Interdisciplinary Experiment. *CSIRO Marine Laboratories, Report* 198, 31pp.

Camerlengo, A.L. and J.J. O'Brien, 1980: Open boundary conditions in rotating fluids. *J. Comput. Physics*, 35, 12-35.

Church, J.A., G.R. Cresswell, and J.S. Godfrey, 1989: The Leeuwin Current. *Poleward Flows along Eastern Ocean Boundaries*, S. Neshyba, C.N.K. Mooers, R.I. Smith, and R.T. Barber, Eds, Springer-Verlag, 230-252.

Condie, S.A., and G.N. Ivey, 1988: Convectively driven coastal currents in a rotating basin. *J. Mar. Res.*, 46, 473-494

Cresswell, G.R., and T.J. Golding, 1980: Observations of a south-flowing current in the southeastern Indian Ocean. *Deep-Sea Res.*, 27A, 449-466.

Cresswell, G.R., and J.L. Peterson, 1993: The Leeuwin Current South of Western Australia. *Aust. J. Mar. Freshwater Res.*, 1993, 44, 285-303.

Gentilli, J., 1972: Theral anomalies in the Eastern Indian Ocean. *Nature (London) Physical Sciences*, 238, 93-95.

Godfrey, J.S., and K.R. Ridgway, 1985: The large-scale environment of the poleward-flowing Leeuwin Current, Western Australia: Longshore steric height gradients, wind stresses and geostrophic flow. *J. Phys. Oceanogr.*, 15, 481-495.

Godfrey, J.S., D.J. Vaudrey, and S.D. Hahn, 1986: Observations of the shelf-edge current south of Australia, winter 1982. *J. Phys. Oceanogr.*, 16, 668-679.

Golding, T.J., and G. Symonds, 1978: Some surface circulation features off Western Australia during 1973-1976. *Aust. J. Mar. Freshwater Res.*, 29, 187-191.

Griffiths, R.W., and A.F. Pearce, 1985B: Instability and eddy pairs on Leeuwin Current south of Australia. *Deep-Sea Res.*, 32, 1511-1534.

Grunlingh, M.L., 1983: Eddies in the southern Indian Ocean and Agulhas Current. In: *Eddies in Marine Science* (A.R. Robinson, Editor), Springer-Verlag, Berlin, 245-264.

Hamon, B.V., 1965: Geostrophic currents in the south-eastern Indian Ocean. Aust. J. Mar. Freshwat. Res. 16, 255-271.

Hamon, B.V., 1972: Geopotential topographies and currents off West Astralia, 1965-69. *CSIRO Division of Fisheries and Oceanography, Technical Paper No.* 32, 11 pp.

Hamon, B.V., and G.R. Cresswell, 1972: Structure functions and intensities of ocean circulation off east and west Australia. *Aust. J. Mar. Freshwater Res.*, 23, 99-103.

Han, Y.-J., 1975: Numerical simulation of mesoscale eddies. PH.D. Thesis, University of California, Los Angeles, 154pp.

Haney, R.L., 1974: A numerical study of the response of an idealized ocean to large-scale surface heat and momentum flux. *J. Phys. Oceanogr.*, 4, 145-167.

Haney, R.L., 1985: Midlatitude sea surface temperature anomalies: A numerical hindcast. *J. Phys. Oceanogr.*, 15, 787-799.

Holland, W.R., 1978: the role of mesoscale eddies in the general circulation of the ocean - numerical experiments using a wind-driven quasigeostrophic model. *J. Phys. Oceanogr.*, 8, 363-392.

Holland, W.R., and M.L. Batteen, 1986: The parameterization of subgrid scale heat diffusion in eddy-resolved ocean circulation models. *J. Phys. Oceanogr.*, 16, 200-206.

Legeckis, R. and G.R. Cresswell, 1981: Satellite observations of sea surface temperature fronts off the coast of Western and South Australia. *Deep-Sea Res.*, 28A, 297-306.

Levitus, S., 1982: Climatological Atlas of the World Ocean. NOAA Professional Paper 13. US Department of Commerce: National Oceanic and Atmospheric Administration. 173pp.

McCreary, J.P., Jr., S.R. Shetye and P.K. Kundu, 1986: Thermohaline forcing of eastern boundary currents: With application to the circulation off the west coast Australia. *J. Mar. Res.*, 44, 71-92.

Parrish, R.H., A. Bakun, D.M. Husby and C.S. Nelson, 1983: Comparative climatology of selected environmental processes in relation to eastern boundary current pelagic fish reproduction. Sharp, G.D., J. Csirke, Eds., *Proc. Expert Consultation to Examine Changes in Abundance and Species of Neritic Fish Resources*, San Jose, Costa Rica, FAO Fish Rep. 291, Vol. 3, 731-778.

Pearce, A.F. and G.R. Cresswell, 1985: Ocean circulation off Western Australia and the Leeuwin Current. *CSIRO Information Service, Sheet No. 16-3*, 4pp.

Pearce, A.F. and R.W. Griffiths, 1991: The mesoscale structure of the Leeuwin Current: A comparison of laboratory models and satellite imagery. *J. Geophys. Res.*, 96, 16,739-16,757, 1991.

Rochford, D.J., 1962: Hydrology of the Indian Ocean. Part II: the surface waters of the south-east Indian Ocean and Arafura Sea in the spring and summer. *Austr. J. Mar. Freshwater Res.*, 13, 226-251.

Rochford, D.J., 1969: Seasonal variations in the Indian Ocean along 110 degrees E. Part I: Hydrological structure of the upper 500 m. *Aust. J. Mar. Freshwater Res.*, 20, 1-50.

Rochford, D.J., 1986: Seasonal changes in the distribution of Leeuwin Current waters off southern Australia. *Aust. J. Mar. Freshwat. Res.*, *37*, 1-10.

Semtner, A.J., and Y. Mintz, 1977: Numerical simulation of the Gulf Stream and midocean eddies. *J. Phys. Oceanogr.*, 7, 208-230.

Semtner, A.J., and R.M. Chervin, 1988: A simulation of the global ocean circulation with resolved eddies. *J. Geophys. Res.*, 93, 15,502-15,522.

Smith, R.L., A. Huyer and J.S. Godfrey, 1991: The Leeuwin Current off Western Australia, 1986_1987. *J. Phys. Oceanogr.*, 21, 323-345.

Thompson, R.O.R.Y., 1984: Observations of the Leeuwin Current off Western Australia. *J. Phys. Oceanogr.*, 14, 623-628.

Thompson, R.O.R.Y., 1987: Continental-shelf-scale model of the Leeuwin Current. *J. Mar. Res.*, 45, 813-827.

Tomczak, Matthias and J. Stuart Godfrey, In, *Regional Oceanography: An Introduction, 1st ed.* (London: Pergamon, 1994) 217-220 pp.

Trenberth, K.E., W.G. Large, and J.G. Olson, 1990: The mean annual cycle in global ocean wind stress. *J. Phys. Oceanogr.*, 20, 1742-1760.

Weatherly, G.L., 1972: A study of the bottom boundary layer of the Florida Current. *J. Phys. Oceanogr.*, 2, 54-72.

Weaver, A.J., and J.H. Middleton, 1988: An analytic model for the Leeuwin Current off Western Australia, School of Mathematics, *Appl. Math. Preprint No. AM 88/31*, University of New South Wales.

Weaver, A.J., and J.H. Middleton, 1989: On the dynamics of the Leeuwin Current. *J. Phys. Oceanogr.*, 19, 626-648.

Weaver, A.J., and J.H. Middleton, 1990: An analytic model for the Leeuwin Current Off Western Australia. *Cont. Shelf Res.*, 10, 105-122.

Wooster, W.S., and J.L. Reid, 1963: Eastern Boundary Currents. In, *The Sea, volume 2*, M.N. Hill, ed., Wiley Interscience, New York, pp. 253-280.

INITIAL DISTRIBUTION LIST

	No. Copies
1. Defense Technical Information Center Cameron Station Alexandria, VA 22304-6145	2
2. Librarian, Code 52 Naval Postgraduate School Monterey, CA 93943-5101	2
3. Chairman (Code OC/Bf) Department of Oceanography Naval Postgraduate School Monterey, CA 93943-5122	1
4. Chairman (Code MR/Hy) Department of Meteorology Naval Postgraduate School Monterey, CA 93943-5114	1
5. Dr. Mary L. Batteen, (Code OC/Bv) Department of Oceanography Naval Postgraduate School Monterey, CA 93943-5122	2
6. Dr. Curtis A. Collins, (Code OC/Co) Department of Oceanography Naval Postgraduate School Monterey, CA 93943-5122	1
7. Mike Cook, (Code OC/Mk) Department of Oceanography Naval Postgraduate School Monterey, CA 93943-5122	1
8. Pete Braccio, (Code OC/Bc) Department of Oceanography Naval Postgraduate School Monterey, CA 93943-5122	1
9. Dr. Richard Lambert National Science Foundation 4201 Wilson Boulevard Arlington VA 22230	1

10. LCDR Christopher L. Butler — 2
826 Harned St. APT 7B
Perth Amboy, NJ 08861

11. Director, Naval Oceanography Division — 1
Naval Observatory
34th and Massachusetts Ave, NW
Washington, DC 20390

12. Commander — 1
Naval Meteorology and Oceanography Command
1020 Balch Boulevard
Stennis Space Center, MS 39529-5005

13. Commanding Officer — 1
Naval Oceanographic Office
Stennis Space Center, MS 39529-5000

14. Commanding Officer — 1
Fleet Numerical Meteorology and Oceanography Center
7 Grace Hopper Avenue, STOP 1
Monterey, CA 93943-5001

15. Dr. Tom Kinder — 1
Office of Naval Research
800 N. Quincy Street
Arlington, VA 22217-5000

16. Alan Pearce — 1
CSIRO, Division of Oceangraphy
P.O. BOX 20
North Beach, WA 6020
AUSTRALIA